Preliminary design of a foundation for a Tall Lunar Tower

A. van der Pauw

Image: (Airwolfhound, 2020)

Foster + Partners

TU Delft

Preliminary design of a foundation for a Tall Lunar Tower

by

A. van der Pauw

Student number:	4590767	
Project duration:	Sep, 2024 – July, 2025	
Thesis committee:	Dr. Giorgia Giardina	TU Delft, supervisor
	Dr. Marina Konstantatou,	Foster + Partners
	Dr.ir. Mandy Korff	TU Delft
	Dr. Dipl.-Ing. H.H. (Henriette) Bier	TU Delft

TU Delft

Preface

This Master thesis is part of the thesis of the Master Civil Engineering – Track Geotechnical Engineering. This thesis was written in collaboration with Foster + Partners and TU Delft. It serves as a guide for geotechnical engineers who wish to explore the current possibilities for foundation design on the lunar surface, based on the available information.

I would like to thank Giorgia Giardina and Marina Konstantatou, who provided valuable feedback and discussions as my supervisors. Giorgia, in particular, who listened and understood the difficult situations I found myself in and gave me the space and support to deal with everything at my own pace while still challenging me to grow.

Mahtab Foroughnia, Murat Sahin, Jan Koune, Hao Kuai, Rafael Ramirez Eudave, Dominika Malinowska, and Valentina Macchiarulo, thank you all for your kind words and advice during the group meetings. I enjoyed our time together and had a great time getting to know you all. I hope to see you again someday during our next adventures!

Additionally, I would like to thank Mandy Korff and Luca Flessati for their brainstorming sessions with me. Your advice inspired me to explore different directions and expand my knowledge on seismic design.

Lastly, I would like to thank my friends, who helped me through the difficult times while I was writing this report. You are the best, and I look forward to spending many more years together.

A. van der Pauw
Delft, 2025

Abstract

The Artemis program is the start of this new era of space exploration, where NASA aims to develop infrastructure that enables sustained scientific research, exploration, and industrial activity on the Moon. The Tall Lunar Tower is one of the concepts designed to provide power generation and communication, position, navigation, and timing architecture that needs to be established during this era. However, the foundation design is underdeveloped and is critical for transferring loads from the structure to the lunar regolith and for providing stability under microgravity and moonquake loading. Additionally, the lunar environment presents unique challenges for the design process, and only limited information is available on geotechnical design parameters and the seismic hazard posed by shallow moonquakes. This thesis provides a preliminary design of a foundation for a Tall Lunar Tower under microgravity and shallow moonquake loading, within the constraints posed by the extraterrestrial lunar environment, and gives insights into soil-structure interaction and uncertainties in lunar foundation design. An extensive literature review was conducted to identify relevant requirements, boundary conditions, evaluation criteria, and uncertainties. To develop concepts, historical and current foundation designs were investigated and evaluated using a multi-criteria analysis, and the chosen concept was verified using the NEN-1997 and NEN-1998 design standards. The design considers the high cost of transporting material and equipment by leveraging the current capacities of lightweight equipment and using locally produced materials that withstand extreme temperatures and radiation. It was concluded that the soil parameters influence the shear strength and deformation behaviour of the lunar regolith, thereby dictating the required foundation size. However, the limited measurements available from different sites introduce uncertainty into soil behaviour, seismic hazard, and the source of shallow moonquake events. A slab foundation can serve as a prototype for a lunar foundation, given its simple construction, the option to use local materials and limited excavation depth. Small seismic excitations can yield large displacements at the top of the tower, and to achieve stability, a large, shallow foundation is necessary. This results in substantial settlements and an increased risk of rotational failure. To reduce the foundation size, anchored post-tensioning tendons or external wires can recenter the tower, or structural parameters can be adjusted to influence the tip displacement. This thesis has considered the state of the art to perform preliminary design calculations, thereby identifying the research gaps for geotechnical engineering on the lunar surface and outlining paths forward to make lunar colonisation a reality.

Contents

1 Introduction **1**
1.1 Motivation . . . 1
1.2 Scope . . . 2
1.3 Outline . . . 2

2 Literature Review **6**
2.1 Lunar environment . . . 6
2.2 Tall Lunar Tower . . . 7
2.3 Location Artemis base camp . . . 8
2.4 Illumination conditions . . . 12
2.5 Geology . . . 15
2.6 Seismicity . . . 21
2.6.1 Types of moonquakes . . . 21
2.6.2 Seismic Hazard . . . 23
2.7 In Situ Resource Utilization . . . 24
2.7.1 Available materials . . . 25
2.7.2 Construction techniques . . . 27
2.8 Excavation and drilling possibilities . . . 29
2.8.1 Excavators . . . 29
2.8.2 Drills . . . 29
2.9 Anchoring possiblities . . . 30
2.10 Program of Requirements . . . 32
2.10.1 Requirements . . . 32
2.10.2 Boundary conditions . . . 33
2.10.3 Evaluation criteria . . . 33

3 Design **35**
3.1 Development of Concepts . . . 35
3.1.1 Historical foundations . . . 35
3.1.2 Eurocode 8 foundation design . . . 36
3.1.3 Multi Criteria Analysis . . . 38
3.2 Design Input . . . 40
3.2.1 Structure Input . . . 40
3.2.2 Soil Input . . . 40
3.2.3 Seismic Input . . . 40
3.2.4 Foundation Input . . . 45

4 Static analysis **46**
4.1 Overview . . . 46
4.2 Methodology . . . 47
4.2.1 Stability . . . 47
4.2.2 Bearing Capacity . . . 47
4.2.3 Sliding . . . 50
4.2.4 Rotational Failure . . . 50
4.2.5 Failure due to horizontal movement foundation . . . 51
4.2.6 Settlements . . . 51
4.3 Results . . . 52
4.3.1 Bearing capacity . . . 52
4.3.2 Settlements . . . 54
4.4 Discussion . . . 55

5 Seismic analysis **61**
5.1 Seismic analysis - no second order effects . . . 61
5.1.1 Overview . . . 61
5.1.2 Methodology . . . 61
5.1.3 Results . . . 65
5.1.4 Discussion . . . 67
5.2 Seismic analysis - with second order effects . . . 73
5.2.1 Overview . . . 73
5.2.2 Results . . . 73
5.2.3 Discussion . . . 75

6 Final Design **86**
6.1 Final Design Configuration . . . 86
6.2 Material options . . . 86
6.3 Shallow Foundation Size Reduction . . . 89
6.3.1 Post-tensioning . . . 89
6.3.2 Anchoring in lunar regolith . . . 91
6.3.3 Using fill material . . . 92
6.4 Difference from Earth . . . 94
6.4.1 Design process . . . 94
6.4.2 Design standard . . . 95

7 Conclusions & Recommendations **97**
7.1 Conclusions . . . 97
7.2 Future recommendations . . . 99

References **104**

A Appendix A: Consideration MCA scores **111**

B Appendix B: Alternative Pile Foundation **115**
B.1 Methodology . . . 115
B.2 Results . . . 118
B.3 Discussion . . . 119

1 Introduction

1.1. Motivation

Since the Apollo 11 flight, no humans have set foot on the moon. Many scientific discoveries were made possible thanks to the observations and collected samples from a single visit. Therefore, the importance of lunar exploration cannot be underestimated (Creech et al., 2022; Moriarty et al., 2021; Young et al., 2021). NASA set seven objectives for the new Artemis program, which aims to start a new era of lunar exploration for "science, national posture and inspiration" (NASA, 2023). To do this, it is necessary to establish lunar infrastructure, where three specific objectives described by NASA (2023) are:

> *"LI-1: Develop an incremental lunar power generation and distribution system that is evolvable to support continuous robotic/human operation and is capable of scaling to global power utilization and industrial power levels."*
>
> *"LI-2: "Develop a lunar surface, orbital, and Moon-to-Earth communications architecture capable of scaling to support long-term science, exploration, and industrial needs."*
>
> *"LI-3: "Develop a lunar position, navigation, and timing architecture capable of scaling to support long-term science, exploration, and industrial needs."*

For the first objective, solar power must be harvested to provide power to lunar surface assets. The lunar surface is highly irregular, creating large regions of low illumination. Ross et al. (2021) proposed that the "Peaks of Eternal Light", elevated areas that are almost continuously illuminated and are therefore mostly unaffected by the shadows of surrounding terrain, could be utilised to generate sufficient power. However, this significantly limits the area available for solar power generation to a few km^2 (Gläser et al., 2014). To increase solar power generation, therefore, Ross et al. (2021) and Doggett et al. (2022) suggest building higher to improve the illumination of the solar panels and increase the lunar surface area that can potentially be used for solar power generation. Additionally, a single tall power module reduces the total mass compared to multiple shorter modules, which is relevant for the energy required for material production, transport, and assembly. It also makes it possible to vertically stagger solar arrays, allowing more solar power modules to inhabit the same area. More height also reduces the sensitivity to inaccuracies in the current terrain data.

Edwards (2023) and Edwards et al. (2023) state that a robust communications and navigation system, named LunaNet, providing proper coverage, is being investigated by NASA to achieve the second and third objectives. In the earlier Artemis missions, satellites could be enhanced to provide these Communication, Position, Navigation and Timing (CPNT) services. However, when user numbers increase considerably in future phases of the project, the use of surface-to-surface communications can no longer be provided solely by lunar satellites. Therefore, there is a need for a lunar surface wireless network to provide an alternative path for data. Early results from lunar terrain models show that a single Base Terrain Station (BTS) can provide a high percentage of coverage at known locations. However, when more lunar surface area or different locations need to be covered, one BTS is no longer sufficient. Increasing the height of the station is an option to expand the coverage area for a single BTS.

One of the concepts being developed by NASA in collaboration with Foster + Partners to provide these services is the Tall Lunar Tower (TLT). The current tower concepts are truss structures that can be robotically assembled and can reach great heights. One identified underdeveloped part of the design is that these towers need a foundation (Tiffin & Mahlin, 2023). A fixed connection to the lunar surface is currently assumed in the existing literature (Edwards, 2023; Song, Mikulas, et al., 2023), meaning that the tower is unable to move or rotate at the base .

A foundation is crucial for transferring loads from the structure to the ground and providing the necessary constraints for the structure's stability. In the lunar environment, one of the loads that could lead to structural instability is moonquakes. The equipment or structure could be damaged during a seismic event if no proper foundation is designed to transfer these loads. Additionally, since the tower serves as a power source, nearby lunar assets may be affected. Therefore, it is essential to design a foundation that supports the structure and resists moonquake events to reduce this risk.

This project aims to provide a preliminary conceptual design of a foundation for a Tall Lunar Tower that considers the unique environmental loads and available materials on the moon, providing a fixed connection to ensure the stability of the TLT and resistance to moonquakes. This preliminary design can be used to take another step in making lunar exploration possible by giving insights into the behaviour of the lunar soil and the soil-structure interaction, as well as identifying risks and uncertainties for foundation design on the lunar surface. If proper stability and resistance to moonquakes can be guaranteed in the future, the risk of damaging the TLT can be reduced. With the necessary CPNT and power services in place, a new era of lunar exploration can begin.

Problem Statement:
A foundation is critical for connecting a Tall Lunar Tower to the lunar surface, and relevant concepts are underdeveloped. Therefore, the stability of the Tall Lunar Tower under moonquake and microgravity loading cannot be guaranteed.

Design objective:
This thesis aims to provide a preliminary design of a foundation for a Tall Lunar Tower that guarantees stability and provides shallow moonquake resistance, within the constraints posed by the extraterrestrial lunar environment.

Table 1.1: The problem statement and design objective that were identified for the design project.

1.2. Scope

When using the elementary design cycle as presented in Figure 1.1, eight stages are identified with multiple iterative jumps. The number of times the design cycle and iterations can be repeated had to be limited to fit within the timeframe of a Master Thesis. This resulted in the unfeasibility of detailed modelling of the foundation and structure. Therefore, it was chosen to perform only a preliminary design and to validate the results with the Eurocode design standards where possible. In addition, only one tower design was considered as input to the design calculations, as varying it would introduce too many variables to the design process.

1.3. Outline

In Chapter 2, an extensive literature review is described, covering steps one and two of the elementary design cycle. First, the lunar environment is investigated to identify factors that influence the requirements, boundary conditions, and evaluation criteria for foundation design. Then, the current state of development of the TLT is investigated, where the loads that need to be imposed on the foundation and other requirements are identified, as well as the goals and future plans for TLT design that will impact the location. Based on these findings, the factors influencing the location of the future Artemis Base Camp are investigated to identify the necessary elements that will enable compliance with both future scientific objectives and the purpose of the TLT. Since the TLT is designed to provide solar energy, the illumination conditions are identified at the found locations to determine the location where

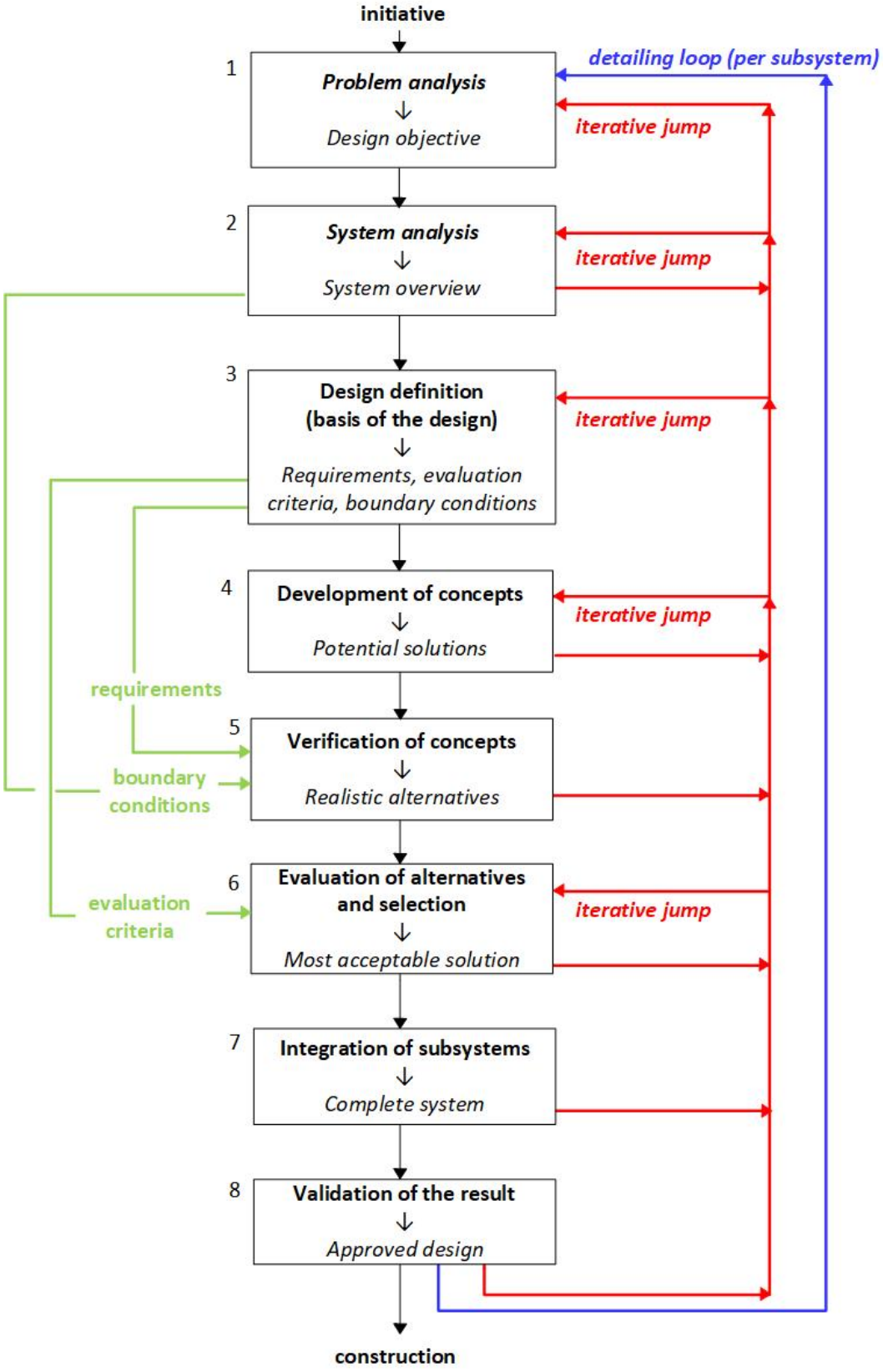

Figure 1.1: The elementary design cycle (Thesis Prep course, n.d.).

boundary conditions can be obtained. In this location, the geology and soil parameters are gathered and examined. Since the design objective requires moonquake resistance, the seismicity of the Moon is investigated in conjunction with the potential seismic hazard. Lastly, due to the unique challenges posed by extraterrestrial construction, the current state of In Situ Resource Utilisation (ISRU) is described, where materials are produced from the local resources on the lunar surface. The state of the excavation and drilling possibilities, as well as anchoring, is also described. These factors result in additional requirements, constraints, and evaluation criteria for the foundation design. In Section 2.10, the findings of the literature review are summarised in requirements and boundary conditions. In addition, evaluation criteria are presented to consider the different verified foundation concepts based on what is preferred when constructing in an extraterrestrial environment. This concludes step three of the elementary design cycle.

The development of concepts and verification of the found concepts are the fourth and fifth steps of the cycle, after which the evaluation of the concepts follows. Therefore, with the requirements and boundary conditions known, the first part of Chapter 3 discusses different concepts that were developed based on historical and state-of-the-art concepts from literature. Moreover, the recommended foundation configurations for seismic loading conditions, as outlined in the Eurocode, are compiled. Methods to increase earthquake resistance are discussed, and their potential application on the lunar surface, combined with their feasibility for the TLT structure, is explored. Then, the evaluation criteria from Section 2.10 are used to perform a Multi-Criteria Analysis to determine the most feasible foundation configuration for performing preliminary design calculations, finishing step six of the design cycle. The second half of Chapter 3 describes all the input parameters and assumptions necessary to perform preliminary design calculations as described in the Eurocodes and validate the foundation concept. First, the structural input from the TLT is discussed, followed by a summary of the input used for soil parameters. Afterwards, the seismic input is discussed to determine which parts of the Eurocode to apply. First, the site categorisation based on shear wave velocities is done. This is followed by the definition of a consequence class, along with the limitations of this definition in the unique case of construction on the lunar surface. This is used as input to determine the seismic class of the lunar soil, allowing for the inclusion or exclusion of inertial forces in the design calculations. With this information known, and the seismic hazard for different return periods obtained in Chapter 2, the peak ground acceleration and structure acceleration are determined. This chapter concludes with a foundation configuration used as input for various analyses, validating whether the foundation can withstand all loads and completing the design cycle.

In Chapter 4, the foundation configuration is validated against the static loads. The method for calculating failure mechanisms related to stability bearing capacity, sliding, rotational failure, failure due to horizontal movement of the foundation, and settlements is described. The governing failure mechanisms for the static load case are calculated for the foundation input described in Section 3.2. To obtain insights into the effects of different aspects of the design process, the following research questions are discussed in the final part of each analysis:

- How do the soil parameters influence foundation design under static and seismic loading conditions?
- How does the foundation configuration affect the failure mechanisms given by the Eurocode design standards?
- How do the structural parameters of the TLT influence the foundation configuration?
- How does microgravity influence the possible foundation configurations for the static and seismic load cases?

Chapter 5 uses the same structure as the static analysis and regards the seismic load case. First, the methodology is discussed in relation to the Eurocode design standards for the relevant failure mechanisms under seismic loads, including sliding failure, exceedance of bearing capacity, rotational failure, and settlements. The relevant failure mechanisms are validated for the foundation input, and a similar discussion is conducted using the same research questions as posed above. The last analysis accounts for the second-order effect and the corresponding loads. The same failure mechanisms are checked, and the discussion uses the same structure.

Chapter 6 summarises the found configurations and discusses potential material options that can be used in the lunar environment, the advantages and disadvantages, and what should be checked in the future when using one of the options. Moreover, various methods to enhance stability and minimise the size of shallow foundations, thereby reducing material consumption, are discussed. Lastly, the differences between the design process in lunar conditions and how it normally occurs on Earth are highlighted, along with the inputs required for a future lunar design standard.

The final chapter, Chapter 7, presents a reflection on whether the problem is solved and the design objective has been achieved, along with the assumptions under which this is the case. The major insights obtained from the discussions are summarised, and finally, the recommended topics for future research or experiments are detailed.

2

Literature Review

2.1. Lunar environment

The lunar environment presents unique challenges to designing a foundation for a TLT. Compared to Earth, the gravity on the lunar surface is about 1/6th of Earth's gravitational acceleration, approximately 1.2 m/s^2. This reduces the load on the foundation; however, this also impacts inertia effects.

Due to the nature of the lunar regolith, which is discussed in depth in Section 2.5, minor disturbances can create a lot of dust that can potentially damage or block equipment due to its unique electrostatic and magnetic properties (Valinia et al., 2022). Jablonski and Ogden (2008), Kalapodis et al. (2020), and Ruess et al. (2006) state that the upper layer of the regolith is a loose, fine material that is easily disturbed. This indicates the need to disturb the ground as little as possible during the construction of the tower, remove this layer entirely, and take time to let the dust settle slowly. This will prevent robotic equipment needed to construct the tower from being impacted by the dust too extensively.

The seismic environment of the moon differs from that on Earth (Oberst & Nakamura, 1992). These ground motions could be an underestimated hazard for lunar structures (Jablonski & Ogden, 2008; Kalapodis et al., 2020; Oberst & Nakamura, 1992). The risk of a seismic event damaging the solar towers, possibly disrupting experiments and leaving lunar surface assets without power, needs to be minimised. A risk of building higher towers in a seismic environment is that small horizontal loads due to seismic accelerations can quickly lead to large moments being imposed on the foundation, potentially causing instability of the TLT. This depends on the material used for the tower and the mass of solar panels attached to the top. The details about the preliminary design of the TLT and future developments are discussed in section 2.2. The exact nature of these events and their characteristics are described in section 2.6.

Additionally, the Moon lacks an atmosphere. This has a positive effect on the tower as it prevents horizontal wind loads on the tower; however, according to Jablonski and Ogden (2008), Kalapodis et al. (2020), and Ruess et al. (2006), not having a protective layer around the Moon causes large thermal gradients, radiation, and meteoroid impacts.

Valinia et al. (2022) conclude that extreme thermal fluctuations over the lunar surface are present, due to the moon's topology capable of casting long shadows, combined with the properties of the lunar regolith exhibiting low thermal conductivity and high emissivity. The 29.5-day duration of the lunar day and night cycle causes temperatures to range from -255 degrees to 127 degrees. The long shadows result in illumination conditions relevant to solar power energy generation, as well as the required height of the TLT and potential locations for the Artemis Base Camp. The light conditions are therefore discussed in section 2.4 and the potential locations in section 2.3. For the structure of the TLT, this could lead to high thermal stresses in joints and a possible thermal fatigue effect. The materials used for a foundation need to be able to withstand these extreme temperatures.

Jablonski and Ogden (2008) and Ruess et al. (2006) summarise that the radiation on the lunar surface consists of 2 types: electromagnetic and ionising, where solar winds, solar cosmic rays, and galactic cosmic radiation cause the latter. This again impacts the equipment, but in addition, temperature fluctuations and these ionising radiation particles influence the materials used to construct the tower. Since humans cannot survive in environments with high radiation levels, extreme temperatures,

and a lack of oxygen without special measures, innovative construction methods need to be developed and are discussed in Section 2.7. This section also discusses the possible materials that can be used for the design.

Furthermore, the lack of atmosphere causes meteoroid impacts (Jablonski & Ogden, 2008). Meteoroid impacts are stochastic in nature, making it difficult to accurately model this hazard. For the scope of this Master thesis, meteoroid impacts are not considered.

2.2. Tall Lunar Tower

Tall Towers can be more easily achieved on the Moon than on Earth. Because of the lack of atmosphere, no horizontal wind forces are present in the lunar environment. This enables us to build higher than we normally would on Earth and unlocks the preferred height for CPNT services and solar power generation. One preliminary design was created by Ruppert et al. (2022), investigating the stability of a tower made of lunar concrete. The analytic approach showed that concrete towers on the Moon are stable, even at a kilometre scale, against compressive failure and buckling in this simplified design.

One issue with building higher is that both the amount of material required increases, and the construction method becomes limited. Transporting materials or equipment from Earth to the lunar environment is extremely expensive; therefore, solutions must be found to reduce the mass and volume of the tower.

It was found by Doggett et al. (2022) that using metal truss frame towers can reduce transportation mass, allowing for the choice of towers that can be assembled on the lunar surface or those that utilise a telescoping tube. It was concluded that the assembled towers require 1/3 of the mass of a telescoping tube tower, and 1/14th to 1/25th times the volume for the power modules in the 50 kW to 200 kW range. The assembled towers can also be packaged more efficiently than tubes when transporting materials from Earth.

Another option is the use of locally produced materials. Ruppert et al. (2022) suggest using lunar regolith as an ingredient for the concrete used to build the tower, sparking the idea of using local material as a building block for lunar infrastructure. The transportation of material to the lunar surface can be reduced; however, the mass and volume of the tower are still relevant since it requires lunar material and power to produce the structural members.

When using locally produced material, power quickly becomes one of the major factors in building and developing infrastructure on the lunar surface. A single TLT will not be sufficient as the power and CPNT demand grow (Carrio et al., 2023; Tiffin & Mahlin, 2023). In the Lunar Economy Analysis Platform (LEAP) model developed by Carrio et al. (2023), Lunar Vertical Solar Array Technology (LVSAT) elements and Fission Surface Power (FSP) elements can be placed to design power grid layouts based on supply and demand. In the earlier stages of the Artemis era, the surface elements are mobile. Once infrastructure is developed, however, the elements become fixed based on the optimal configuration for illumination conditions of the worst-case lunar day. This timeline is illustrated in Figure 2.1.

Tiffin and Mahlin (2023) show that a grid of autonomously constructed TLTs in the right location would then be able to provide both a power supply and CPNT coverage as the height increases. As infrastructure grows, the towers become more beneficial by reducing the battery mass of lunar surface assets, as these no longer need to rely on their own power generation and storage, thereby making the infrastructure more robust. As demand grows, the grid can be easily upgraded with additional towers, eventually providing power to a large number of users. One argument against using TLTs for CPNT is that a lander or rover could be outfitted with these capabilities. However, this is still an expensive and complex development, and navigating rovers is also complicated. Once they break, their repair options are limited. In contrast, a Robotic Construction Rover (RCR) could assemble multiple TLTs, introducing redundancy, scalability, and robustness to failure. The TLT can be repaired, inspected, and outfitted by the same robotics.

As the lunar environment, with its high temperature fluctuations and lack of breathable oxygen, is not a suitable place for humans to construct infrastructure themselves, autonomous construction through robotics is preferred. Song, Mikulas, et al. (2023) studied the robotic assembly of the tower, and, once assembled, the design, modelling, fabrication, and testing of a truss structure and structural joints. This design serves as a reference in this thesis to inform the preliminary design calculations. The TLT can be modelled as a clamped beam element, with a tip mass and distributed mass due to the microgravity. With this mechanical scheme, information about the natural frequency of the tower, its buckling

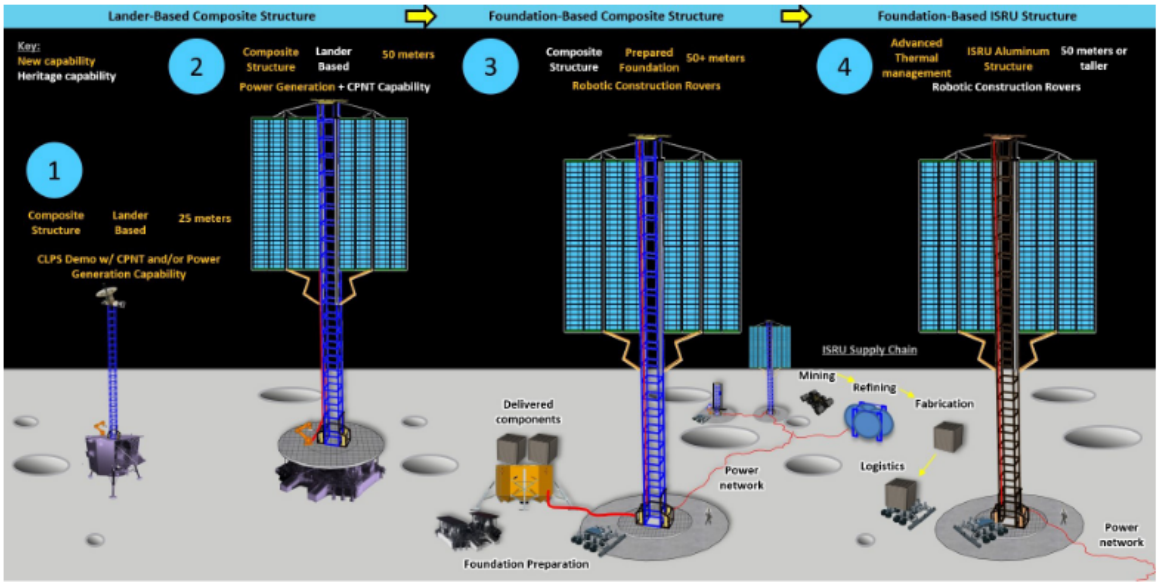

Figure 2.1: The roadmap for the development of TLT structures. Here, the TLT structure is visualised in different phases of lunar colonisation (Tiffin & Mahlin, 2023)

response, and the static deflection could be obtained. Song, Stark, et al. (2023) performed a detailed analysis on the buckling responses for different payloads and materials, and a thermal-structural analysis of the same structure. The latter resulted in minimal tip displacement at significant temperature gradients, not generating additional moments on the foundation. Moonquakes were not specifically considered; they were only taken into account in the safety factor. Another design by Konstantatou et al. (2025) uses local materials and 3D printing techniques to create a helical diagrid geometry, using the tower geometry as rails to achieve the required height of the structure. The slender aspect ratio is identified as a stability risk under moonquake loading and thermal gradients. Options to use tie rings or explore post-tensioning approaches are given to reduce the risk of instability; however, the interaction with the foundation remains unexplored. Therefore, the effect of moonquake loading on the TLT structure, particularly when considering soil-structure interaction, remains unknown.

2.3. Location Artemis base camp

As it is difficult and costly to move assets from Earth to the lunar surface, efforts are focused on determining the most useful locations to send them. Lawrence (2022) states that the most advantageous area for future Artemis missions is the Lunar South Pole. In this zone lies the South Pole-Aitken Basin, the oldest and largest impact basin, which can reveal information on how the Moon formed. By taking samples there, the bombardment history and origin of the Moon can be studied, as well as the impact processes that shaped it. Moreover, an investigation of the moon's internal structure will reveal more information about the nature of lunar tectonism. Additionally, the rock diversity of the lunar crust, volcanism, and regolith processes can be explored. This can lead to an understanding of the geotechnical and physical properties of the regolith, advancing engineering on the lunar surface.

The area's topography is illustrated in Figure 2.2. New technologies will be tested here to expand the possibilities on the lunar surface. With this knowledge, we can prepare our systems for eventually going to Mars (National Space Council, 2020). According to Mazarico et al. (2011), the South Pole is also of interest because of the Earth's visibility for communications (Figure 2.3a), as no CPNT network is available on the lunar surface during the earlier stages of lunar colonisation. Additionally, the NASA (2022b) mentions the presence of areas with nearly continuous sunlight (more in section 2.4) for solar power generation, permanently shadowed areas (Figure 2.3b) where volatiles can be found, and the geological diversity as other reasons to investigate the Lunar South Pole more closely.

It was concluded by NASA (2022b) that long-duration illumination zones are thermally stable, resulting in more effective solar power generation with reduced battery power requirements during periods of darkness. The dependency on the times of year with long illumination durations will decrease by having

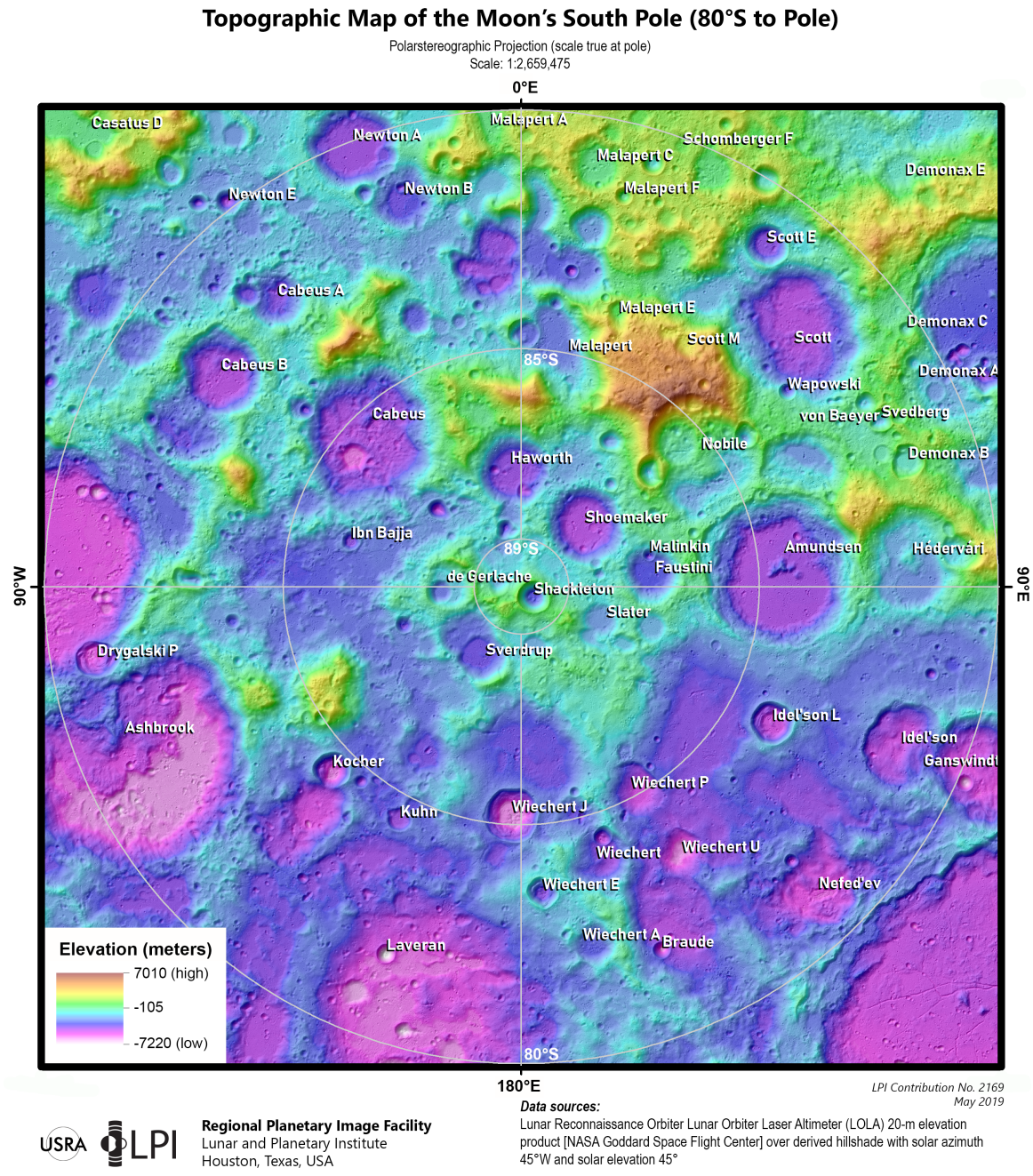

Figure 2.2: The topography of the Lunar South Pole. The focus during the Artemis era will be on the area around Shackleton crater, which is located directly next to the South Pole (Stopar & Meyer, 2019).

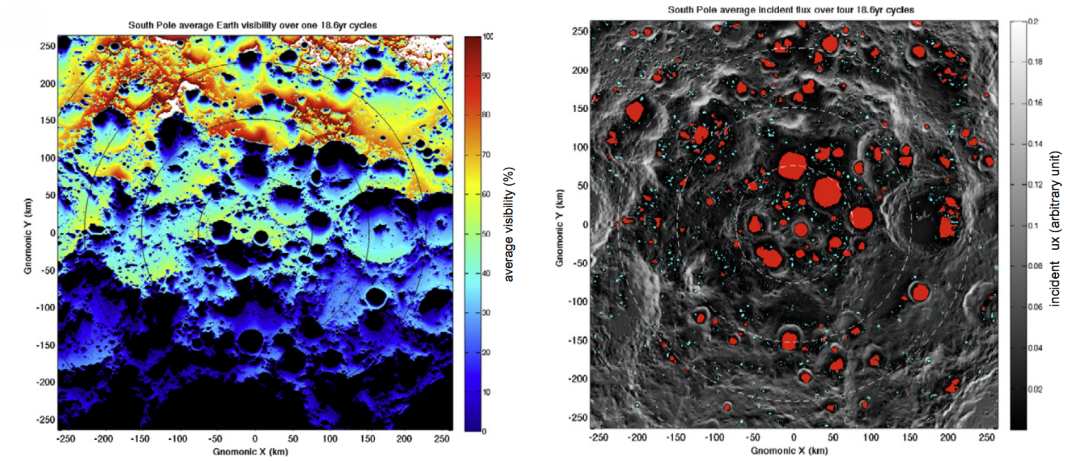

(a) The visibility of the Earth is an important factor to ensure early communication before a local network is available (Mazarico et al., 2011).

(b) The location of Permanently Shadowed Regions on the South Pole that likely contain volatiles. The red areas describe the 150 largest permanently shadowed regions, where the cyan areas describe smaller PSRs (Mazarico et al., 2011).

Figure 2.3: The Earth visibility and location of Permanently Shadowed Regions on the South Pole area of the Moon.

local power supplies that harness power by using their height above the surface to their advantage . Thermal stability also reduces the loads on the structure and materials of lunar infrastructure.

The zones with permanent shadows are protected from solar winds and likely contain volatiles trapped in ice (NASA, 2022b). These volatiles contain scientific knowledge about the history of the Moon (Hu et al., 2023), Sun (National Space Council, 2020), and Earth systems and can serve as valuable resources (Hu et al., 2023; National Space Council, 2020). Utilising local water and hydrogen sources that can be extracted from volatiles enables the production of fuel, water, and oxygen to support a human habitat (Hu et al., 2023; National Space Council, 2020). These volatiles can also be found near the surface in only partially illuminated areas (Hu et al., 2023; NASA, 2022b), making them accessible for sampling (NASA, 2022b) or mining (National Space Council, 2020). Mining on a greater scale, however, can only be realised once a suitable power supply system and lunar infrastructure are in place. As the mined material needs to be not only excavated, but also transported over the lunar surface from areas of permanent shadow, where no power can be harnessed from the sun. This will require the development of specialised excavators and drills capable of penetrating the lunar regolith under vacuum conditions and in extreme temperatures. Section 2.8 summarises the current state of development for this specialised equipment.

To transport and build on the lunar surface, the National Space Council (2020) aims to develop new autonomous techniques. However, as shown in Figure 2.2, the elevation on the Lunar South Pole can vary significantly. When you consider that PSRs are likely located in craters, autonomous vehicles need to be able to lower themselves and pull themselves up on steep slopes to access that area and its resources. Additionally, lunar dust poses a significant risk to equipment, and mitigation measures need to be developed. During the process of constructing infrastructure on the Moon, we will gain a deeper understanding of how to design in these extreme environments.

Lawrence (2022) summarises the scientific factors relating to the site selection process as follows:

- Sufficient illumination
- Availability range of sizes of craters for radial traverses and sampling
- Comprehensive sampling
- Accessibility of large blocks to enable sampling of large crater ejecta
- Proximity and accessibility mostly / permanently shadowed regions to understand volatile processes
- Proximity multiple geologic units of different time-stratigraphic age

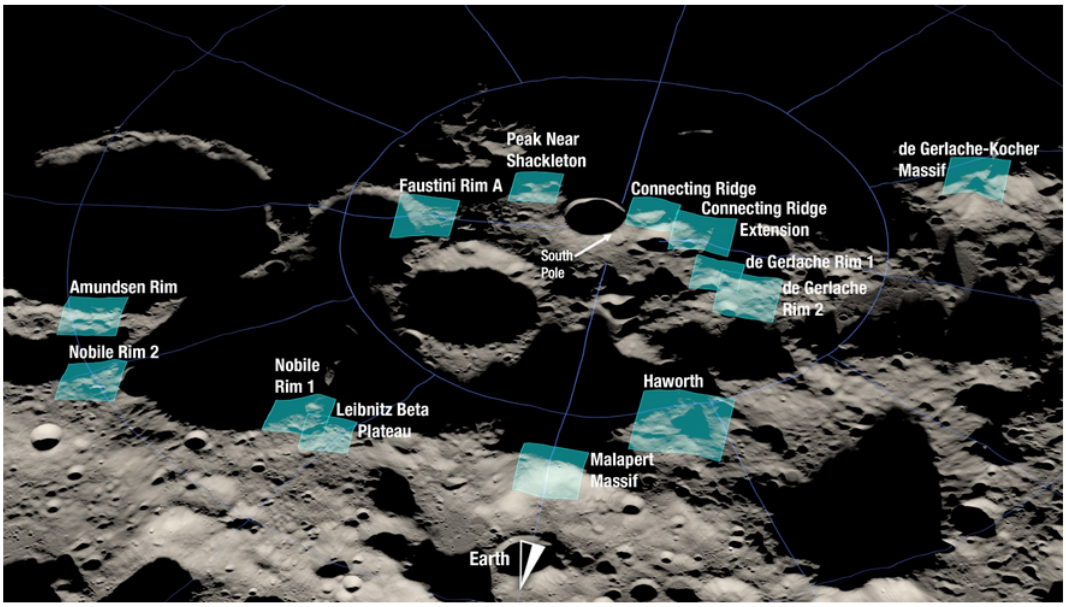

Figure 2.4: The candidate locations identified by NASA on the lunar South Pole (NASA, 2022a)

- Proximity geologic units that enable specific, high-priority investigations (Lawrence, 2022, p. 50)

In addition to these scientific goals, Hu et al. (2023) voices that the early missions must consider three engineering factors to ensure the landers carrying lunar assets can safely touch down on the lunar surface. Here, the slope and ruggedness of the surface, as well as the presence of blocks or small impact craters, are crucial factors in ensuring a safe landing and providing an area to start constructing infrastructure. Lighting conditions are important for sustaining exploration and facilities by harnessing solar power and minimising large thermal gradients that can damage equipment. In the case of a TLT, lighting conditions are especially significant, as these towers will primarily be used for solar power generation, leveraging their height to their advantage. Placing an object with a significant height on a sloped surface will result in large tip displacements and extra moment loads, and is therefore discouraged for foundation design. On the Lunar South Pole, areas with high illumination throughout the year, present near PSRs, and with a low angle slope are of interest for these purposes. Time periods restrict the available locations, as illumination conditions are not stable at every site throughout the year (Bleacher et al., 2024; Lawrence, 2022; Valinia et al., 2022). With these factors in mind, site selection becomes an iterative process that updates when more knowledge becomes available. In the later stages of the Artemis era, when scientific goals are achieved, the locations of interest will similarly change. Ultimately, the comparison of scientific goals with engineering restrictions involves finding the balance between ”where we want to go” and ”where we can go” (Bleacher et al., 2024).

NASA has already identified candidate regions for the next Moon landing. In Figure 2.4 the 13 candidate regions are visible, consisting of ”Faustini Rim A, Peak Near Shackleton, Connecting Ridge, Connecting Ridge Extension, de Gerlache Rim 1, de Gerlache Rim 2, de Gerlache-Kocher Massif, Haworth, Malapert Massif, Leibnitz Beta Plateau, Nobile Rim 1, Nobile Rim 2 and Amundsen Rim” (NASA, 2022a). They are still being updated (Taveau, 2024), indicating that ongoing discussions between experts and stakeholders are taking place.

Currently, analyses are being conducted using modern techniques to investigate the factors most important in decision-making for selecting the location of Artemis Base Camp. One study by Feng et al. (2024) uses deep learning techniques to select the optimal landing sites for an International Lunar Research Station (ILRS). Their model considers 12 factors related to the goals described above for site selection. When examining the results of the influence of the different factors, sun visibility is deemed the most important factor for the future ILRS, followed by the presence of water-ice, as evident in the analysis results in Figure 2.5.

Feng et al. (2024) conclude that the region near Shackleton Crater is a favourite because of its high sunlight points and geological diversity. It is also near other craters like Sverdrup Henson, and de Gerlache, that contain permanently shadowed regions and water-ice. The Shackleton region was also

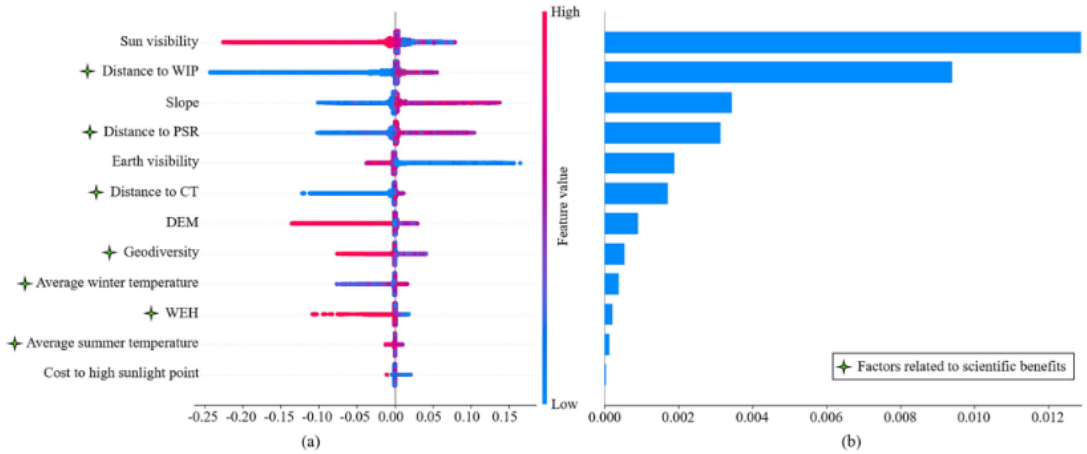

Figure 2.5: Factors identified by Feng et al. (2024) that influence site selection. The factors are: elevation from digital elevation models (DEM), slope, sun visibility, earth visibility, distance to cold trap (CT), distance to water-ice bearing pixels (WIP), distance to PSR, average summer temperature, average winter temperature, water equivalent hydrogen (WEH), geodiversity, and cost to high sunlight point (Feng et al., 2024). The infrastructure suitability assessment for the found areas was then evaluated for "Resource Utilization, Energy Supply, Expandability, Earth visibility and Scientific benefits." (Feng et al., 2024). The values on the x-axis represent the interpretation of the used Convolutional Neural Network model and present Shapley additive explanations (SHAP).

explored by Valinia et al. (2022) as an area of interest for lunar exploration due to the relatively long duration of illumination and the vicinity of many different PSRs around the Shackleton crater.

Another study by Csank (2023) identified the Connecting Ridge and Shackleton Crater Rim within the Shackleton region as primary targets for future lunar surface operations and a possible power grid, as they are located near multiple PSRs, such as Shackleton Crater, Sverdrup-Henson Crater, and the De Gerlache Craters. Here, the power supply for mining resources in the craters for ISRU practices could be implemented. The future focus lies on developing an advanced electrical power system that can provide the necessary values of resilience, reliability, and autonomy.

When examining tall towers to provide this power source, Tiffin and Mahlin (2023) and Doggett et al. (2022) mention the Connecting Ridge, the area that connects De Gerlache Crater and Shackleton Crater, as a suitable location for a solar farm, as well as the advantages of using an increasing standoff height on that location. Since the slope of the area becomes an important factor as described above when increasing the height of the structure, the slope measurements on the Shackleton region are visualised in Figure 2.6. As the discussion on the optimal site remains a current topic of conversation and research, this thesis will assume the Connecting Ridge as an area of potential interest for a solar farm. To investigate the available area with a low slope and proper illumination to obtain the required height of the TLT, lighting conditions are summarised in section 2.4. The local geology of this area is described in section 2.5.

2.4. Illumination conditions

To determine the height of the TLT, it is necessary to investigate the lighting conditions on the Connecting Ridge. Fincannon (2008) found that the lunar South Pole experiences varying lighting conditions, depending on the terrain elevation and the Sun's position. Around Shackleton crater, the lighting conditions can vary considerably over a lunar year, as illustrated for the best and worst lunar days in Figures 2.7a and 2.7b. Peaks of light can be observed around Shackleton Crater even with the worst light conditions; these areas, as stated in Section 2.3, are of interest for solar power generation. When measuring the illumination at these peaks in storage hours at surface level and at 100 meters in height, the number of energy storage hours decreases by approximately 15 to 21%. However, Fincannon (2007) determined that the results derived from these images could be influenced by errors caused by the resolution of the then-available data, that may lead to an error in the shadow cast by Malapert Mountain on the Shackleton region.

This error can be reduced with Kaguya and LOLA satellite data to obtain proper illumination conditions to provide a reference for the height of a future TLT (Bussey et al., 2010; Mazarico et al., 2011).

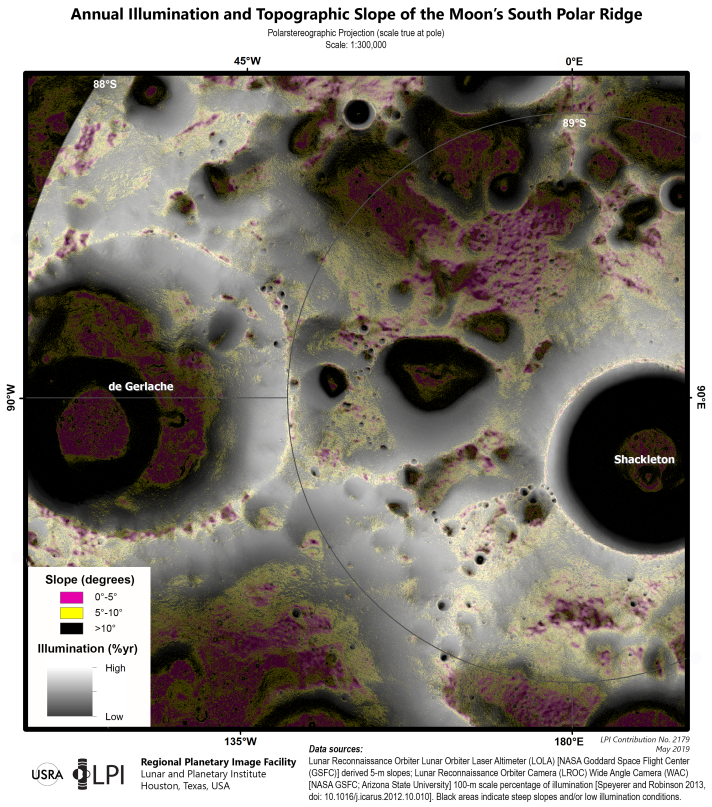

Figure 2.6: Map that combines slope information with illumination conditions to identify suitable locations in the region around Shackleton Crater (Stopar & Meyer, 2019).

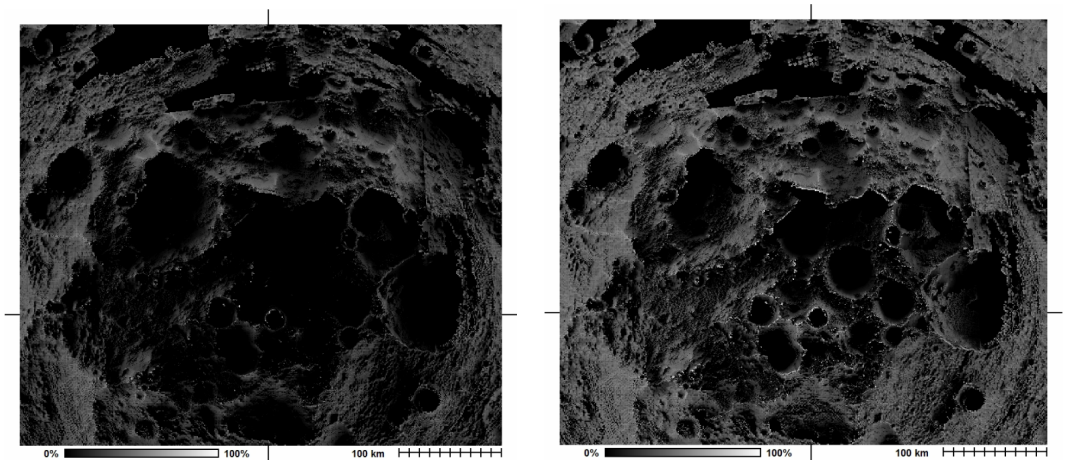

(a) Average illumination worst case lunar day (Fincannon, 2008) (b) Average illumination best case lunar day (Fincannon, 2008)

Figure 2.7: The vastly different lighting conditions on the lunar South Pole that can be observed in a lunar year.

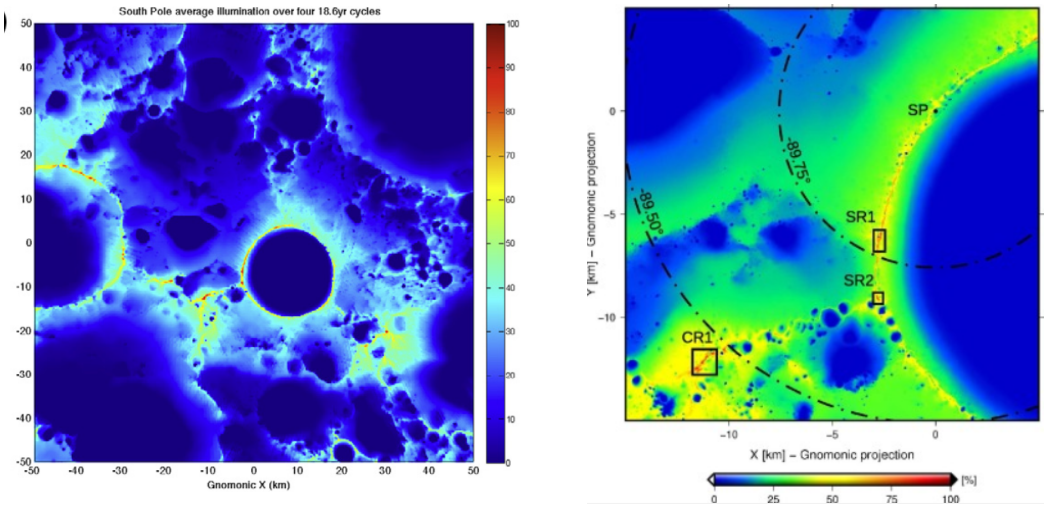

(a) The average illumination derived from LOLA satellite data around Shackleton Crater (Mazarico et al., 2011)

(b) The average illumination zoomed in on the Lunar South Pole. Three regions with high illumination percentages were identified. CR1 is the Connecting Ridge, where SR1 and SR2 are two locations on the Shackleton Rim. (Gläser et al., 2014)

Figure 2.8: The illumination conditions on different in the region around Shackleton crater.

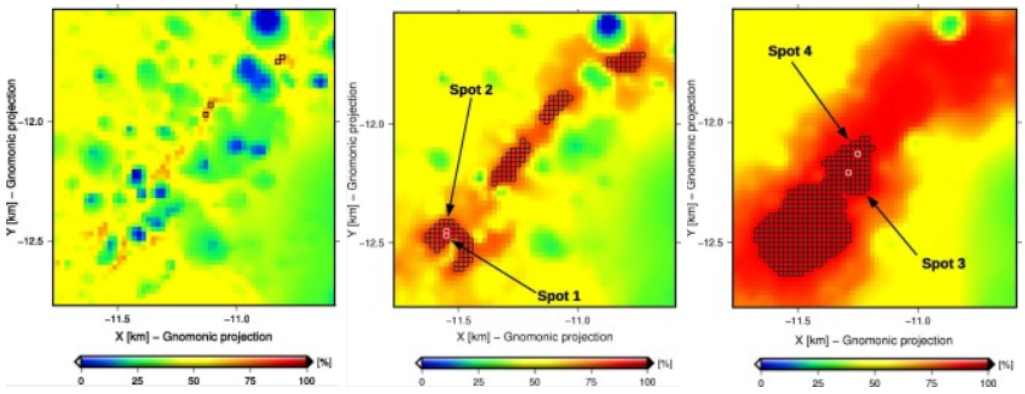

(a) Illumination percentage at surface level.

(b) Illumination percentage at 2 meter height.

(c) Illumination percentage at 10 meter height.

Figure 2.9: The increase in available highly illuminated area with height on the Connecting Ridge (Gläser et al., 2014).

Figure 2.8a shows the illumination in the region of Shackleton crater. When zooming in on the Connecting Ridge and the illumination conditions there, as illustrated by Figure 2.8b, three regions are identified with an average illumination of 80.62 - 86.62 % at two meters above surface level and a slope <5 °. The Connecting Ridge contains many red pixels, indicating an area of approximately 120000 m² available for a solar farm. Most slopes on the Connecting Ridge are smaller than 3 °.

The effect of the increase in available area with height can be seen in Figure 2.9. The black outlined spots in Figure 2.9a represent average illumination > 70 %, Figure 2.9b > 80 %, and Figure 2.9c > 92 %, where the highest average illumination spots are white outlined and indicated. At 10 meters, the illumination even reaches 95.65 % in spot 4. However, the area does not increase indefinitely; the roughness of the terrain becomes a more limiting factor than illumination with an increase in height (Gläser et al., 2014). Moreover, the uncertainties stemming from the used Digital Elevation Model data for the height and slope are approximately 0.30 - 0.50 meters for the height and 1.5 - 2.5 ° for the slope (Barker et al., 2021).

The required height of the towers, however, is not only focused on achieving the highest illumination conditions and thus the highest possible tower height; instead, it can be limited by the required power generation for, for example, planned mining activities in the area. The effect of tall towers of different heights on the available area on the Connecting Ridge for different illumination percentages is illustrated in Figure 2.10. According to Ross et al. (2021), the phenomenon that is not considered in this illustration

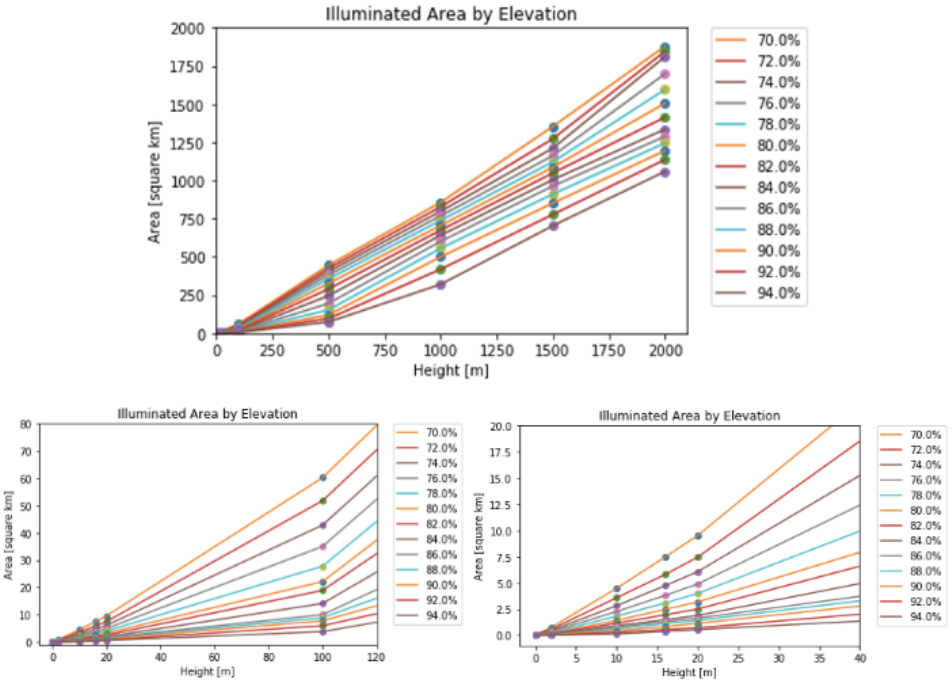

Figure 2.10: The effect of increasing the height of a tower on the available area for different illumination percentages (Ross et al., 2021).

is the effect of overshadowing. Depending on the exact configuration of solar towers, they can block the light for others when they are close together or positioned in the same direction as the light source.

In the near future, towers of 100 meters can be deployed and provide solar power in the order of hundreds of megawatts (Ross et al., 2021). Higher towers up to two kilometres in height can provide even more energy; however, they are considered a subject for future research. As the properties of a tower of 50 metres were already studied in detail by Song, Stark, et al. (2023) and Song, Mikulas, et al. (2023), and the illumination that can be reached is between 70 and 94 %, a height of 50 - 100 meters is assumed. Additionally, a slope of 5 degrees with a possible deviation of 2.5 degrees is assumed for the design location.

2.5. Geology

The Connecting Ridge is the region that connects Shackleton Crater and de Gerlache Crater and lies near the Lunar South Pole. To understand the expected stratigraphy at this location, the events that formed the lunar landscape were investigated.

Kramer (2020) describes the timescale of the lunar stratigraphy as follows: The Pre-Nectarian period is the start of the lunar system, the formation of the moon and the large impacts that continued to reshape the surface. This period is followed by the short Nectarian period, during which 12 basins were formed by a heavy bombardment of the lunar surface. This period ends with the Imbrium impact, starting a period in which volcanic eruptions littered the surface. When volcanism was reduced to only moderate levels in the mare regions, the timescale extends into the Erastosthenian period. The mare volcanism, however, slowly ceased over time, and the surface was bombarded with new impacts. This marks the last, and thus the current, Copernican system.

When trying to place the Connecting Ridge in one of these time periods to determine which stratigraphy can be expected, Gawronska et al. (2020) found that the Connecting Ridge was formed in the same period as de Gerlache crater, which is estimated to be Pre-Nectarian or Nectarian, and is likely the result of the formation of the South Pole-Aitken basin. As stated earlier, this basin is the largest and oldest impact basin from Pre-Nectarian times. The Shackleton crater is assigned an Erasthonian age, and has likely scattered ancient material over the area that is of interest to understand the geologic evolution of the South Pole region.

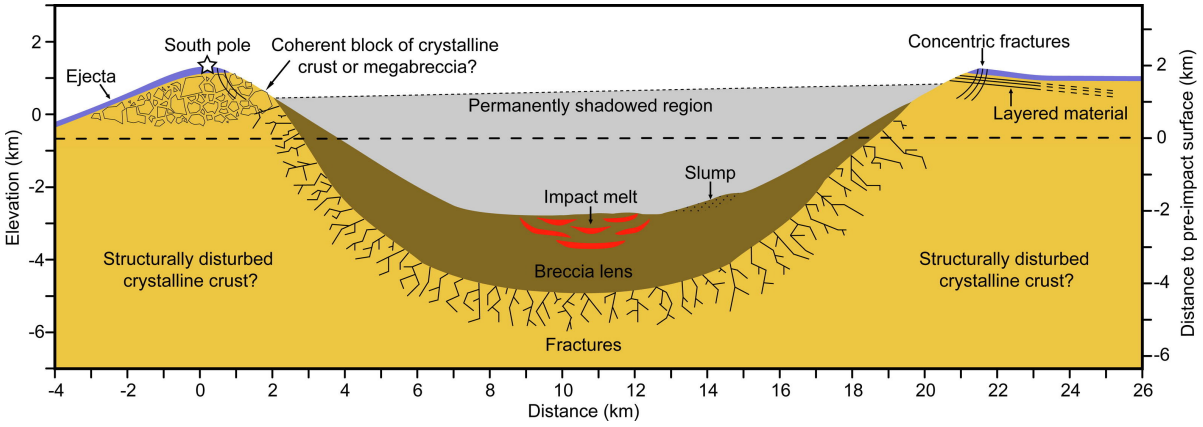

Figure 2.11: The cross section of Shackleton crater that presents the geology of impact craters (Gawronska et al., 2020).

The formation process of craters that determines the types of material found in and around impact craters is described by Gawronska et al. (2020) and Kramer (2020). When a crater is formed by an impact, the older material beneath the impact location is exposed and subjected to high temperatures and pressures, resulting in the creation of new materials from the original ones. The impact also causes ejecta of exposed material to spread around the crater, where new impacts and weathering can transform the rocks. This process can be seen in Figure 2.11. This ancient crustal material in ejecta is of interest for sampling activities during the Artemis era. The build-up of the underground on the lunar surface is therefore caused by the process of impact ejecta being sedimented, combined with new impacts, space weathering and slope processes.

Kramer (2020) summarises that the bombardment process, combined with space weathering, causes 4 groups of rocks to appear on the moon: ”basaltic volcanic rocks, pristine rocks, breccias and impact melts, and lunar soil” (Kramer, 2020). The lunar soil consists of debris smaller than one centimetre, is unconsolidated and covers the lunar surface. This layer is very loose and has electrostatically cohesive properties, causing dust to form on the equipment. The physical properties are uniform, while the chemical composition of individual grains may vary considerably.

According to Slyuta (2014), the impact processes on the moon control the grain sizes that can be observed, as they fragment and agglutinate the lunar regolith and spread it over the surface. As the mean size of found regolith is very small, the regolith is likely more mature and less disturbed. The regolith layer will be thick and mature. Usually, the lunar regolith samples exhibit bimodal size distributions, as a portion of the lunar regolith is mature, another portion is more coarse, and a third portion is fresh ejecta. Therefore, the expected grain sizes are determined by geologic and geomorphologic properties, as well as by the chemical and mineral composition of the regolith at that location. In general, lunar regolith is a poorly sorted sand-aleuritic soil, with particle sizes varying from 40 to 130 μm. The sizes vary by layer, and over depth, they vary due to different regolith layers distributed by different events. This means that even though the regolith is in a deeper layer, the particles may be smaller than those of the soil above. This could lead to weak soil pockets that affect the behaviour of the lunar regolith once loaded. With future data, this phenomenon should be investigated.

At the Connecting Ridge, several factors influenced the formation of the lunar soil. Gawronska et al. (2020) describes that the ejecta of these impacts, along with the corresponding weathering process, resulted in different layers of deposits that were mixed through ballistic sedimentation. These layers were also observed in the walls of the Shackleton crater. A geomorphic map of the current situation at the surface was produced by Bernhardt et al. (2022) and is shown in Figure 2.12. When looking at the geomorphology, the Connecting Ridge area is located on Cratered highlands surface, meaning that the slopes are smaller than 10 degrees and that the area is mostly undisturbed by slope processes, which include tracks of ejecta rolling of slopes, landslides or weathering effects. In the stratigraphic cross-section through the Connecting Ridge produced by Krasilnikov et al. (2024), the layers of interest at Site 1 on the Connecting Ridge are Upper Imbrain craters, with some areas containing satellitic and secondary craters. As stated before, deeper ancient pre-Nectarian material is also present here, caused by impacts later than the impact that created the Amundsen-Ganswindt craters.

One aspect worth noting, indicated by Boazman et al. (2022), is the potential presence of boulders on the Connecting Ridge. This could pose a risk to excavating and introduces uncertainty in assump-

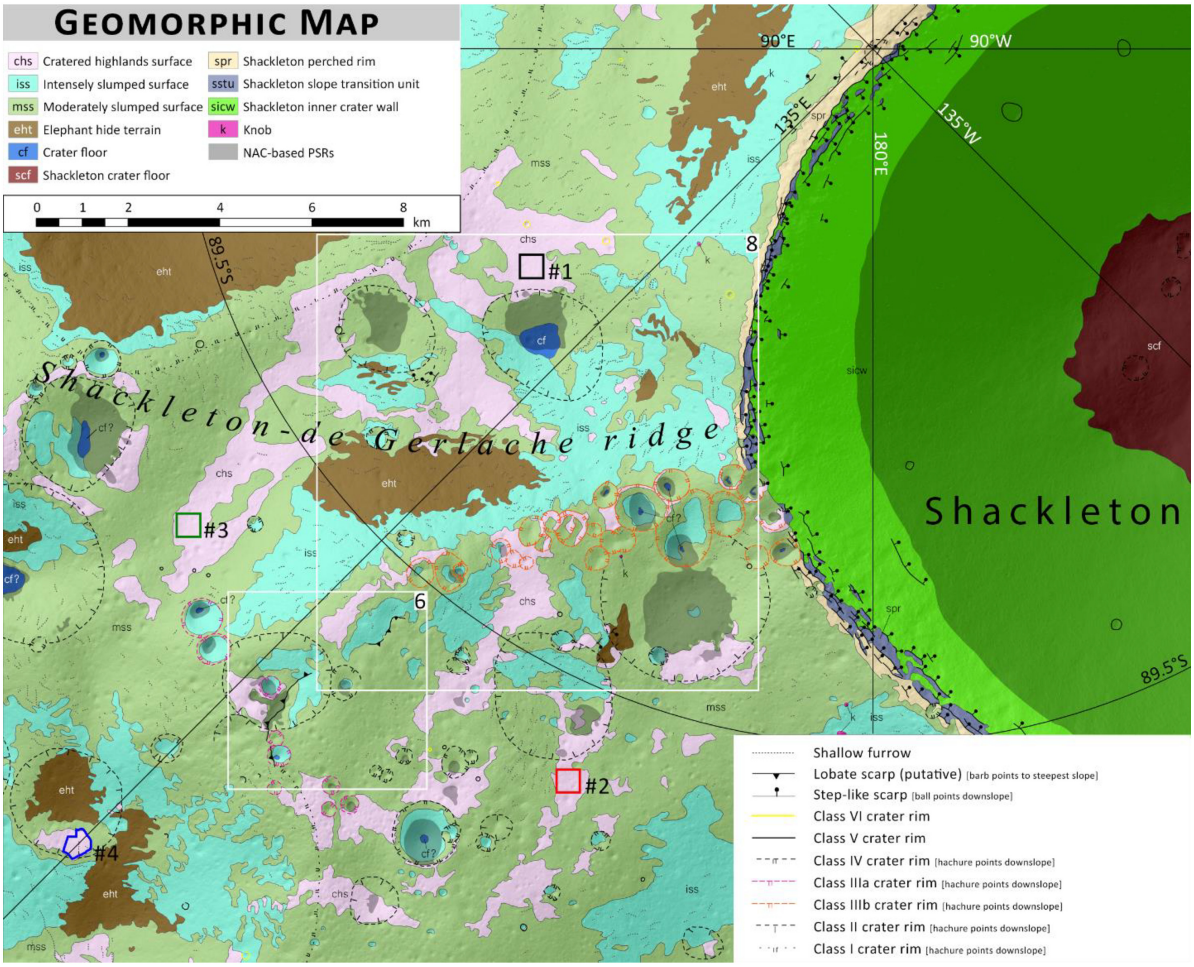

Figure 2.12: The geomorphic map of the Connecting Ridge (Bernhardt et al., 2022).

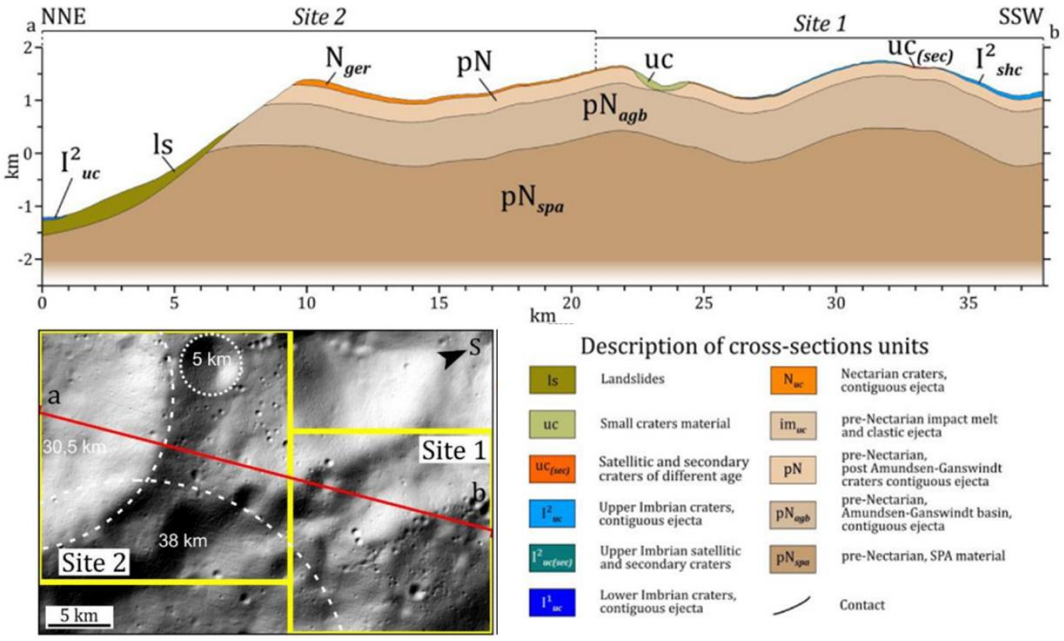

Figure 2.13: The estimated stratigraphy of the Connecting Ridge (Krasilnikov et al., 2024).

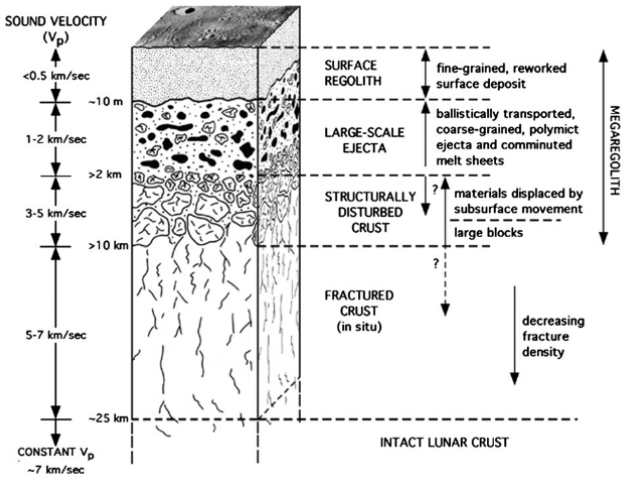

(a) The idealized cross-section of the lunar subsurface (Hiesinger, 2006).

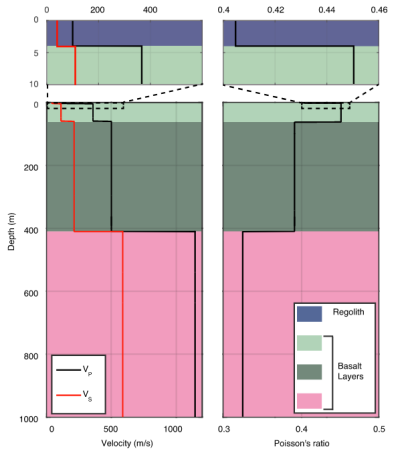

(b) The model developed by Sollberger et al. (2016), presenting the sound velocities and expected Poisson's ratio of the different layers of the lunar crust.

Figure 2.14: Two different models for the layers of the lunar subsurface and their corresponding sound velocities.

tions for modelling the underground. However, the approximate locations of these boulders have been mapped and can, therefore, be considered for more detailed designs in the future. This thesis will not consider the risk of encountering boulders in the underground.

The general estimated build-up of the moon's crust is illustrated in Figure 2.14a. In this idealised cross-section by Hiesinger (2006), the upper 10 meters consists of surface regolith, followed by coarse-grained material containing ejecta and melted material. With a novel waveform analysis technique, Sollberger et al. (2016) identified shear waves in the recorded seismograms to make a model of the lunar crust. The results are visualised in Figure 2.14b. They identify that the upper layer of lunar regolith is only four meters thick, before jumping to a layer of basalt. The sound velocities, however, fall within the same range as the cross-section presented earlier. The surface regolith is a fine-grained material formed by heavy bombardments and weathering (Jaumann et al., 2012). As excavation methods are limited, only the surface regolith and the first basalt layer are reached.

However, data on accurate shear wave velocities of the different layers of the moon is still unknown (Sollberger et al., 2016). These velocities are an important parameter in seismic design, as they determine the depth of the bedrock and thus which layers are affected by seismic excitation. Sollberger et al. (2016) explains that during the Apollo missions, seismic waves were recorded on geophones placed on the lunar surface; although, due to the intense scattering in the near-surface layer of the Moon, it is challenging to accurately identify the exact arrival times. In addition, the available data is measured near Earth, providing limited information on the layer build-up at the Lunar South Pole.

Slyuta (2014) summarises the parameters available for civil engineering purposes. Limited samples were acquired during the Apollo missions, and the results of all tests performed on the material are presented in Table 2.1. However, it is worth noting that these properties are based on samples from a different area of the moon than the future location of the TLT. Therefore, there is uncertainty involved that can be reduced by using data from future Artemis missions.

Kalapodis et al. (2020) state that the relative density $D_r(\%)$, cohesion c' and internal friction angle ϕ' are relevant parameters for civil engineering design, as they represent the shear strength of the lunar regolith. These can be calculated by using the following formulas:

$$\phi' = arctan(\frac{\tau - c'}{\sigma'})$$

$$D_r = \frac{\rho_{max}}{\rho} * \frac{\rho - \rho_{min}}{\rho_{max} - \rho_{min}} * 100\%$$

where:

σ' is the effective normal stress in kPa,

τ is the shear stress in kPa

ρ is the bulk density of the Lunar regolith in kg/m^3,

ρ_{min} is the minimum value of the Lunar regolith's bulk density in kg/m^3,

ρ_{min} is the maximum value of the Lunar regolith's bulk density in kg/m^3,

ϕ' is the internal friction angle in $^\circ$,

D_r is the relative density in $\%$.

Characteristics		Numerical value
Soil density	Surface layer	1.3 g/cm^3
	At the depth of 15.0 cm	1.5 g/cm^3
	At the depth of 60 cm	1.66 g/cm^3
	At the depth of 200 cm	1.9 g/cm^3
Density variation	To the depth of 200 cm	$\rho = 1.92(z + 12.2)/(z + 18)$
Soil porosity	Surface layer 0–15 cm	$52 \pm 2\%$
	At the depth of 30–60 cm	$44 \pm 2\%$
Porosity variation	To the depth of 200 cm	≤40%
Percentage (%) of grains larger than the assumed value for the typical lunar regolith $N_{>d}\% = -23.205\ln(d) + 143.586$	>841 μm	1%
	>250 μm	15%
	>105 μm	35%
	>53 μm	50%
	>20 μm	78%
Soil deformation modulus	Surface layer	15.6–29 kPa
	At the depth of 200 cm	240 kPa
Deformation modulus variation	To the depth of 200 cm	15.6–240 kPa
Poisson ratio of the soil (mean value)	To the depth of 200 cm	0.2
Shear strength of the soil	At the depth of 5 cm	0.1–2.5 kPa
	At the depth of 50 cm	1–3.5 kPa
	At the depth of 100 cm	2–4 kPa
	At the depth of 200 cm	4–8 kPa
Shear strength variation	To the depth of 200 cm	0.1–8 kPa
Cohesion of grains (mean value)	At the depth of 0–15 cm	0.52 kPa
	At the depth of 10–20 cm	0.6 kPa
	At the depth of 0–30 cm	0.90 kPa
	At the depth of 30–60 cm	3.0 kPa
	At the depth of 0–60 cm	1.6 kPa
Cohesion variation	To the depth of 200 cm	0.1–3.5 kPa
Variation of the internal friction angle	To the depth of 200 cm	30°–50°

Table 2.1: The properties from the lunar soil (Slyuta, 2014).

As reported by Slyuta (2014), the specific density of the lunar regolith varies widely depending on the minerals and chemicals present in the sample and directly influences the bulk density. This is also impacted by the porosity. The porosity represents the free space between the grains of the soil and inside the grains, this configuration of pores and particles influences whether the soil is in a loose or a dense state. During the Apollo missions, astronauts left footprints on the lunar surface. In these footprints, measurements were taken on the crater rims and intercrater space to find the porosity. The estimation of porosity is based solely on a one- and 10-cm dip of an astronaut's footprint, and therefore, can only be used as an indicative measurement for deeper layers. More data, preferably in situ measurements, are necessary to determine the proper state of the lunar regolith over depth.

Slyuta (2014) states that the measurements of the bulk density in the Apollo region were made using rovers, by the previously mentioned bootprints of the astronauts, and through an indirect analysis of the indentation left behind by the rover. Additionally, samples were taken to a depth of up to 3 meters to more accurately determine the bulk density values. It was observed that the bulk density increases with depth. From 60 cm, the value stabilises and only increases slightly. Due to the bombardment of the surface with meteoroids, the upper layers are very loose, while the deeper layers get compacted.

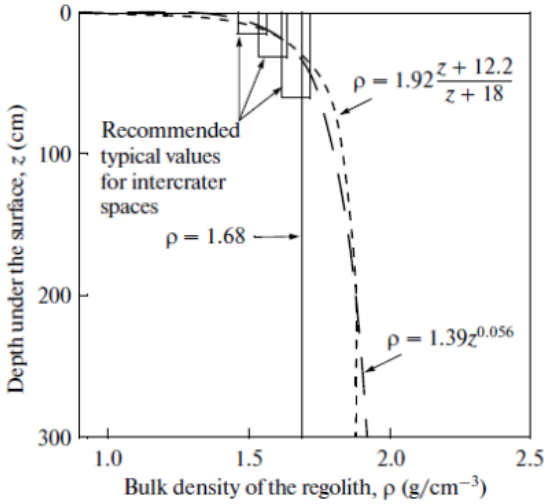

Figure 2.15: The relationship of bulk density and depth for lunar regolith (Heiken et al., 1991).

Increasing the depth, therefore, influences the compactness of the soil, influencing the bulk density and, thus, cohesion and internal friction angle. The effect on bulk density is visualised in Figure 2.15.

Because these measurements are taken from a location other than the Lunar South Pole, it is difficult to determine the expected range of bulk density on the Connecting Ridge. As the Connecting Ridge is likely Pre-Nectarian, the density of deeper layers could be higher. However, later impacts could have scattered new material over the Ridge, leaving it in a looser state.

Regarding the strength parameters of lunar regolith, Knez and Zamani (2021) notes that similar cohesion values are found in most soils on Earth, except for those with high cohesion, such as clays. The average internal friction angle is higher than that of soils on Earth due to the formation process caused by meteorite bombardment, which produces sharper grains and results in a higher maximum shear stress.

Slyuta (2014) summarises that astronauts experienced the cohesion of the lunar regolith, which tends to stick together in clumps but is easily crushed under weight. When the lunar regolith is in a loose state, the cohesion is insignificant, and the internal friction angle similarly so. In a denser state, cohesion forces increase, and the internal friction angle increases as the soil becomes more compact, with soil particles closer together and experiencing greater friction. Under shear, the bulk density increases when normal pressure is applied above 10 kPa, and the lunar regolith reaches a denser state, thereby increasing the strength parameters of the soil and, consequently, the shear strength of the lunar regolith.

The values for cohesion and internal friction angles presented in Table 2.1 are, according to Slyuta (2014), the result of measurements performed on the lunar surface by the astronauts. With rovers, hand core tube sampler, manual penetrometer and self-recording penetrometers, cohesion values of up to 1.3 kPa and internal friction angles of 46.5 ° were measured by the Apollo 16 crew. A hole was drilled to a depth of 218 cm, and the soil barely crumbled due to the cohesion of the lunar regolith and the high friction angle. It can be concluded that the values depend on the location and depth at which the sample is taken. In Apollo missions, penetrometers were used to reach even higher depths.

Knowledge about the deformation is necessary to evaluate the impact of placing a load on the lunar surface. Slyuta (2014) gives a summary of relevant deformation parameters. The Poisson's ratio was measured by Luna-16 and Luna-20, both of which contained Coulomb's instruments. The results were a value of 0.31 and 0.2. Usually, a value of 0.2 is estimated. A flat punch test was performed on samples taken by the Luna-16 spacecraft, and it was found that the resisting force increased when deeper, denser lunar regolith was encountered. As is known, the upper layer of the lunar regolith is very loose and therefore has a very low modulus of deformation, ranging from 15 to 29 kPa. In deeper layers, as the bulk density increases, the modulus of deformation increases rapidly to around 240 kPa at depths of 30-60 cm. Other estimates of the modulus of deformation are based on the footprints of the astronauts and the impression depth of the support of the lunar module.

The dependence on the state of the soil similarly holds true for the compressibility coefficient of the lunar soil. When testing samples from Luna-16 and later Luna-20, Slyuta (2014) reports that the

porosity initially decreases before the soil particles break and move closer together, transferring loads through the contact points. Eventually, the maximum compaction is reached, and the soil compressibility becomes very low. In the Apollo 12 mission, the compressibility coefficient for samples returned to Earth ranged from 0.01 to 0.11. The recommended value to take for design is 0.05 (Heiken et al., 1991).

Considering the bulk density of the lunar regolith at the Connecting Ridge is unknown, the deformation modulus may differ from the values mentioned here. A deformation modulus of around 250 kPa is deemed very low for soils on Earth. The loads of a TLT with a foundation are significantly larger than those of a lunar module, which is designed to be as lightweight as possible for launch from Earth. With a deformation modulus this low, a considerable risk of settlements is present. Additionally, the potential presence of loose or more weathered regolith pockets in the subsurface can result in differential settlement. As the upper layers have even lower deformation moduli, it is recommended to remove them or provide proper densification before construction.

2.6. Seismicity

Between 1969 and 1972, a seismic network was active at the lunar surface during the Apollo missions (Nakamura et al., 1982). Before then, it was theorised that the Moon lacked significant lunar tectonism since no surface features could indicate tectonic activity (Latham et al., 1971). However, when the seismic stations were active, over 12000 seismic events were recorded (Nakamura et al., 1982).

Nunn et al. (2020) describes the four different experiments were performed during the Apollo missions. The Passive Seismic Experiment (PSE) used 3-component displacement sensors and a vertical component sensor to capture natural seismic events. The Active Seismic Experiment (ASE) utilised a small array of geophones, combined with controlled seismic sources in the form of explosives. With the propagation of the waves through the subsurface, it was used to evaluate its structure. The same geophones were used in the Lunar Seismic Profiling Experiment (LSPE), combined with eight explosive packages placed by astronauts. The goal was to explore the subsurface even deeper than with the ASE. The Lunar Surface Gravimeter (LSG) was supposed to be used for observing gravitational waves. However, the instrument was unable to generate valuable data due to a miscalculation. The recorded natural events exhibited slight variations in sampling rates. This was due to the temperature variations present on the Moon. The artificial impacts from the explosives and the measurements when the Apollo 12 Lunar Module ascended, combined with the impact of Apollo 13 Saturn boosters, yielded a reference point to reconstruct the time of seismic events.

Latham et al. (1970) and Oberst and Nakamura (1992) found that the data suggest that the seismic activity on the Moon is significantly different from that on Earth. The activity is much lower, events have a very long duration, and the attenuation is much lower than on Earth. It takes time for the moonquake to reach its peak, and then it undergoes an extremely slow decay. This likely means that the energy from a moonquake can spread over a larger area from the epicentre. Another notable difference compared to earthquakes is that the seismic waves experience intense scattering, in particular near the surface. These results indicate that the Moon's seismic energy release is significantly lower than Earth's. Goins et al. (1981) concluded that the seismic character of a planet appears to be controlled by its state, which is related to its size and the distribution of temperature in the subsurface. The lithosphere of the Moon is thick compared to the Earth, presumably preventing strong motions. According to Oberst and Nakamura (1992), the prolonged duration of a moonquake would result in slower dispersion, potentially reducing damage compared to earthquakes of similar magnitude. The scattering in the subsurface also prevents the propagation of surface waves, which are usually responsible for the most earthquake damage. This could reduce the hazard of the seismic activity on the Moon. However, there is no evidence to conclude whether these effects reduce the seismic impact on lunar structures.

2.6.1. Types of moonquakes

From the recorded seismograms, four distinct types of seismic activity were identified that were not artificially created by humans: meteoroid impacts, thermal moonquakes, deep moonquakes and shallow moonquakes (Nakamura et al., 1982). Their signals show distinct features, and four of them can be observed in Figure 2.16.

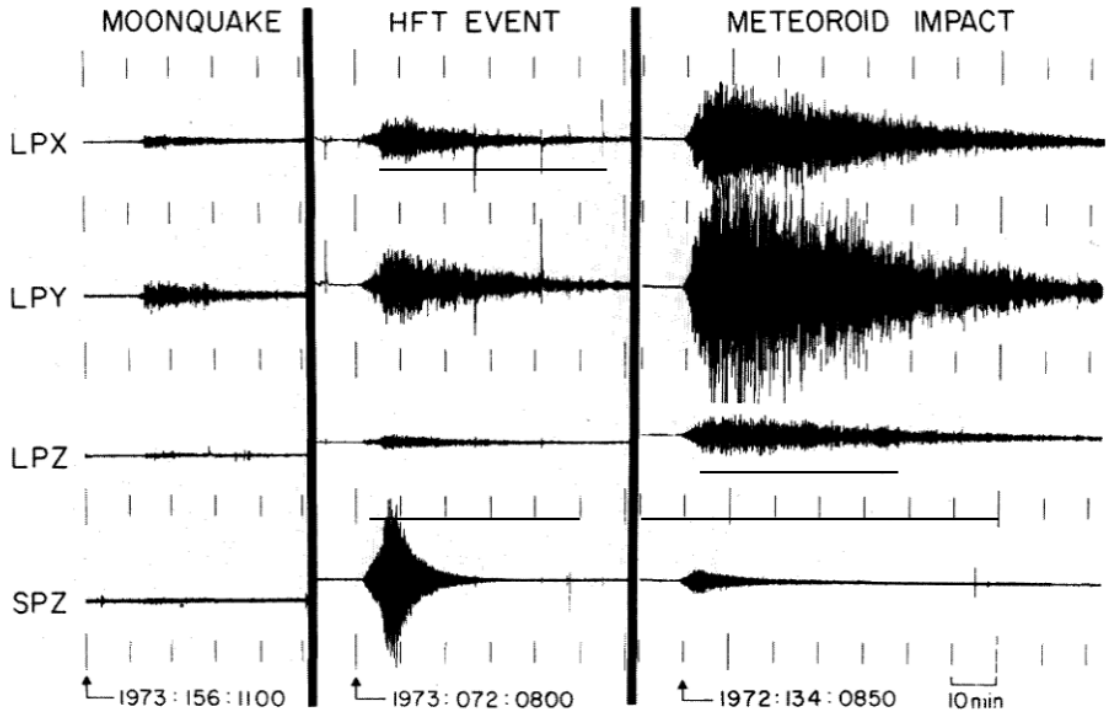

Figure 2.16: The recorded types of seismic activity. The LPX, LPY and LPZ are the three long-period instrument orthogonal components, where the SPZ is for vertical components of the short-period instrument. On the x-axis, the duration of the moonquake event is described (Nakamura, 1977).

Meteoroid impact
The lack of atmosphere makes meteoroid impacts more frequent on the Moon than on Earth (Kalapodis et al., 2020). Nakamura et al. (1982) reports that their origin is from outside the lunar environment, making it an essential source of information for the interplanetary environment. The seismic data show clustering, which is correlated with known meteor streams. In a review by Kalapodis et al. (2020), it is reported that frequent impacts are associated with small meteoroids, whereas rare events involve large mass meteoroids. They are important hazards for lunar infrastructure. However, large meteoroids are hard to predict since they do not correlate with known meteoroid showers. The stochastic nature of modelling meteoroid impact is deemed out of scope for the duration of this project.

Thermal Moonquakes
These moonquakes are very small events theorised to be caused by temperature variations (Nakamura et al., 1982). Kalapodis et al. (2020) report that they are correlated with diurnal changes, meaning the cycles of day and night on the Moon and the corresponding movement of regolith. Due to their small size, these types of seismic events are unlikely to pose a threat to infrastructure.

Deep Moonquakes
The most recorded seismic events during the Apollo experiments have been labelled deep moonquakes (Nakamura et al., 1982). Latham et al. (1971) states that they exhibit low-stress levels and are, therefore, of small magnitude. They are correlated with the generation of tides caused by the relative motions of the sun and Earth (Latham et al., 1970, 1971; Nakamura et al., 1982). Their sources are present at large depths in the interior of the Moon (Latham et al., 1971; Nakamura et al., 1982). Their exact mechanism remains unknown (Lammlein et al., 1974; Latham et al., 1970, 1971; Nakamura et al., 1982), although many theories exist. Since these moonquakes are only of small magnitude, they are not expected to influence early lunar infrastructure as much as shallow moonquakes.

Shallow Moonquakes
Among all the measured signals during the Apollo seismic experiments, the seismic events with the highest frequency are referred to as shallow moonquakes. In earlier years, they were described by

Nakamura (1977) as high-frequency teleseismic (HFT) events. In contrast to deep moonquakes, they show no correlation with tidal events. They are rare compared to other seismic events and appear to originate from a finite shallow depth. Still, their exact origin is complex to determine due to the intense scattering of the seismic waves. They are likely tectonic in origin, occur from finite depths and exhibit similarities to intraplate earthquakes (Nakamura et al., 1979; Nakamura, 1982). The stress drops of the most significant events measured are estimated as $\delta\sigma$ > 100 MPa with corresponding body wave magnitudes m_B > 5.5 on the Richter scale (Oberst, 1987).

The exact origin of shallow moonquakes is still a topic of research today. Gillet et al. (2017) concluded that the source of shallow moonquakes can be found at 50 km depth $\pm$ 20 km and are explained by fractures in the interior of the Moon, located in the mantle and crust. However, the exact location of the boundary between these layers is uncertain. Current velocity models remain divided on the interior and number of layers of the Moon, and new theories are still being developed in the modern age (Gillet et al., 2017; Heffels et al., 2017; Nunn et al., 2020). Another theory uses an origin outside of the Moon itself; the passage of nuggets of strange quark matter could induce shallow moonquakes (Frohlich & Nakamura, 2006). A recent paper by Onodera (2024) theorised fault activities around rifts filled with lava driven by the contraction of the entire Moon. Sources near the surface would explain other shallow quakes. An interesting observation from this dataset, which contains more shallow moonquake events, is a distinct regional pattern, suggesting that the southern part of the Moon is less seismically active than the northern part. The hemisphere where Artemis Base Camp will be located might result in a more peaceful seismic environment. A lack of data on these shallow events prevents the determination of the exact cause and corresponding mechanism. It also prevents conclusions on the precise location of focal depths and whether there is a difference in seismicity between the north and south of the lunar surface.

In literature, these shallow moonquakes are considered a threat to lunar infrastructure (Goins et al., 1981; Oberst & Nakamura, 1992). Even with limited measurements, many moonquakes have been detected and identified, and even more events are currently being found from the Apollo experiment data using modern techniques (Knapmeyer-Endrun & Hammer, 2015; Onodera, 2024). This suggests that the Moon might even be more seismic than believed (Onodera, 2024). Due to the limited recording time of the Apollo experiments, shallow moonquakes could contain even higher frequencies than already measured. When calculated to a practical value for lunar infrastructure, Oberst and Nakamura (1992) suggested that the structure likely experiences a shallow moonquake with a body wave magnitude m_B > 4.5 on the Richter scale within 100 km, once every 400 years. In the current era, this would be the same as a ground motion exceeding 10% probability in 50 years or otherwise described as an earthquake with a 475-year return period (Kalapodis et al., 2020). This thesis, therefore, takes a shallow moonquake event with a 475-year return period as a governing design situation. For future projects, more data will need to be gathered during the Artemis missions to reveal the exact nature and source of shallow moonquakes.

2.6.2. Seismic Hazard

The design philosophy behind earthquake-resistant design standards is explained by Paul and Wamelink (2017) and is based on defining a seismic hazard. The area where a structure is located, along with the intensity and magnitude of an earthquake, determines how to define this probability. The intensity of an earthquake provides a measure of the consequences in terms of loss of life, damage to structures, or environmental damage. The magnitude of an earthquake refers to the amount of energy released during the earthquake. The definition of seismic hazard becomes: ”The probability that an earthquake will occur in a given geographic area, within a given window of time and with ground motion intensity exceeding a given threshold.” (Paul & Wamelink, 2017). A design parameter often used to represent an earthquake is the Peak Ground Acceleration (PGA), which is the amplitude of the maximum acceleration measured by an accelerometer. The Eurocode utilises PGA values and seismic hazard to define steps for calculating and modelling the response of structures to seismic loading, as well as measures to enhance earthquake resistance. Next to the seismic hazard and PGA values, the allowed performance level and limit state of the structure need to be defined, as they relate to the amount of damage and risk of experiencing this damage level.

Paul and Wamelink (2017) further note that the most damaging factor for structures is usually the horizontal component of the seismic load. This load needs to be guided through the structure; it is therefore preferred that the structure contains redundant load paths. The structure has its own natural

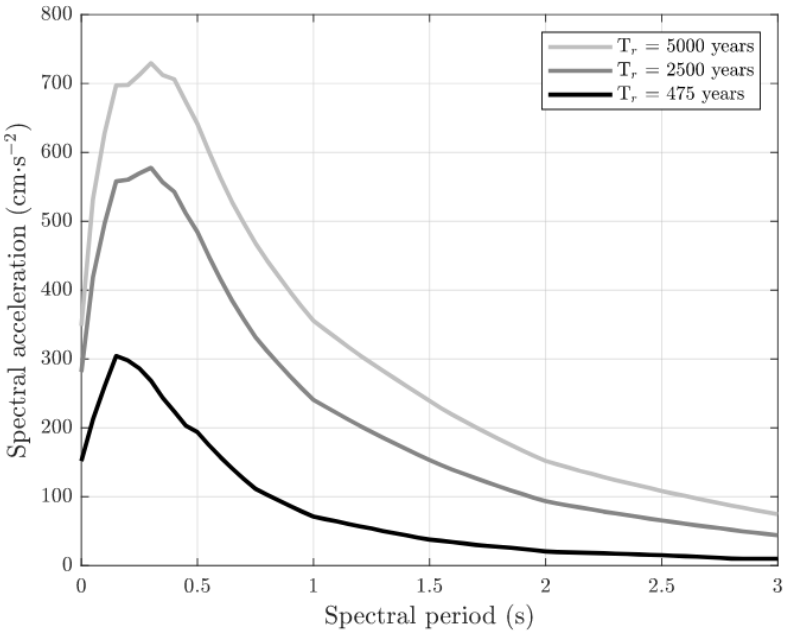

Figure 2.17: The Uniform Hazard spectra for different return periods at the Apollo 17 landing site from a preliminary Probabilistic Seismic Hazard Analysis (Ruiz et al., 2022).

frequency and response spectrum, meaning it behaves differently at different frequencies of dynamic movement and can even resonate at a frequency close to its natural frequency.

One of the first steps, according to Paul and Wamelink (2017), to take is to obtain information about the site's response to seismic movement. Softer soils can, for example, enhance the amplitude of the seismic signal. On the Lunar South Pole, however, there is no data available on the site's response, and therefore, applying design rules becomes difficult. A Probabilistic Seismic Hazard Analysis (PSHA) was performed by Ruiz et al. (2022) to obtain the PGA value associated with a shallow moonquake event of different return periods. As the origin of moonquakes remains unknown, it is unclear whether moonquakes are caused by tectonic movements. It was assumed that the source of the shallow moonquake events was a fault represented by the Lee-Lincoln lobate scarp in Tarus Littrow Valley, located at the Apollo 17 site, where measurements of shallow moonquakes were obtained. In addition, they assumed a fault dip angle and depth.

However, Ruiz et al. (2022) reports that due to the lack of data on shallow moonquake events and the seismicity on the Moon, the Ground Motion Prediction Equations (GMPE) necessary for performing a PSHA on the Moon do not exist. A GMPE can be used to input possible combinations of magnitude and distance from the seismic source in the study area to predict mean values of the intensity measure parameter for different spectral periods. They require input parameters related to the site and source of the quake, as well as data on the magnitude of the events, and are relevant for different spectral periods. To mitigate this lack of data, various developed GMPEs for the Earth were combined for different magnitudes, distances, and spectral periods. Synthetic values of PGA were generated based on the few measurements of shallow moonquake events, as the measured PGA values were only measured at large distances from the assumed source.

With this information, Ruiz et al. (2022) obtained deterministic values of PGA associated with specific return periods, as well as the events that cause a certain hazard level by deaggregating the result. For different spectral periods and rates of occurrence, PGA values were obtained to generate a Uniform Hazard Spectrum, which can be used to identify the hazard posed to the TLT structure and its foundation. The Uniform Hazard Spectra that was obtained is shown in Figure 2.17.

2.7. In Situ Resource Utilization

Wu et al. (2024) reports that developing construction materials that can be locally produced and withstand the lunar environment is a crucial aspect of designing lunar infrastructure, especially since con-

Chemical oxides (wt%)	Apollo 11 (Mare)	Apollo 12 (Mare)	Apollo 14 (Highlands)	Apollo 15 (Highlands)	Apollo 16 (Interface Area)	Apollo 17 (Interface Area)
SiO_2	42.15	46.30	48.10	46.95	45.26	40.95
TiO_2	7.80	3.20	1.70	1.60	0.66	7.61
Al_2O_3	13.65	13.35	17.40	12.70	25.48	12.78
Cr_2O_3	0.30	0.38	-	0.47	0.25	0.46
Fe_2O_3	-	-	-	-	-	-
FeO	15.55	16.30	10.40	16.29	6.58	15.76
MnO	0.20	0.22	0.14	0.22	0.34	0.21
MgO	7.85	9.70	9.40	10.75	6.19	9.99
CaO	11.95	10.65	10.70	10.49	15.17	11.03
Na_2O	0.49	0.46	0.70	0.33	0.45	0.32
K_2O	0.13	0.24	0.55	0.09	0.13	0.08
P_2O_5	0.08	-	0.51	0.16	0.11	0.06
S	-	-	-	0.07	0.07	0.12
LOI	0.12	-	-	-	0.07	-

Notes: "LOI" denotes loss of ignition, and "-" denotes absence of the substance detected.

Table 2.2: The chemical composition of the lunar regolith samples taken during different Apollo missions at locations in the highlands and at mare areas (Zarzycki & Katzer, 2019).

struction materials on Earth usually incorporate water as the binder, a scarce resource on the Moon and contained in ice in PSRs. Different techniques were developed to use lunar regolith as a resource and utilise special materials to address the lack of water. This section explores the techniques available for constructing on the moon and the materials made from local resources that can resist the lunar environment.

Toklu and Akpinar (2022) concluded that the lunar regolith is the most abundant resource on the lunar surface. Depending on whether you are in a mare area or on the ancient highlands, it contains basalt rich in iron and titanium or anorthosite and feldspar. Regolith can be used as aggregates or to extract necessary elements for space concrete (Wu et al., 2024). The chemical compositions of the samples taken during Apollo missions are visible in Table 2.2.

2.7.1. Available materials

Wu et al. (2024) summarises that any used material must withstand large thermal fluctuations and maintain its physical properties. The temperature that the foundation material needs to withstand is directly related to the temperature of the surrounding soil and, thus, the lighting conditions. As is known, the lighting conditions vary considerably over the lunar year. Therefore, these materials also need to withstand thermal fatigue over long periods of enduring these fluctuations. Several types of materials are available that can withstand the lunar environment and are produced by ISRU techniques. These are described below.

Space concrete

Wu et al. (2024) explains that one material of interest is space concrete. Making standard concrete on the Moon is not feasible. Since water is scarce, new types of concrete using local lunar materials with alternative binding agents that require less or no water have been developed. These concrete types do not require high energy or temperatures for manufacturing and can be made from local lunar materials. They have high compressive strength and durability and are engineered to withstand the local environment. The low gravity and vacuum conditions, for example, alter the processes to make concrete

and, therefore, influence the final properties, whereas radiation after casting can change molecular structures.

There currently exist six different types of space concrete that can be produced, taking normal concrete using Portland cement as a reference point.

- Calcium aluminate concrete is described by Wu et al. (2024) and is bonded together by a high-temperature process with limestone and bauxite. It uses less water than traditional concrete but needs careful water management. It hardens swiftly, is chemically resilient and durable, has high initial strength and can withstand extreme temperature variations. However, this type of concrete still requires water. Anorthite, which is aluminium-rich, can serve as a local resource for this cement. However, this requires a high amount of energy to process.

- Sulfur concrete can be produced without water (Wu et al., 2024), utilises sulfur as a binding agent (Gracia & Casanova, 2012; Grugel & Toutanji, 2008), has robust mechanical performance and can incorporate fibres and additives (Meyers & Toutanji, 2007). Meyers and Toutanji (2007) found that metal fibres can be incorporated to increase compressive strength and ductility, while glass fibres can heighten flexural-tensile strength. Wu et al. (2024) reports that sulfur can be extracted from sulfide materials, such as pyrite, using heat. Aggregates, like basalts, can be obtained from local regolith. However, physical and chemical properties can change significantly in vacuum conditions and extreme temperatures, making it an unstable material in the lunar environment.

- Ockleston (1950) found that sorel concrete requires little water and is composed of magnesium oxide and magnesium chloride. Concrete made with this alternative binding method showed robust mechanical properties. Wu et al. (2024) adds that it is resistant to corrosion, energy-efficient, and thermally stable. An experiment by Osio-Norgaard et al. (2021) confirmed that sintering can be used to produce this concrete, even recovering the used water in the process, and that this concrete is suitable for 3D printing techniques.

- Magnesia silica concrete was investigated by Scott and Oze (2018) does not use water, but a reaction between MgO and SiO_2 to set and has a similar microstructure compared to using Portland cement. It is mainly a material of interest for Martian infrastructure, as this type of concrete is very compatible with the resources available on Mars.

- Polymer concrete is based on the principle of binding aggregates with polymers (Ferdous et al., 2020). Studies by Agavriloaie et al. (2012), Jung et al. (2014), and More et al. (2021) concluded that these polymers enhance the compressive strength, durability and resistance against environmental factors. However, it is expensive and difficult to manufacture and cure on an extraterrestrial site (Wu et al., 2024).

- Geopolymer concrete, according to Wu et al. (2024), uses a reaction between silicates and aluminates to bind the concrete together. Both mineral types are readily available in lunar regolith in the shape of olivine, pyroxene and silica. It has a low carbon footprint, is eco-friendly and requires little water. The chemical stability of this concrete is excellent (Xiong et al., 2022). In addition, Pilehvar et al. (2020) demonstrated that it can incorporate superplasticisers for workability, unlocking the potential for 3D printing technology with this type of concrete.

Wu et al. (2024) conclude in their review on space concrete that geopolymer concrete is best suited for building in the lunar environment. It cures rapidly and has low water demand. It is chemically stable and has high mechanical strength. The most suitable concrete depends on the exact usage in the extraterrestrial environment. When using 3D printing technology, Sorel concrete also appears to be a good candidate. However, the mechanical properties of this type of concrete are less advantageous than those of geopolymer concrete. Therefore, this thesis assumes the use of geopolymer concrete as a viable material option.

Sintered materials

Sintering can be used to create building materials (Cheng et al., 2024). Kalapodis et al. (2020) explains that in this process, a porous material is heated, causing its particles to approach their melting point and bind together. Different sintering methods exist, namely Solar / Laser / Melt Sintering and Microwave Sintering (Mueller et al., 2016). Sintering techniques enable the production of regolith bricks or similar

regular shapes (Cheng et al., 2024), unlocking construction components for lunar construction. These processes can also be used to obtain fibres and glass materials (Cheng et al., 2024).

Metals / alloys
Cheng et al. (2024) reports that lunar regolith contains common metal materials, including Aluminium, Magnesium, Iron, and Titanium. Researchers are exploring the use of pyrolysis, electrolysis, and chemical reduction by microorganisms to extract these metals from the lunar surface. These metals can be used for construction materials or structural components.

Cast basalt
Instead of binding material with additives and sintering techniques, Ruess et al. (2006) states that cast regolith can be obtained by simply melting regolith and controlling the cooling process. This process is improved by the vacuum conditions on the moon. After cooling, the cast basalt has high compressive strength, and when subjected to tensile forces, it exhibits moderate tensile strength. After casting, however, it becomes impossible to process due to its hardness. Moreover, it becomes a brittle material, thus requiring tensile reinforcement. This casting method enables the creation of structural elements resistant to dust and corrosion. The downside of this method is the high energy cost of melting regolith.

Fabricating basalt fibres can be of interest for serving as reinforcement in potential structural components and enhancing the feasibility of cast basalt components (Zhang et al., 2023). Fibres made from various materials have also been manufactured from local lunar material and can enhance tensile resistance (Becker et al., 2019; Xing et al., 2020).

2.7.2. Construction techniques

Currently, four different types of construction techniques are being investigated for extra-terrestrial construction and exploration and are discussed below.

3D printing technology
This Additive Manufacturing (AM) technique uses local material combined with additives to 3D print constructions (Kalapodis et al., 2020). Using the precision of 3D printing, it is possible to print objects of intricate shapes from tens of meters to a few micrometres (Cheng et al., 2024), minimising waste and maximising efficiency (Wu et al., 2024). In addition, Wu et al. (2024) states that it is energy-efficient, can produce stable constructions, and is resilient against the lunar environment. Several new developments are concrete printing (Cheng et al., 2024), contour crafting (Cheng et al., 2024; Wu et al., 2024; Zhang et al., 2023), D-Shape printing (Wu et al., 2024; Zhang et al., 2023) and powder binder jet printing (Cheng et al., 2024; Wu et al., 2024). A counter-crafted structure can be seen in Figure 2.18a. Simulants that have rubber-like properties that can be 3D printed have been developed by Jakus et al. (2017) and could be of interest for damping the effect of moonquakes. However, challenges regarding 3D printing in a microgravity situation and the viability of getting the right equipment to the lunar surface remain (Cheng et al., 2024; Wu et al., 2024; Zhang et al., 2023).

Automated robot technology
Cheng et al. (2024), El Samid et al. (2008), Kalapodis et al. (2020), and Wu et al. (2024) explain that robots are a solution for construction in challenging environments. As mentioned above, robots can be used to apply 3D printing technologies. In addition, excavation or assembling premade construction components could be done robotically. When examining premade construction components, Cheng et al. (2024) and Kalapodis et al. (2020) note that interlocking components offer significant flexibility. Structures made of these use the principles of topology to make various shapes from prefabricated blocks . An example of a structure using these blocks is visualised in 2.18b.

Automated filling and stacking of regolith bags
This innovative technique, described by Cheng et al. (2024), is a recent development in which bags are filled with regolith and stacked to form a structure, as illustrated in Figure 2.18c. It does not require any water and can utilise raw materials, making it a highly energy-efficient construction method. However, the structures have low strength and require complex operations to construct.

(a) A contour crafted landing pad using 3D printing technology (ICON, 2021).

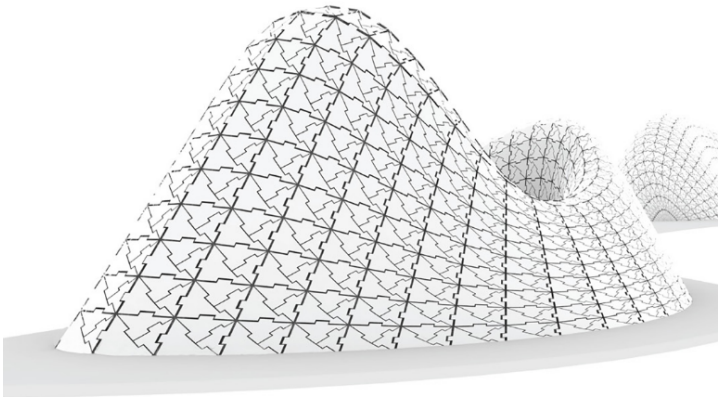

(b) A structure made from interlocking tiles that could be assembled using automated robot technology (Yazici, 2018).

(c) A small arch structure made from regolith bags (Bao et al., 2024).

Figure 2.18: Different construction technologies that can be applied on the lunar surface.

Hybrid construction technology
This construction technology encompasses all possible combinations of the above-mentioned technologies (Cheng et al., 2024). Utilising the benefits of multiple technologies can advance the design of extraterrestrial structures and present new challenges.

2.8. Excavation and drilling possibilities

In the lunar environment, excavating becomes difficult since the methods used on Earth are no longer sufficient and feasible. Limited data is accessible from earlier geotechnical experiments on the behaviour of lunar regolith when excavated. As described in section 2.5, the lunar regolith first consists of a loose layer and then gets denser with depth. This, in turn, means that going deeper into the soil will require more energy and time, generate more dust, and necessitate more powerful equipment. Therefore, one requirement would be to excavate as little material as possible. Since completely avoiding excavations will likely be impossible, the current possibilities need to be investigated. According to Zacny (2012), the development of these excavation or drilling methods faces significant challenges, such as transporting large instruments to the moon and the instruments' capabilities to excavate in vacuum and low-gravity conditions. In this section, the excavation and drill possibilities and limitations of the current state-of-the-art methods were investigated.

2.8.1. Excavators

Hilburger (2024) states that due to the lunar environment and the limitations of transporting large equipment to the moon, special excavators are being developed. These excavators will be used for ISRU-based resource production, regolith manipulation and site preparation. The current goal is to excavate to a depth of three meters, although current concepts attempt to reach a minimum excavation threshold of one meter. Jayathilake et al. (2022) concludes that in general, the regolith is well-defined up to a depth of three meters; however, due to the abrasive nature of dense regolith, economically feasible excavations would be limited to 30 cm unless new developments in excavation techniques are made. This thesis assumes boundary conditions for excavation of one meter to a maximum depth of three meters, which is considered a feasible excavation depth in the near future.

2.8.2. Drills

Drilling techniques are investigated for applications such as water extraction, sample acquisition, mining, and anchoring (Knez & Zamani, 2021). Wang et al. (2024) explains that drills can penetrate the hardest rocks on Earth and could pose an advantage in penetrating the highly compacted lunar regolith at depth. However, they are unsuitable for excavating large quantities and cannot take advantage of the same reaction force on the drill bit that Earth's greater gravity provides. Furthermore, the stability of the drill rig itself in microgravity also needs to be governed (Wang et al., 2024; Zacny, 2012). In addition, Knez and Zamani (2021) reports that the limited power available on the lunar surface necessitates the design of drilling tools with very low power demands that can be supported by solar energy and can deal with the abrasive nature of lunar soil that can quickly cause wear on the drill. Therefore, drilling at extra-terrestrial locations remains an important research topic. The deepest hole to date was drilled to a depth of 2.92 meters (Heiken et al., 1991), highlighting the current limitations of drilling techniques on the lunar surface. It is mentioned that increasing the drilling depth will increase the risk of encountering large ejecta, a risk that needs to be considered. In the future, it may be possible to drill 5-10 meters into the lunar regolith.

Drill fluid is used to stabilise the holes in the soil and remove cuttings during auger drilling on Earth. This material is unavailable on the lunar surface, and in addition, the lack of atmosphere and the varying temperatures will cause the drilling fluid to behave differently. However, it is noted that due to the cohesion and large friction angle of the lunar regolith at depth, drilling fluid can be avoided, as astronauts observed during the drilling of a 218 cm deep hole that the soil barely crumbled (Slyuta, 2014). This gives rise to the option of filling the borehole with material to create a simple pile foundation. In the design, auger-drilled pile foundations may be an option when it is assumed that this technology is available.

2.9. Anchoring possiblities

Anchors are of potential interest for stabilising infrastructure and preventing deep excavations on extraterrestrial surfaces. When looking at literature regarding anchoring on the lunar surface, the focus lies on the anchoring of rovers or surface-based landers (Ebert & Larochelle, 2016). Four types of anchoring systems have been investigated: Helical anchoring (Figure 2.19a), suction drilling (Figure 2.19b), circular wedge anchoring (Figure 2.19c), and claw anchoring (Figure 2.19d) (Kalapodis et al., 2020; Knez & Zamani, 2021). These are shown in Figure 2.19.

Suction drilling and claw anchoring are small-scale experimental anchors, where their usage focuses on drilling with the aim of sampling (Faßwald et al., 2012) or providing stability for rovers or landing systems (Ebert & Larochelle, 2016). These systems, therefore, are brought from Earth and do not comply with the ISRU principles required for long-term infrastructure on the lunar surface. The helical anchors and circular wedge anchors are currently Earth-produced as well. With 3D printing techniques, these anchors could potentially be produced using ISRU material.

Considering anchoring used in, for example, deep excavations, the anchors rely on the shear force between the grout and the soil. As stated before, grout is unavailable on the lunar surface, and its behaviour in microgravity and under lunar temperature conditions is unknown. The proposed method by Faßwald et al. (2012) to use a suction drill using cold gas for ejecting debris on the JSC-1A simulant has been experimentally tested. This, however, is only at a small experimental scale; the true power requirement and gas supply necessary for a relatively large suction anchor for a TLT are unknown. Moreover, the grain size distribution at the Connecting Ridge is unknown; therefore, it cannot be stated that the cold gas is capable of transporting the soil particles.

When considering helical anchoring and circular wedge anchoring, both types require the soil to resist the pulling force exerted by the anchor. The shear forces are generated through the shear strength and the weight of the soil of the wedge. It is known that the internal friction angle of lunar regolith is quite high, having a positive effect on the maximum pull-out force. The microgravity, however, will reduce the weight of the soil. The circular wedge anchoring is in development for larger infrastructure; experimental tests will need to determine if this anchoring method is sufficient on Earth to translate the results to the lunar environment.

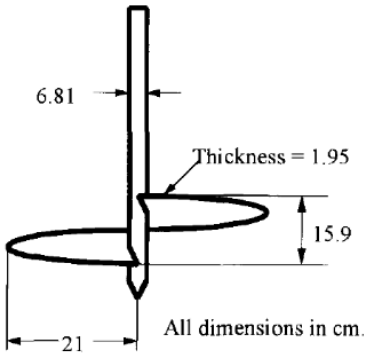

(a) The helical anchoring method developed by Klosky et al. (1998).

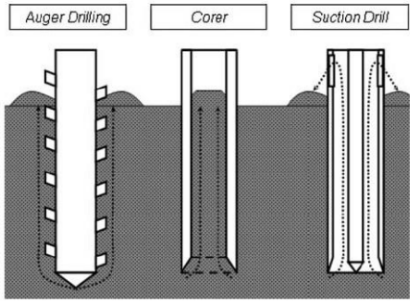

(b) The suction drilling principle (Faßwald et al., 2012).

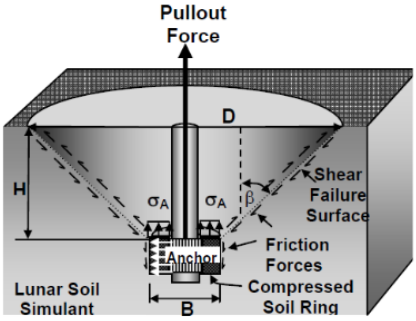

(c) Circular wedge anchoring (Chang et al., 2010).

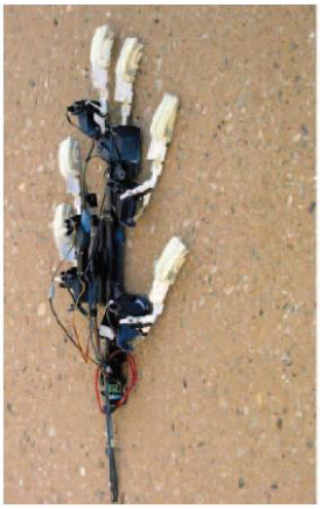

(d) Claw anchoring (Ebert & Larochelle, 2016).

Figure 2.19: Different types of anchoring technologies.

2.10. Program of Requirements

After the literature review, the challenges related to the lunar environment and uncertainties in input parameters were identified, along with the assumptions made to address the constraints. The information is divided into three categories: requirements, boundary conditions and evaluation criteria. This section summarises these three components that serve as input for the preliminary foundation design. As inspiration, the general requirements and evaluation criteria that are defined by Ruess et al. (2006) were used.

2.10.1. Requirements

This section describes the requirements for the foundation. In other words, what the situation demands of the foundation and the function it needs to fulfil. This relates to the loads the foundation needs to carry from the TLT and requirements for stability under microgravity and moonquake loading. As construction on the Moon presents unique challenges, several additional requirements are defined for designing in an extraterrestrial environment.

Structural Adequacy:

- The foundation needs to provide a connection of the TLT to the lunar surface to ensure stability within safety limits.
- The foundation needs to support the vertical load of the TLT.
- The foundation needs to support the load caused by the solar panels.
- The structure and foundation need to be able to withstand microgravity and moonquake loading.
  - Microgravity loading = 1/6th of Earth's gravity.
  - Moonquake loading = shallow moonquake with m_b > 4.5 on the Richter scale once every 400 years / earthquake with a return period of 475 years.
  - The PGA value for the 475 year return period event is 300 cm/s^2, based on Figure 2.17.
- The foundation shall transfer the seismic action effects in the structure, from the structure to the ground, without unacceptable permanent displacements.

Energy Efficiency:

- The foundation design needs to minimise the amount of locally produced material.

Compatibility:

- The foundation needs to be compatible with the current truss structure for a TLT.
- The foundation size needs to be small enough so that, in the future, other TLT structures can be built adjacent.

Transportation:

- If material is brought from earth, this material needs to be as compact and lightweight as possible.
- If equipment is brought from Earth, it must be as compact and lightweight as possible.

Materials:

- Most materials need to be produced from local resources and follow ISRU principles.
- All materials need to withstand lunar environmental conditions.
  - When space concrete is used, geopolymer concrete is assumed.
  - Other material types described in section 2.7 are assumed to meet this requirement.

Maintenance:

- The surface of the foundation needs to be as flat as possible so robots can still reach the TLT for maintenance.
- The foundation must be aligned to the surface or use a slope for accessibility.

Ease of Construction:

- Use one of the construction techniques described in section 2.7 to ensure the feasibility of the construction process of the foundation.
- Keep the foundation design as simple and small as possible.
- Make sure that the design requires no heavy construction equipment.
- Disturb the regolith as little as possible to prevent dust generation.

Excavation:

- Excavation on the lunar surface is difficult, and it only increases with going deeper. Therefore, excavate as shallow as possible or eliminate it completely.
- Excavate the top layer of the regolith, as this material is too loose and fine and easily disturbed.

Settlements:

- Keep the settlements in the surrounding area as small as possible.
- Keep the range of influence on the subsurface as small as possible.

2.10.2. Boundary conditions

In extraterrestrial construction, there is limited information about the environment in which the structure needs to be built. This results in the current state of the art of equipment being taken as boundaries, and the current limited information as guidance for the design process. This section gives the boundary conditions that the design needs to consider.

- The foundation needs to be built on the Connecting Ridge.
- A tower length of 50-100 meters is assumed.
- The surface slope at the Connecting ridge is assumed to be 5 degrees with a possible deviation of 2.5 degrees.
- The soil conditions are assumed to be as described in section 2.5 for layers beneath the top layer, as this is an unfeasible material to build on.
- Excavations are assumed to be feasible between 1-3 meters in depth.
- Drilling 5-10 meters into the lunar regolith is assumed possible in the future.
- It is assumed that anchoring techniques exist and that small anchors are feasible in the near future; however, they are presumed to be brought from Earth.
- No drilling fluid is available.
- No large equipment for piles, drilling or tunnelling is available.

2.10.3. Evaluation criteria

Evaluation criteria are proposed to compare the different conceptual design options. These are based on the evaluation criteria defined by Ruess et al. (2006), and extended based on the information obtained during the literature review and system analysis. They relate to concepts important in extraterrestrial construction. In Table 2.3, the criteria are described. They can be used to score conceptual designs on a scale of 1 to 10 for each criterion.

Evaluation criteria	**Description**
Transportation cost	Mass / Volume of non-ISRU material Mass / Volume equipment Mass / Volume non-ISRU construction components
Material production energy	Amount and type of locally produced material used
Ease of construction	How simple is the design? How easy is it to obtain construction components? Which technique can be used to construct this design?
Use of local materials	How much of the design is from local materials?
Excavatability	How much soil needs to be excavated?
Experience with construction methods on Earth	How similar is the foundation method used to Earth?
Sensitivity to settlements	Expected impact on the surrounding surface and settlements.

Table 2.3: Criteria for evaluating the verified conceptual designs.

3

Design

3.1. Development of Concepts

After gathering all necessary information to inform design decisions, this section describes the development of concepts that comply with the defined requirements and boundary conditions. Foundations in history were researched, and the current state of earthquake foundation design was examined.

3.1.1. Historical foundations

From history, we can learn how people in the past worked to build a foundation without the equipment available today. When going to the moon, similar to the historical situation, a lack of equipment is present to build foundations in the way we do currently. Therefore, it is of interest to look to the past for inspiration. Przwerlócki and Świniański (2005) reports that between the 5th and 10th centuries, buildings were constructed on piles of rubble, held together by mortar. In later centuries, this concept was refined by selecting larger boulders for the exterior and filling the interior with smaller debris. This is called a Gothic foundation, and is illustrated in Figure 3.1a. Between the 12th and 16th centuries, the mortar used was of higher quality, and blocks were carefully selected. Outer layers were lined with ashlars, which are cubic rocks.

On the lunar surface, such a foundation would be achievable by making blocks and mortar from the lunar regolith. Robots could arrange the blocks in a structure, and mortar could be poured to bind them all together. The entire foundation could thus be assembled on the lunar surface. The downside of this method is the selection of aggregates for the blocks of lunar regolith, that may result in blocks with varying mechanical properties. The sizes and locations of the lunar regolith aggregates in the mortar mix can vary by foundation, resulting in different properties and potential weak spots. Especially in a seismic environment, this can quickly become problematic as local failure propagates.

When considering a more controlled approach to this historical foundation concept, bricks with mortar or interlocking bricks could be used as a column to support the tower. This gives a more structured approach to the Gothic foundation principle. This is illustrated in Figure 3.1b. An issue with using masonry is the decreased resistance to earthquakes; therefore, this needs to be considered during the evaluation of a lunar foundation under moonquake loading and modelled accurately.

When examining earthquake resistance in history, Zhong and Christopoulos (2022) found that the design of earthquake-resistant buildings was not well understood. Although ancient builders used freestanding columns in the past to support their structures, many of these structures are still present today and have survived multiple earthquake events. The resistance of these structures stems from the rocking and sliding of the blocks that make up the column, providing the entire structure with a self-rocking and self-centering capability.

For a lunar application, the TLT could be founded on columns designed to provide this self-rocking and self-centering capability. This concept is shown in Figure 3.1c. However, it needs to be investigated and modelled in detail whether the stability of the TLT can be maintained once a moonquake occurs. Similarly, the excavation depth necessary to achieve this self-rocking behaviour raises questions about the viability of this concept.

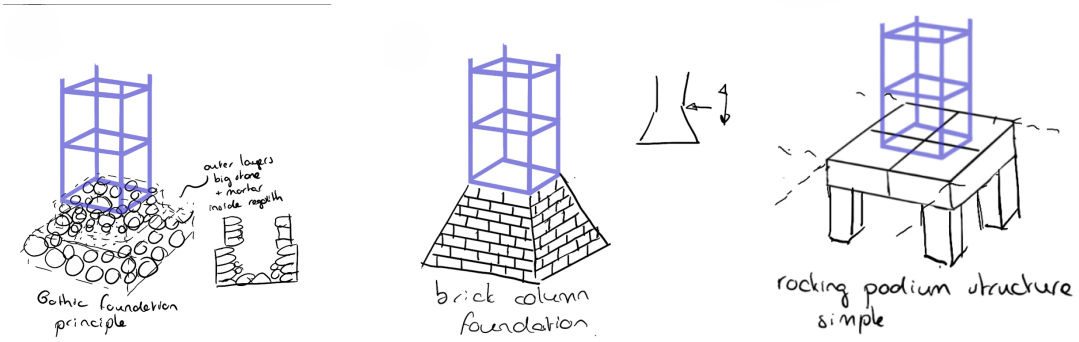

(a) Gothic foundation concept, where large boulders fill the exterior and small debris is used to fill the center space. The foundation is held together by mortar.

(b) A more refined version of the Gothic foundation using bricks. These bricks could potentially utilise an interlocking mechanism to eliminate the need for mortar altogether.

(c) Rocking podium foundation concept, where columns provide a self-rocking and self-centering capability.

Figure 3.1: Historical foundation concepts

3.1.2. Eurocode 8 foundation design

Foundations are classified into two groups according to NEN-EN 1998-5: surface and shallow-embedded foundations, and pile foundations. In the current design philosophy, the earthquake resistance is built into the structure by exploiting the ductile behaviour of components. This way, failure will cause plastic hinges to develop in these locations, allowing for larger deformations and preventing brittle failure and collapse. The foundations are designed to accommodate the extra earthquake load, but are otherwise similar to the static situation. There are several ways to enhance earthquake resistance by modifying the foundation. These are discussed in Section 3.1.2.

Shallow foundations

A shallow foundation resists forces by utilising friction and soil pressures to counteract weight, sliding forces, and moments. Shallow foundations need to be tested on their resistance to sliding, stability, rotational failure, exceeding the soil bearing capacity and structural failure in the Ultimate Limit State. In the Serviceability limit state, the horizontal movement and settlements need to be verified. In its simplest form, the shallow foundation is a simple slab foundation (see Figure 3.2a). In the lunar environment, the slab foundation can be made from different materials. To provide extra support against lateral movement, it is possible to brace the tower with anchors, as can be seen in Figure 3.2b. However, the method for securing these anchors in the lunar regolith remains a topic of investigation, as does the feasibility of making the materials for the anchors and the anchors themselves using ISRU practices.

Since the amount of material is preferable to be limited in the design, a slab foundation could also be a strap foundation, where the individual vertical trusses and beams of the TLT are at the bottom supported by small strip foundations that are connected to each other. An example of such a strap foundation can be seen in Figure 3.2c. One notable risk associated with a strip foundation is differential settlements, which can cause the foundation to rotate and, in turn, affect the moment load on the foundation.

A shallow foundation should be able to support the TLT, and the amount of material should be enough to withstand the vertical load posed by the mass of the structure and the horizontal force caused by the moonquake loading. This could lead to the slab's dimensions becoming unfeasible or otherwise requiring an increased amount of material and a deeper excavation.

Deep foundations

The other subsection of foundations is deep foundations, which are classified as pile foundations in the Eurocode. Piles transfer loads through a combination of shaft resistance and the tip bearing capacity. A simple version of a pile foundation is illustrated in Figure 3.3a. With a pile foundation, attention must be given to the potential breakage of piles and settlements. As mentioned earlier, the technology to create piles in the lunar environment and achieve the proper depth does not exist, as it requires a deep excavation using drills or augers, along with the in situ construction of the piles. Additionally, transport-

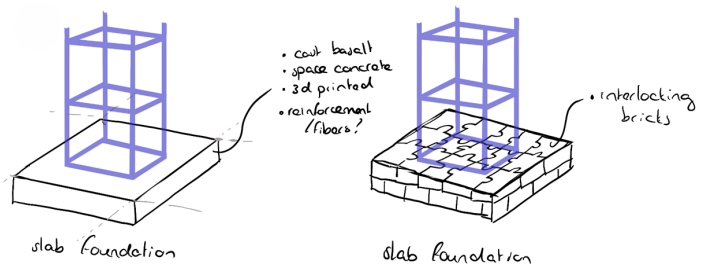

(a) A slab foundation, which is a type of shallow foundation. It can be made from different types of materials.

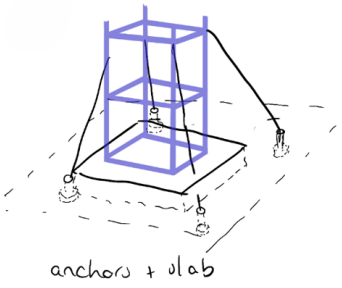

(b) A small slab foundation, with multiple anchors that provide stability to the structure.

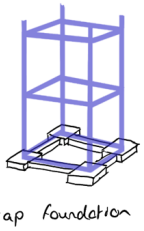

(c) A strap foundation that prevents material usage by only placing strips and small slabs under the structure itself.

Figure 3.2: Different shallow foundation concepts from the Eurocode 8 design standard.

ing and operating a pile-driving rig that can function in the extreme lunar environment is considered unlikely.

Piles can also be combined with rafts (see Figure 3.3b), increasing the resistance and giving the possibility to connect the raft to another (see Figure 3.3c), increasing the lateral resistance to moonquake loading. Another application of these connecting beams is to provide room for the energy supply system (Baker et al., 2022). In the case of the TLT, this can be used to safely store the cables to the battery storage. Compared to other foundation concepts, a pile raft foundation requires more material and has the same disadvantages as the simple pile foundation.

Increasing Earthquake Resistance

Measures are defined in the Eurocode to enhance earthquake resistance. If a building with a shallow foundation slid frictionlessly as one block over the surface after applying horizontal forces without deforming, there would be no damage to the structure. As this is not realistic in real-life applications, however, additional measures are needed to reduce the acceleration acting on the structure to prevent large deformations and damage.

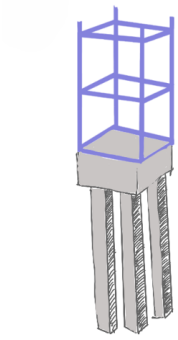

(a) A simple pile foundation.

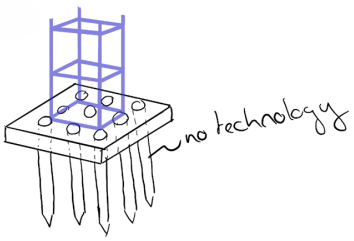

(b) An unconnected piled raft foundation.

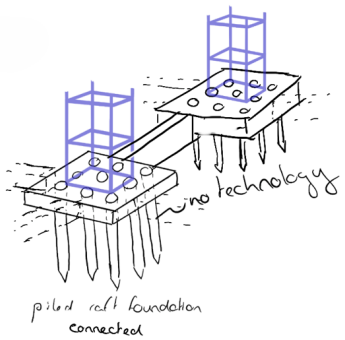

(c) A connected piled raft foundation.

Figure 3.3: Different deep foundation concepts from the Eurocode 8 design standard.

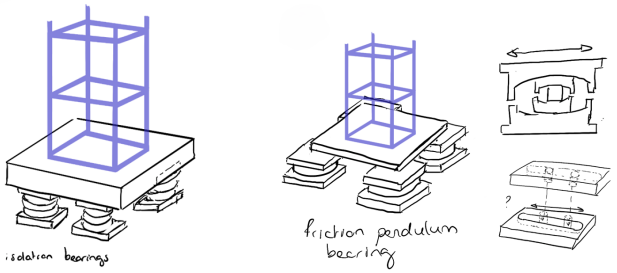

(a) A foundation with isolation bearings.

(b) A foundation with a friction pendulum bearing. Potentially, an interlocking system could be used that allows for movement in response to seismic excitation.

Figure 3.4: Options for increasing earthquake resistance by changing the foundation structure.

The design code mentions two different additions to structures to help protect structures from seismic loads: base isolation and energy dissipation devices. The latter requires adjustments to the Tall Lunar Tower design and is therefore not considered an option for the foundation design. The first one, base isolation, can be done in two different ways. By using elastomeric or friction sliding-based isolators as visualised in Figure 3.4a. It is known that elastic material can be produced from lunar regolith, as mentioned in Chapter 2.7. The friction pendulum bearing often utilises high-precision steel members, which are likely to require production and transportation from Earth and can be seen in Figure 3.4b.

In recent years, a new design philosophy was developed by Anastasopoulos et al. (2010) for shallow foundations by underdesigning the foundation, and thereby inviting failure into the soil. Instead of forming plastic hinges in the structure itself that can cause damage and necessitate repairs after an event, the structure rocks as a whole and is subjected to rotation and settlement. As long as the structure itself does not become unstable after these movements, the deformation gets located in the soil. For a lunar application, damage at the lunar surface would be a more accessible type of damage to repair than if robots had to scale the meter-high tower. It also allows structural design choices that would compromise ductility in the structure itself, as the options for construction on the lunar surface are already limited. The amount of rotation after an event, considering the height of the tower, is something that needs to be investigated to prevent instability. With a small rotation, displacements can become significant in the higher regions of the TLT. This causes the tip mass to move out of its location compared to the static situation, increasing the risk of structural instability.

3.1.3. Multi Criteria Analysis

With all options for foundation designs and their limitations now known, a multi-criteria analysis was performed based on the evaluation criteria defined in Chapter 2.10. It is assumed that for this thesis, the ease of construction, use of local materials and excavatability are more important for foundation design than the other criteria. In the future, stakeholders should decide which criteria are most important for foundation design, as all stakeholders will have different sets of priorities. The scoring is done on a scale of 1-10, where 1 represents the worst-case scenario, and 10 represents the best. The result of this process can be seen in Table 3.1.

From this analysis, it can be concluded that a slab foundation is the most convenient to construct in a lunar environment, due to its simplicity and the option to use ISRU materials. After that, a strap foundation is selected, followed by a brick column foundation. The reasoning behind the scores can be found in Appendix A.

To investigate the possibilities of a shallow foundation on the surface, a slab foundation is designed for the TLT. The downside of the slab foundation is its resistance to moonquakes. The dimensions of the slab will increase to counteract a larger moment due to seismic activity, negatively impacting the other evaluation criteria. The resulting size increase and how to mitigate this effect were therefore investigated in this thesis. Another risk is settlements, due to the low deformation modulus of the lunar regolith. Options for ISRU materials were also investigated.

	Transportation cost	Material Production Energy	Ease of construction	Use of local materials	Excavatability	Experience with construction method on Earth	Sensitivity to settlements		
Weight	0.1	0.1	0.2	0.2	0.2	0.1	0.1	**SUM**	**WSUM**
Slab	8	6	8	10	8	10	4	54	8
Slab + anchors	6	7	8	5	8	7	5	46	6.7
Pile	5	5	7	10	1	10	8	46	6.4
Piled raft	5	1	3	10	1	10	8	38	5.2
Rocking podium	8	3	7	10	3	5	7	43	6.3
Isolation bearing	7	4	3	10	4	8	6	42	5.9
Friction pendulum bearing	1	9	5	2	4	8	6	33	4.2
Gothic	9	8	9	10	6	3	3	40	5.7
Brick column	8	7	8	10	6	5	6	50	7.4
Strap	8	6	7	10	8	10	3	52	7.7

Table 3.1: Multicriteria analysis for the different conceptual designs based on the evaluation criteria. The weights for each criterion are described, as well as the sum of all scores (SUM), and the weighted sum (WSUM), where the score is multiplied by the weight before addition.

3.2. Design Input

This section describes the input for the different analyses performed to investigate the dimensions of a slab foundation for a TLT. These design calculations are based on the Eurocode, where the situation was translated to the lunar environment. The Eurocodes used are NEN-EN 1997-1, related to geotechnical aspects, NEN-EN 1998-1 for general rules on seismic design, and NEN-EN 1998-5 for geotechnical aspects, foundations, and underground construction in seismic design situations.

These calculations are used only to obtain indicative dimensions for the foundation, as it is unknown how many of these relationships can be applied to the lunar environment. The behaviour of the soil in microgravity and vacuum conditions, and whether the soil will fail in a similar manner as on Earth, is also unknown. For this preliminary design, it is assumed that the formulas provide a good first step in gaining insights into the behaviour of lunar soil and the soil-structure interaction.

3.2.1. Structure Input

The tower itself has parameters that are necessary for the preliminary design calculations. These are described in Table 3.2

Parameter	Description	Value
m_{TLT}	The mass of the TLT (Song, Mikulas, et al., 2023).	200 kg
m_{solar}	The mass of the solar panels (Song, Mikulas, et al., 2023).	1500 kg
E	The stiffness of the tower (Song, Mikulas, et al., 2023).	$70 * 10^9$ Pa
I	The moment of inertia of the tower (Song, Mikulas, et al., 2023).	$2.21 * 10^{-4} m^4$
h_{tower}	The height of the tower.	50 m

Table 3.2: The input parameters for the structure used in the analyses for the preliminary design. Each parameter is paired with its corresponding description and value.

3.2.2. Soil Input

Soil parameters were assumed to serve as input for the static and seismic analyses and are summarised in Table 3.3. There is limited data available on the properties of lunar regolith as discussed earlier in section 2.5. The values presented are extracted from Table 2.1. Mostly, average parameters were calculated from the available data up till 2 meters of depth, since the shallow foundation covers most of that range. To be conservative however, some values are chosen based on the lower values of the shallower regolith. If another source was used, this is specified in Table 3.3.

The values of the upper layer of the lunar regolith are not considered. This layer consists mainly of dust with a lower density than the deeper lunar regolith. The problem, however, lies primarily in the deformation modulus, which varies between 15.6 and 29 kPa for the surface layer. This material is unsuitable for building on, due to its low strength and risk of densification, and needs to be removed.

3.2.3. Seismic Input

The Eurocode prescribes two different approaches for calculating seismic effects on geotechnical structures. According to EN 1998-5, Section 4.5, seismic action effects on geotechnical structures can be calculated using either a force-based approach or a displacement-based approach. Since this thesis only deals with a preliminary design, a force-based approach was taken to get an initial indication of how the system behaves. This section describes the seismic input parameters necessary to use the force-based approach.

Site categorisation

For seismic calculations, shear wave velocities are an important parameter. In the upper 10 meters, according to Figure 2.14a, the upper layer is estimated to have velocities lower than 0.5 km/sec. According to Sollberger et al. (2016), the shear wave velocity is even lower, at 30 meters, and they estimate it around 90 m/s.

According to NEN-EN 1998-1, Table 5.1, there are two possibilities: category A and category B. With the depth of the seismic bedrock formation, where velocities are ≥ 800 m/s, lower than 30 meters, the site categorisation is B.

Parameter	Description	Calculation	Value
γ_ϕ γ_c γ_γ	The partial factor for ϕ, c and γ from NEN-EN 1997-1, Table A.4a, Annex A.3.2 for a shallow foundation.	-	1.15 1.6 1.1
ϕ_k	Angle of internal friction. In literature, it ranges from $30° - 50°$. It was chosen to assume an average of these values for the preliminary analyses.	-	40°
ϕ_d	The design value of the angle of internal friction.	$\frac{\phi_k}{\gamma_\phi} = 40/1.15$	35°
c_k	Cohesion. In literature, the cohesion varies between 0.1-3.5 kPa in the first 2 meters. Again, an average value is presumed.	-	1.6 kPa
c_d	The design value of the cohesion.	$\frac{c_k}{\gamma_c} = 1.6/1.6$	1.0 kPa
ρ_{gem}	The density of the lunar regolith. The conservative value at 15 cm depth was chosen.	$(1.5/1000) * 100 * 100 * 100$	1500 kg/m^3
γ_k	The volumetric weight of the lunar regolith.	$\rho_{gem} * g_{moon}/1000 = (1500 * 1/6 * 9.81)/1000$	2.45 kN/m^3
γ_d	The design value of the volumetric weight.	$\frac{\gamma_k}{\gamma_\gamma} = 2.45/1.1$	2.23 kN/m^3
C_c	Primary compression index (Heiken et al., 1991).	-	0.05
C_α	Secondary compression index. Unknown in literature.	-	-
n	Porosity, becomes lower at depth, value taken from the literature at 30-60 cm depth.	-	0.44
e	Void ratio.	$\frac{n}{(1-n)} = 0.44/(1 - 0.44)$	0.79
K_0	Coefficient of lateral stress (Heiken et al., 1991)	-	0.45

Table 3.3: The input parameters for the soil used in the analyses for the preliminary design. Each parameter is paired with its corresponding description and, where applicable, an optional calculation.

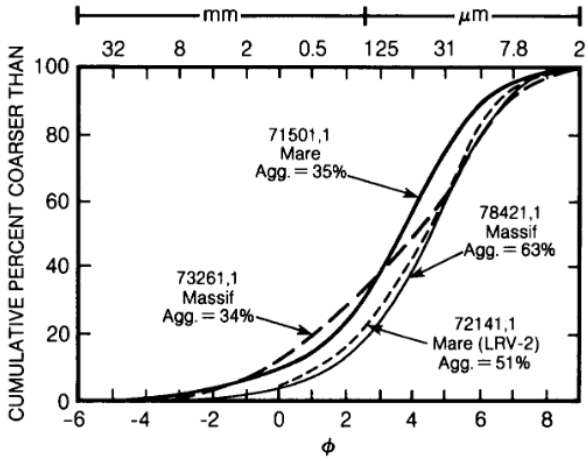

Figure 3.5: Cumulative size-frequency versus grain sizes by Heiken et al. (1991) for lunar samples. As can be seen, most particles are only micrometres in grain size. The lunar regolith has grain size properties of a silty sand, with some cobbles or pebbles.

Using the grain sizes from Figure 3.5, it can be concluded that the upper layers are partially in the silt and in the fine sand category. This suggests that calculations should be made for fine-grained soils. One thing of note here is that these samples are not taken from the Lunar South Pole, but from the area where the Apollo missions took place. It is therefore uncertain if the grain size distribution is similar at the South Pole.

Consequence class

For certain design parameters in the Eurocode, the consequence class is an important factor. A consequence class defines the importance of a structure based on the consequences of the structure failing. These consequences come in different forms, namely the loss of human life or injury, and economic, social or environmental loss according to NEN-EN 1990.

It is assumed that when TLTs are installed on the lunar surface, redundancy will be introduced in the form of multiple towers and backup power facilities. There is still a risk that a TLT structurally failing will result in a loss of power that could lead to loss of human life. In addition, the cost of having to rebuild the tower could become considerable, considering the extra-terrestrial component in the building process. Since the consequence classes are defined for structures on the Earth, it cannot be said that these categories and their influence on the calculations are suitable. For now, assuming that the loss of a TLT could result in loss of human life and a considerable economic loss, a consequence class of CC2 is proposed. Depending on the exact configuration of the power supply system on the moon and the progress in its colonisation, in future analyses, a consequence class of CC1 or CC3 could be more appropriate or a new system could be devised for the lunar situation.

Seismic class

Next to the consequence class, it is essential to determine the seismic class of the lunar surface on the Connecting Ridge to assess whether inertia forces of the soil should be incorporated into shallow foundation calculations in NEN-EN-1998-5. The NEN-EN 1998-1 states that the seismic action index is necessary to define the seismic action class using Table 4.1. The seismic action index is defined as:

$$S_\delta = \delta * F_\alpha * F_T * S_{\alpha,475} \tag{3.1}$$

$S_{\alpha,475}$ is the maximum spectral acceleration for a return period of 475 years from a uniform hazard spectrum. From Figure 2.17, this is chosen as 300 cm/s^2, or 3 m/s^2.

F_T is the topography amplification factor defined in NEN-EN 1998-1 5.2.2.2., Table 5.5. Since the topography on the Connecting Ridge is assumed to have no irregularities, $F_T = 1.0$.

δ is related to the consequence class of the structure, and is assumed to be CC2. In Table 4.2, chapter 4.2 from the NEN-EN 1998-5, $\delta = 1$ for CC2.

F_α is the site amplification factor defined in NEN-EN 1998-1, Section 5.2.2.2, Table 5.4. The default value column with formulas is assumed, since the uncertainty in the shear velocity parameters is large. Since the return period for T=475 year is already known, the $S_{\alpha,RP}$ is simply $S_{\alpha,475}$. This results in F_α taking the value:

$$F_\alpha = 1.3 * ((1 - 0,1S_{\alpha,RP}/g) = 1.3 * (1 - 0.1 * 3/(1/6 * 9.81)) = 1.06.$$

The seismic action index is then calculated as:

$$S_\delta = 1 * 1.06 * 1 * 3 = 3.18 m/s^2$$

According to Table 4.1 in NEN-EN 1998-1, this seismic action index is just 0.06 m/s^2 under the treshold to be included in a moderate seismic action class, so it officially classifies as a low seismic action class. The NEN-EN 1998-5 then prescribes in Section 9.4.2.1.3(3) to exclude inertial forces for a low and moderate seismic class with fine-grained soils. Since it is unknown in the microgravity environment whether the inertial forces will indeed be negligible, and the uncertainty in the parameters of the lunar soil, combined with the limited knowledge on the moon's seismicity, it was decided to consider the inertial forces in this preliminary analysis, when these forces stay within the limits of the formulas.

Peak ground acceleration
For calculating the seismic design situation, a peak ground acceleration is necessary to determine the horizontal force on the system. This horizontal ground acceleration is given in NEN-EN 1998-5, Section 5.2, and is defined as:

$$a_H = \frac{\beta_H}{\chi_H}\frac{S_\alpha}{F_A} = \frac{\beta_H}{\chi_H} PGA_e \tag{3.2}$$

S_α are the same as the previously defined $S_{alpha,475} = 3m/s^2$, representing the peak of the UHS diagram in Figure 2.17.

F_A is the ratio between the starting platform of the UHS and the top in Figure 2.17, determined as $3/1.5 = 2$.

β_H is related to spatial variation and varies with the type of analysis performed. Usually, in this thesis, $\beta_H = 1$ is taken as a conservative approach.

χ_H is related to permanent displacements of the system and is determined by its consequence class and limit state. Per type of analysis and structure, these values are defined.

PGA_e the peak ground acceleration. $PGA_e = 3/1.5 = 2m/s^2$,

a_H is the horizontal ground acceleration in m/s^2. This value is determined in the input for the different scenarios below.

Structure acceleration
The structure itself has a natural frequency at which it resonates in response to an excitation by a moonquake event. In this case, the largest horizontal deformations will occur at the top of the tower, leading to significant moments due to the large tip mass of the solar panels. The acceleration that the structure will be exposed to can be read from the Uniform Hazard Spectra in Figure 2.17 for the corresponding natural frequency. In Figure 3.6, the tower frequencies have been calculated using a formula for cantilever beams with a tip mass proposed by De M. Wahrhaftig et al. (2013).

For a tower of 50 meters, the natural frequencies of the tower vary between 0.01 and 0.045 Hz. This gives the structure natural periods T of 100 - 22 seconds. When looking at the UHS diagram in Figure 2.17, the accelerations are far to the right of the diagram. This means that the structure will only be subjected to very small accelerations. It is warranted that there currently exist few measurements of shallow moonquake events, which could have greater magnitudes than those measured during the Apollo seismic experiment. Additionally, the UHS is based on multiple assumptions (see Section 2.6. If a conservative number is chosen, $a_s = 10cm/s^2$ or lower is a worst-case scenario estimation. This does not yield large forces on the structure; however, a second-order effect, due to the height of the tower, is a governing factor in the foundation design.

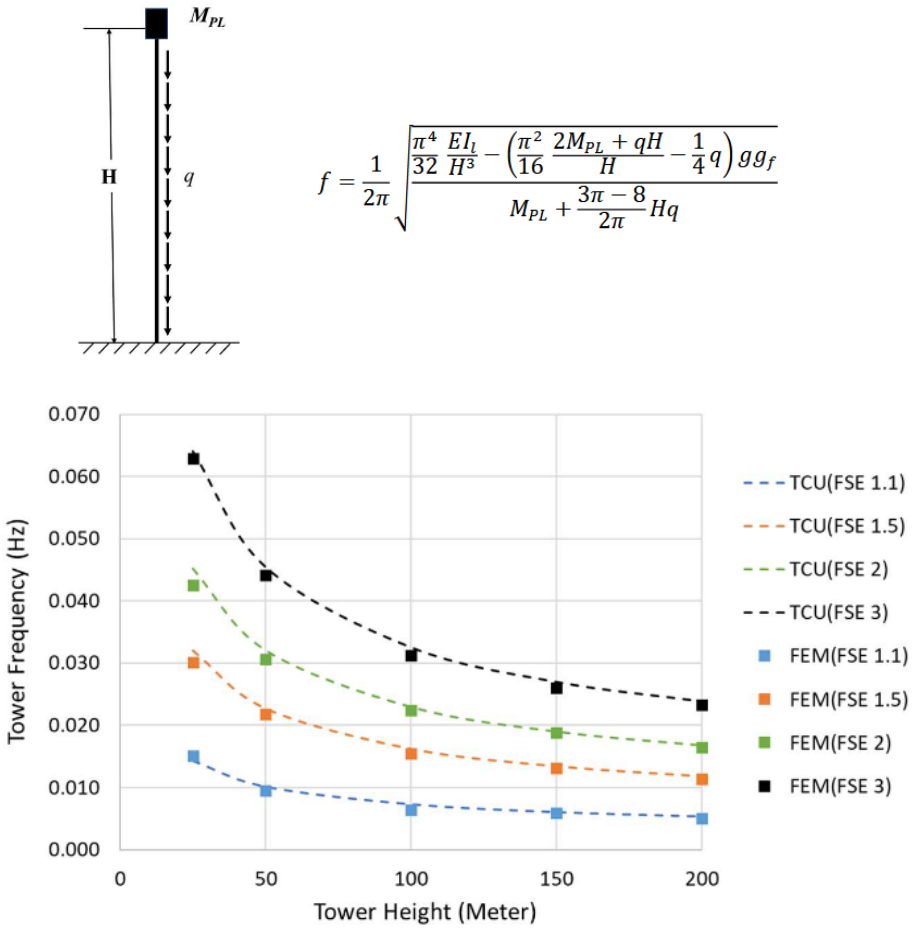

Figure 3.6: The natural frequencies of different heights of the TLT tower concept. A simplified model was tested against a Finite Element Model (FEM) for different safety factors related to the Euler buckling load on the structure (Song, Mikulas, et al., 2023).

3.2.4. Foundation Input

The parameters for the foundation dimensions can be seen in Figure 3.7, where the detailed parameters for the results are summarised in Table 3.4.

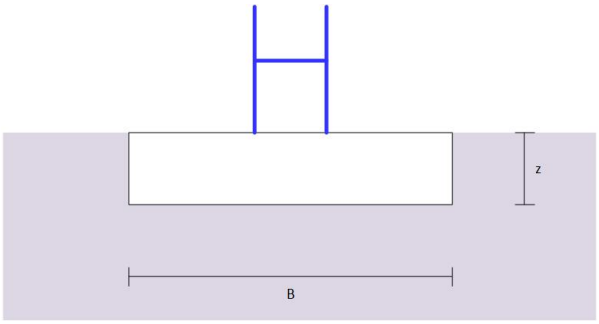

Figure 3.7: The defined dimensions for the slab foundation design.

Parameter	Description	Value
B	The width of the foundation.	7 m
L	The length of the foundation, a symmetric foundation is assumed.	7 m
z	The depth of the foundation.	2 m
slope	A tilt of the underground will cause a large extra moment on the foundation. It is therefore recommended to level the surface before beginning construction.	0°
$\rho_{foundation}$	The density of the foundation material. This will be the density of the geopolymer concrete used, for a value corresponding to regular concrete is assumed.	2500 kg/m^3
$\gamma_{foundation}$	The volumetric weight of the foundation: $\rho_{foundation} * g_{moon} = 2500 * 1/6 * 9.81$	4088 N/m^3

Table 3.4: The input for the foundation and the material used for the analyses.

4

Static analysis

4.1. Overview

This situation primarily concerns the vertical force acting on the foundation caused by the weight of the TLT, the solar panels and the self-weight of the foundation. There are no horizontal loads due to the absence of atmospheric pressure and the structure's symmetry, resulting in no eccentric loads and thus moments. In Table 4.1, the input for the static situation is described, and in Figure 4.1, the load case is visualised.

Parameter	Description	Calculation	Value
γ_G	The safety factor for the permanent loads. NEN 1997-1, Table A.3.	-	1.35
$N_{d,TLT+solar}$	The vertical force due to the mass of the TLT and the solar panels.	$\gamma_G * g_{moon} * (m_{TLT} + m_{solar})/1000 = 1.35 * 1/6 * 9.81 * (200 + 1500)/1000$	3.9 kN
$N_{d,foundation}$	The vertical force due to mass of the foundation.	$\gamma_G * B * B * z * \gamma_{foundation}/1000 = 1.35 * 7 * 7 * 2 * 4088/1000$	540.8 kN
$N_{d,total}$	The total vertical load.	$N_{d,TLT+solar} + N_{d,foundation} = 3.8 + 540.8$	545 kN
H_d	The horizontal load.	-	0 kN
M_d	The moment load.	-	0 kN

Table 4.1: The safety factors and static loads, their definitions, sources, corresponding calculations, as well as their final value. These parameters are used as input for the other static analyses.

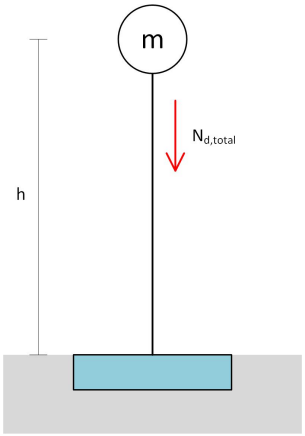

Figure 4.1: The static load case on the TLT modelled as a 1D oscillator. The static case only consists of the vertical load from the mass of the system.

4.2. Methodology

This section describes all the methods to verify the failure mechanisms in the Ultimate Limit State and the Serviceability limit state as described in the Eurocode NEN 1997-1 national Annex for the Netherlands.

4.2.1. Stability

The check prescribed in the Eurocode is related to the slope of the area. This angle needs to be a maximum of $\beta > 0.5 * \phi'_{gem,d}$. When this value is reached, there is a risk of instability, and the sliding behaviour needs to be investigated. As stated earlier, the ground should be levelled to prevent large extra moments. However, even when this is not considered, the current state of the Connecting Ridge has a slope of 5° with a possible deviation of 2.5°. Since the moon is made up of lunar regolith and only a variation in density is present, it is assumed that the $\phi'_{gem,d}$ is just the ϕ_d of lunar regolith. Even with 3 standard deviations, the check becomes: $5 + 3 * 2.5 < 0.5 * 35 = 12.5 < 17.5$., proving that there is no risk for a loss of stability in the static situation.

4.2.2. Bearing Capacity

The bearing capacity of the lunar soil must be calculated to resist the vertical force exerted by the system's mass. To calculate the maximum resisting force, first, the effective area of the foundation needs to be determined:

$$b' = B - 2 * e_B \tag{4.1}$$

$$l' = L - 2 * e_L \tag{4.2}$$

$$A' = b' * l' \tag{4.3}$$

where:

A' is the effective area for the foundation in m^2;

b' is the measurement of the short side of the effective foundation area;

l' is the measurement of the long side of the effective foundation area;

e_B is the absolute value of the eccentricity with respect to the centre of the foundation area in the width direction of the resulting load $N_{d,total}$ in m;

e_L is the absolute value of the eccentricity with respect to the centre of the foundation area in the length direction of the resulting load $N_{d,total}$ in m.

With this effective area, the resisting force can be calculated using the formulas:

$$R_d = \sigma'_{max} * A' \tag{4.4}$$

$$\sigma'_{max} = c'_{gem} * N_c * s_c * b_c * i_c + \sigma'_{v;z;d} * N_q * s_q * b_q * i_q + 0,5 * \gamma'_{gemd;d} * b' * N_{\gamma'} * s_{\gamma'} * b_\gamma * i_{\gamma'} \tag{4.5}$$

where:

R_d is the resisting vertical force from the soil in kN;

σ'_{max} is the maximal effective vertical stress that the soil can bear in kPa;

$c'_{gem;d}$ is the average effective cohesion in KPa;

N_c is the carrying capacity factor for the influence of the cohesion;

s_c is the shape factor for the influence of the cohesion;

b_c is the reduction factor for the influence of the cohesion caused by the inclined underside of the foundation;

i_c is the reduction factor for the influence of the cohesion caused by the inclination of the load;

$\sigma'_{v;z;d}$ is the effective vertical stress of the ground cover on the construction level on depth z in kPa;

N_q is the carrying capacity factor for the influence of the ground cover;

s_q is the shape factor for the influence of the ground cover;

b_q is the reduction factor for the influence of the ground cover caused by the inclined underside of the foundation;

i_q is the reduction factor for the influence of the ground cover caused by the inclination of the load;

$\gamma'_{gem;d}$ is the average effective volumetric weight of the ground under the construction level in kN/m^3;

$N_{\gamma'}$ is the carrying capacity factor for the influence of the effective volume weight of the ground under the foundation;

$s_{\gamma'}$ is the shape factor for the influence of the effective weight of the ground under the foundation area;

$b_{\gamma'}$ is the reduction factor for the influence of the effective weight of the ground under the foundation area caused by the inclined underside of the foundation;

$i_{\gamma'}$ is the reduction factor for the influence of the effective weight of the ground under the foundation area caused by the inclination of the load;

$\phi'_{gem;d}$ is the average effective internal friction angle in °.

To calculate all components of this formula, the average soil parameters across all layers must be determined using these 3 formulas:

$$\phi'_{gem;d} = \frac{\sum_{j=1}^{j=n} h_j * \phi'_{j;d} * X_j}{\sum_{j=n}^{j=1} h_j * X_j} \tag{4.6}$$

$$c'_{gem;d} = \frac{\sum_{j=1}^{j=n} h_j * c'_{j;d} * X_j}{\sum_{j=n}^{j=1} h_j * X_j} \tag{4.7}$$

$$\gamma'_{gem;d} = \frac{\sum_{j=1}^{j=n} h_j * \gamma'_{j;d} * X_j}{\sum_{j=n}^{j=1} h_j * X_j} \tag{4.8}$$

where:

X_j is the distance of the middle of layer j to the influence depth z_e in m;

h_j is the thickness of layer j in m;

n is the number of horizontal layers between influence depth z_e and the bottom of the foundation element;

$\phi'_{j;d}$ is the effective internal friction angle of layer j in °;

$c'_{j;d}$ is the cohesion of layer j in kPa;

$\gamma'_{j;d}$ is the effective weight of layer j in kN/m^3;

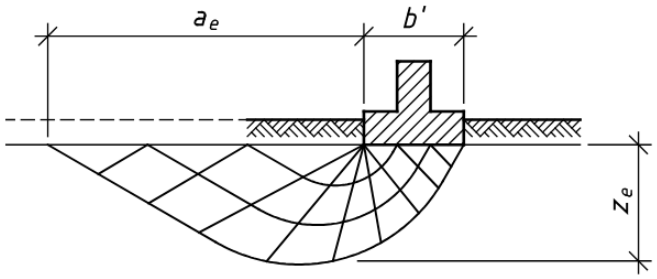

Figure 4.2: The influence zone of a shallow foundation NEN 1997-1 Figure 6.b.

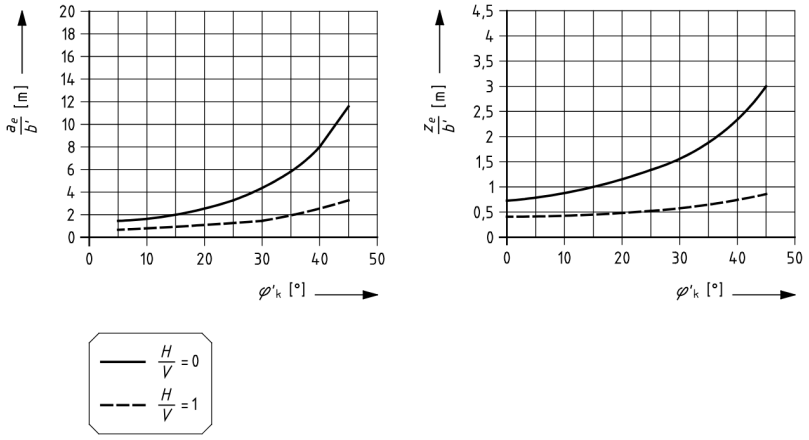

Figure 4.3: The horizontal and vertical influence depth as a function of the effective internal friction and the ratio between the horizontal and vertical resulting force.

z_e is the influence depth according to NEN 1997-1 6.5.2.2(d) in m.

The influence depth is dependent on ϕ'_k and the effective width b' of the foundation, as well as the ratio between the horizontal and vertical forces. It can be determined using Figure 4.2 and Figure 4.3.

The carrying capacity factors can be calculated using these average soil parameters using the following 3 formulas.

$$N_c = (N_q - 1) * cot(\phi'_{gem;d}) \tag{4.9}$$

$$N_q = exp(\pi * tan\phi'_{gem;d}) * tan^2(45° + 0,5 * \phi'_{gem;d}) \tag{4.10}$$

$$N_{\gamma'} = 2 * (N_q - 1) * tan(\phi'_{gem;d}) \tag{4.11}$$

Where the shape factors are dependent on the carrying capacity factors. The formulas for the shape factors are given by:

$$s_c = \frac{s_q * N_q - 1}{N_q - 1} \tag{4.12}$$

$$s_q = 1 + \frac{b'}{l'} * sin(\phi'_{gem;d}) \tag{4.13}$$

$$s_{\gamma'} = 1 + 0,3 * \frac{b'}{l'} \tag{4.14}$$

Lastly, the factors related to the inclination of the load and the inclination of the foundation's underside. The i-factors are related to the inclination of the horizontal load with the foundation. Since there is no horizontal load in this case, all these factors are equal to 1.

$$i_c = 1 \tag{4.15}$$

$$i_q = 1 \tag{4.16}$$

$$i_{gamma'} = 1 \tag{4.17}$$

The factors related to an inclined surface of the foundation itself are given by:

$$b_c = b_q - \frac{(1 - b_q)}{(N_c * tan(\phi'_{gem;d}))} \tag{4.18}$$

$$b_q = (1 - \alpha * tan(\phi'_{gem;d}))^2 \tag{4.19}$$

$$b_\gamma = (1 - \alpha * tan(\phi'_{gem;d}))^2 \tag{4.20}$$

Where α (°) is the slope of the inclined surface.

4.2.3. Sliding

The resistance against sliding originates from the passive ground pressure and the frictional resistance of the foundation surfaces as visualised in Figure 4.4. Since the horizontal force on the foundation in the static situation is $H_d = 0\ kN$, there is no risk of the foundation sliding, because both resistances will always be greater than 0.

4.2.4. Rotational Failure

According to section 6.5.4 of the NEN 1997-1, measures need to be taken when the eccentricity of the load is larger than 1/6th of the width of the foundation. As stated earlier, a symmetric structure is assumed with no eccentricities for the vertical load. This means that the design will remain within the limits for rotational stability as stated in Section 6.5.4 of EN 1997-1. In this scenario, therefore, there is no risk of rotational failure.

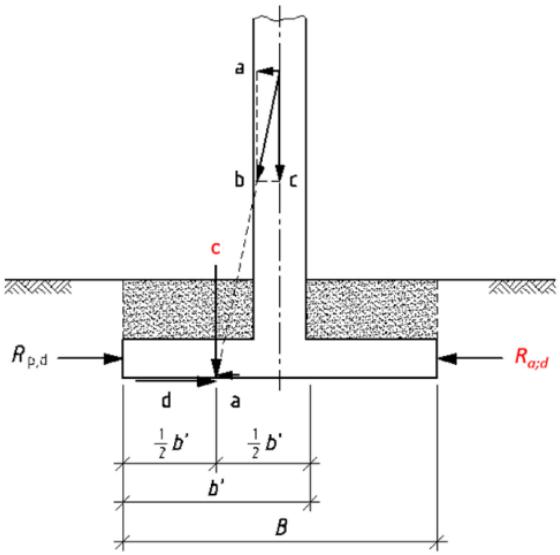

Figure 4.4: The sliding forces used in the calculation.

a is H_d including the active ground pressure $R_{a;d}$;

b is the resulting load $N_{d,total}$;

c is the vertical component of the resulting load, in this case the same as $N_{d,total}$;

d is the resistance of the foundation area R_d and the passive ground pressure $R_{p;d}$.

4.2.5. Failure due to horizontal movement foundation

In the serviceability limit state, the movement due to sliding must be checked by calculating whether the horizontal forces exceed 10% of the vertical forces as mentioned in 6.6.1 of the NEN 1997-1. Since the horizontal force is zero, there is no risk of the foundation moving horizontally.

4.2.6. Settlements

The NEN-EN 1997-1 describes a method to get an indication of possible settlements based on the primary compression index and increase in vertical effective stress. The added vertical stress is calculated by dividing the force of the TLT structure over the effective foundation area, where along a vertical axis the settlements per layer can be calculated.

$$\sigma_{gem,d} = \frac{V_d}{A'_{mom}} \tag{4.21}$$

$$\Delta\sigma'_{v;z;d} = \frac{p_{gem;d}}{\pi} * [(\alpha_1 - \alpha_2) + sin(\alpha_1) * cos(\alpha_1) - sin(\alpha_2) * cos(\alpha_2)] \tag{4.22}$$

A'_{mom} is the effective area of the foundation in m^2;

$\Delta\sigma'_{v;z;d}$ is the effective increase in vertical stress in the middle of a layer at depth z in kPa;

$p_{gem;d}$ is the evenly distributed load given by $\sigma_{gem,d}$ in kPa;

α_1 the angle with the vertical from the left according to Figure 4.5 in $radians$;

α_2 the angle with the vertical from the right according to Figure 4.5 in $radians$;

With the increase in effective stress for each layer known, the primary settlement can be calculated.

$$s1 = \sum_{j=0}^{j=n} \frac{C_{c;j}}{1 + e_j} * d_j * log(\frac{\sigma'_{v;z;0;d} + \Delta\sigma'_{v;z;d}}{\sigma'_{v;z;0;d}}) \tag{4.23}$$

$C_{c;j}$ is the primary compression index of layer j;

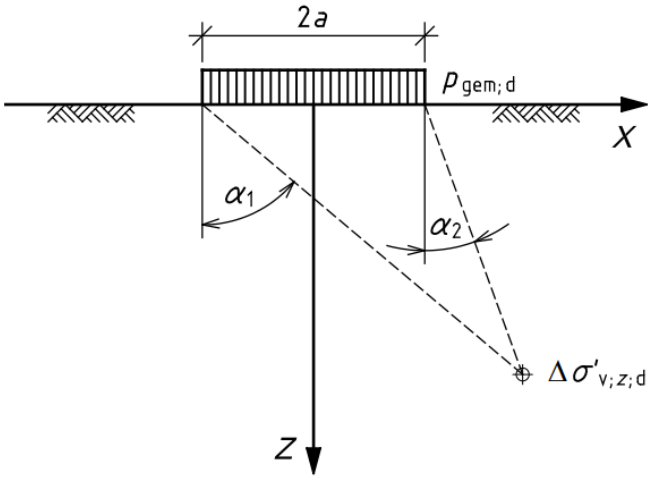

Figure 4.5: The definitions of the parameters used to calculate the increase in effective vertical stress.

e_j is the void ratio of layer j;

d_j is the thickness of layer j;

$\sigma'_{v;z;0;d}$ is the vertical effective stress before adding the load in the middle of a layer at depth z.

4.3. Results

This section contains the necessary calculations for the static case. As mentioned in the previous section, only the bearing capacity and settlements require calculations for the static load case. These calculations are based on the defined foundation input provided below.

4.3.1. Bearing capacity

First, the effective area was calculated using 4.1, 4.2 and 4.3. There is no eccentricity, since the TLT is symmetrical and the load is equally divided. The foundation is assumed to be symmetrical, so e_B and e_L are equal to zero.

$$l' = b' = 7 - 2 * 0 = 7\ m$$

$$A' = b' * b' = 7 * 7 = 49\ m^2$$

Then, the $\phi'_{gem;d}$, $c'_{gem;d}$ and $\gamma'_{gem;d}$ were determined. The important parameter required for this calculation is the influence depth z_e and influence width a_e as defined in Figure 4.2. The influence depth is dependent on the angle of internal friction and the difference between the horizontal and vertical loads, as well as the width of the foundation. Since the friction angle is on average 35°, and $H_d = 0\ kN$, Figure 4.3 can be used to obtain the values a_e/b = 5.77 and z_e/b = 1.9. To calculate a_e and z_e, these can simply be multiplied by B:

$$a_e = a_e/b * B = 5.77 * 7 = 40.4\ m$$
$$z_e = z_e/b * B = 1.9 * 7 = 13.3\ m$$

To obtain $\phi'_{gem;d}$, $c'_{gem;d}$ and $c'_{gem;d}$, 4.6, 4.7 and 4.8 were used. Since there is no known variation in the ground type present in the first 10 meters, the average values were chosen as $\phi'_{gem;d} = 35°$, $c'_{gem;d} = 1.0\ kPa$ and $\gamma'_{gem;d} = 2.23\ kN/m^3$.

The next step was to calculate the carrying capacity factors using 4.9, 4.10 and 4.11.

$$N_c(32.4 - 1) * cot(35°) = 45.2$$

$$N_q = exp(\pi * tan35°) * tan^2(45° + 0,5 * 35°) = 32.4$$

$$N_{\gamma'} = 2 * (32.4 - 1) * tan(35°) = 43.6$$

The shape factors were calculated using the carrying capacity factors from the defined formulas 4.12, 4.13 and 4.14:

$$s_c = \frac{1.57 * 32.4 - 1}{32.4 - 1} = 1.59$$

$$s_q = 1 + \frac{7}{7} * sin(35°) = 1.57$$

$$s_{\gamma'} = 1 + 0.3 * \frac{7}{7} = 1.3$$

As mentioned before in 4.15, 4.16 and 4.17, since there is no inclination of the resulting load assuming H_d = 0, $i_c, i_q, i_{gamma'}$ all have the value one.

The last factors are due to the inclination of the foundation itself using 4.18, 4.19 and 4.20. As mentioned before, the Connecting Ridge has an average of a five-degree incline, which then becomes the α in the formulas. However, it is assumed that an incline of the surface will lead to a large extra moment, and it is preferable to level the surface before constructing. Therefore, for this calculation, the α is taken as zero.

$$\alpha = 0$$

$$b_c = 1 - \frac{(1 - 1)}{(45.2 * tan(35°))} = 1$$

$$b_q = (1 - 0 * tan(35))^2 = 1$$

$$b_\gamma = (1 - 0 * tan(35))^2 = 1$$

Then, only the value for the effective vertical stress at construction level $\sigma'_{v;z;d}$ is left to be able to calculate σ'_{max}. This value was calculated by simply multiplying the effective unit weight of the soil and the depth of the foundation from the surface:

$$\sigma'_{v;z;d} = 2 * 2.23 = 4.46\ kPa$$

With all input for formula 4.5 and 4.4 now complete, the maximum bearing stress and capacity were calculated:

$$\sigma'_{max} = 1.12 * 45.2 * 1.59 * 1 * 1 + 4.46 * 32.4 * 1.57 * 1 * 1 + 0,5 * 2.23 * 7 * 43.6 * 1.3 * 1 * 1 = 741.4\ kPa$$

$$R_d = 741.4 * 49 = 36330.0\ kN$$

The bearing capacity is more than sufficient to carry the mass of the TLT, the solar arrays and the foundation itself:

$$R_d > N_{d,total} = 36330 > 545$$

4.3.2. Settlements

The increase in load at the top of the ground surface is calculated using 4.21.

$$\sigma_{gem,d} = 545/49 = 11.11kPa$$

To calculate the settlements according to formula 4.23, different layers need to be defined, as the load affects the lunar regolith near the surface more than the deeper layers, due to the increasing distribution of stress with depth. The foundation has an influence depth z_e of 13.3 meters, so it was chosen to divide the lunar regolith into three layers of approximately four meters in depth, covering 12 meters of lunar regolith. The original vertical effective stress $\sigma'_{v;0;d}$ in the middle of the defined layers can be calculated using the effective unit weight γ_d.

$$\sigma'_{v;z=2;0;d} = 2 * 2.23 = 4.46\ kPa$$
$$\sigma'_{v;z=6;0;d} = 6 * 2.23 = 13.38\ kPa$$
$$\sigma'_{v;z=10;0;d} = 10 * 2.23 = 22.30\ kPa$$

This load is distributed differently over the layers depending on the depth. The settlements for the 3 layers with centres $2m, 6m, 10m$ were calculated, by first determining the change in vertical effective stress along the vertical directly in the middle of the square foundation, where $a = 1/2 * B$. First, the angles to the vertical were calculated from the two edges of the effective width.

$$a = 1/2 * 7 = 3.5$$

$$\alpha_{1,z=2} = \arctan(3.5/2) = 1.05\ radians$$
$$\alpha_{2,z=2} = -\alpha_{1,z=2} = -1.05\ radians$$

$$\alpha_{1,z=6} = \arctan(3.5/6) = 0.52\ radians$$
$$\alpha_{2,z=6} = -\alpha_{1,z=6} = -0.52\ radians$$

$$\alpha_{1,z=10} = \arctan(3.5/10) = 0.34\ radians$$
$$\alpha_{2,z=10} = -\alpha_{1,z=10} = -0.34\ radians$$

With the locations for the calculations known, the increase in vertical effective stress was calculated with 4.22.

$$\Delta\sigma'_{v;z=2;d} = \frac{11.11}{\pi} * [(1.05 + 1.05) + sin(1.05) * cos(1.05) - sin(-1.05) * cos(-1.05)] = 10.48\ kPa$$
$$\Delta\sigma'_{v;z=4;d} = \frac{11.11}{\pi} * [(0.52 + 0.52) + sin(0.52) * cos(0.52) - sin(-0.52) * cos(-0.52)] = 6.82\ kPa$$
$$\Delta\sigma'_{v;z=6;d} = \frac{11.11}{\pi} * [(0.34 + 0.34) + sin(0.34) * cos(0.34) - sin(-0.34) * cos(-0.34)] = 4.59\ kPa$$

With all the original vertical effective stresses known and the increase of this stress over the 3 layers of 4 meters depth, the primary settlement per layer was calculated .

$$s_{1_1} = \frac{0.05}{1 + 0.79} * 4 * log(\frac{4.46 + 10.48}{4.46}) = 0.14\ m$$
$$s_{1_2} = \frac{0.05}{1 + 0.79} * 4 * log(\frac{13.38 + 6.82}{13.38}) = 0.05\ m$$
$$s_{1_3} = \frac{0.05}{1 + 0.79} * 4 * log(\frac{22.30 + 4.59}{22.30}) = 0.02\ m$$

Summing all the primary settlements across all layers to complete 4.23 yields the total primary settlement after loading the regolith.

$$s_{1_{total}} = s_{1_1} + s_{1_2} + s_{1_3} = 0.14 + 0.05 + 0.02 = 0.20\ m$$

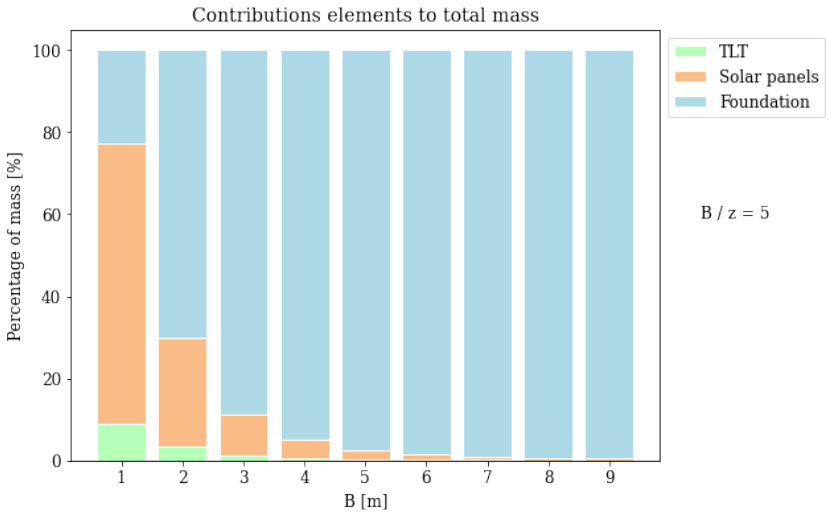

Figure 4.6: The influence of the three elements of the TLT, the solar panels and the foundation on the total system mass. Expressed in percentages of the total mass.

4.4. Discussion

The effect of input parameters on the results is discussed in this section. First, the influence of the increase of width of the foundation and its contribution to the total mass of the system is discussed.

As shown in Figure 4.6, by increasing the width of the foundation, the contribution to the total mass of the TLT and its solar panels decreases quickly, where the foundation's mass becomes the governing load. This highlights the importance of minimising the foundation size whenever possible to prevent excessive loads on the soil. It also shows that the foundation has the largest influence at larger configurations in the static situation, making the weight and thus the influence of the TLT and its solar panels negligible.

The next analysis involves varying the strength parameters and the volumetric weight of the soil to assess the influence on the bearing capacity. These ranges were chosen based on the available data and an estimation of possible deviations. THe results can be seen in Figure 4.7.

The bearing capacity is heavily influenced by the input soil parameters. This influence, however, varies with larger foundation size. The bearing capacity of a smaller foundation is less impacted by the volumetric weight than by the cohesion and internal friction angle. This is likely due to the fact that z=0.2 results in only a small value of vertical effective stress at the depth of the foundation and thus barely contributes to terms in the formula, where the friction angle propagates through the carrying capacity factors and thus heavily influences the outcome. This influence is felt regardless of foundation size. The internal friction angle is therefore a crucial parameter for proper assessment.

Cohesion contributes less when a larger foundation is involved. Since a larger area is available and the value of cohesion is low compared to some of Earth's soils, the contribution of the internal friction angle and volumetric weight over that of cohesion becomes relatively low over larger areas, and its influence diminishes. The influence of volumetric weight is higher with a larger foundation. This is expected, since the depth of the foundation increases, and therefore, the vertical effective stress on the calculation level also increases.

In Figures 4.8 and 4.9, it is visible that the internal friction angle has an exponential influence on the bearing capacity, while the cohesion and volumetric weight contribute linearly. This explains that the internal friction angle has a significant influence on behaviour, especially at higher values of the friction angle. Cohesion and volumetric weight contribute more substantially at lower values of the internal friction angle, but their influence decreases as the friction angle value increases. Since lunar regolith is known for its high friction angle, this parameter should be determined properly to assess the bearing capacity. The influence of the volumetric weight also increases with foundation size, and should therefore be determined properly as well. The cohesion depends on whether the foundation is smaller or larger, and thus depends on the type of structure that is required.

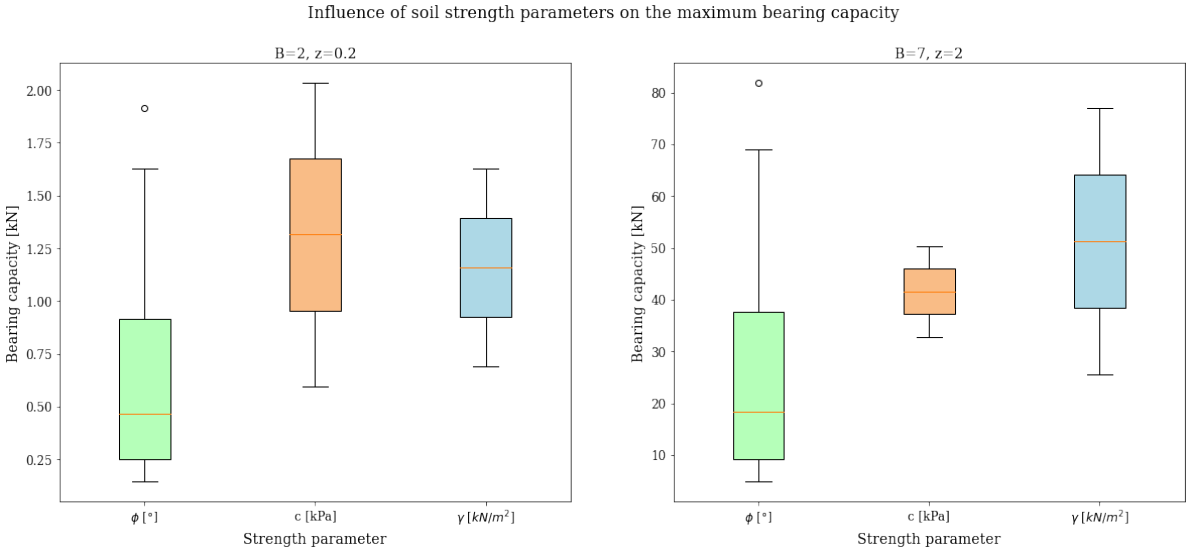

Figure 4.7: The variation in bearing capacity when the strength parameters of the lunar regolith are varied. The variations are: ϕ = 20 - 40°, c = 0 - 5 kPa, γ = 1.5 - 5 kN/m^3. The analysis was performed for two square foundation configurations. One consist of a small foundation with a width of two metres and a depth of 0.2 metres, and the second one is a large foundation witha width of seven metres and the depth 2 metres.

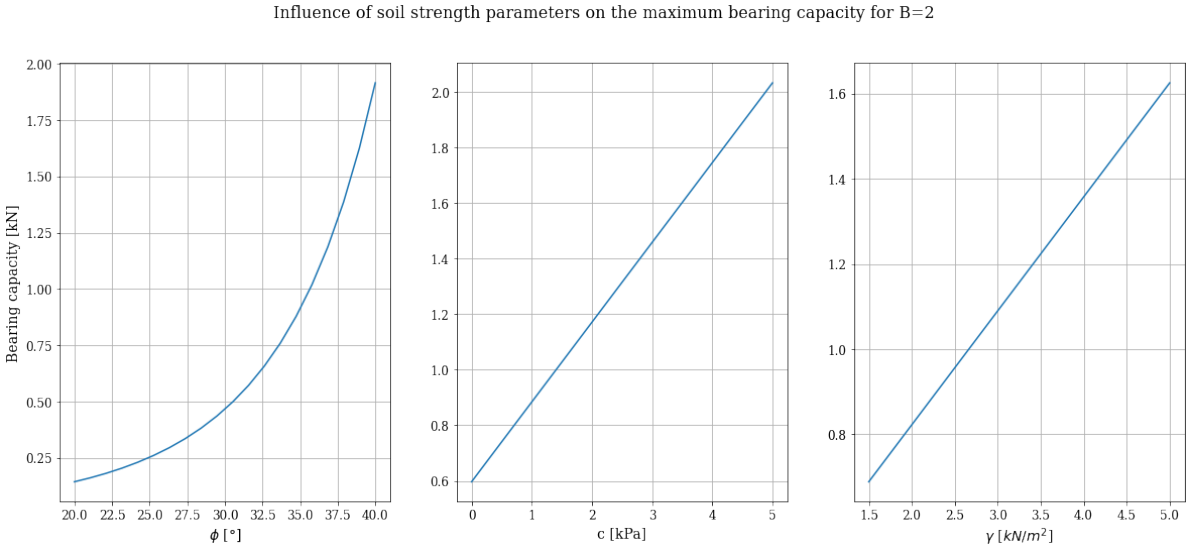

Figure 4.8: The influence of the internal friction angle ϕ, cohesion c and volumetric weight γ on the bearing capacity of the soil for a foundation of two metres width and 0.2 metres depth.

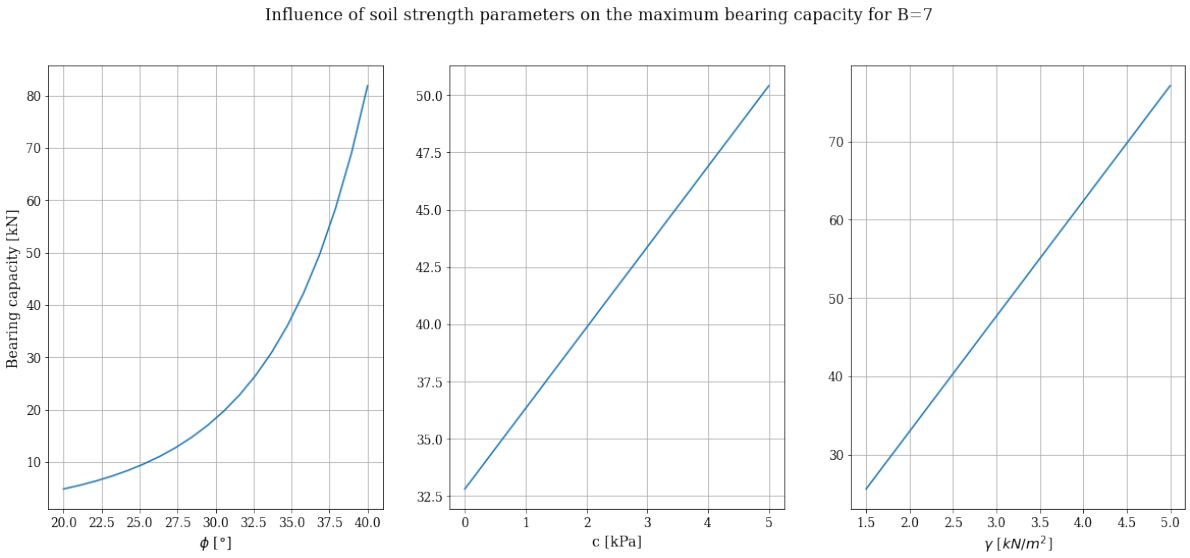

Figure 4.9: The influence of the internal friction angle ϕ, cohesion c and volumetric weight γ on the bearing capacity of the soil for a foundation of seven metres width and two metres depth.

The influence of the width of the foundation on the maximum bearing capacity is visualised in Figure 4.10. With a larger width, the bearing capacity initially increases slowly but accelerates as the width increases. The fact that bearing capacity increases with width is a logical phenomenon. The foundation has more soil to distribute the same weight over a larger width. The width of the foundation is accounted for in the calculations through the shape factors s_q and s_γ, where the second one is then multiplied by the term to consider the contribution of the effective volumetric weight, resulting in an exponential increase with weight. This suggests that the width is an important parameter in foundation design. By decreasing the width to conserve materials and reduce excavation, the bearing capacity will decrease.

One concern with shallow foundation design is the settlements. In Figure 4.11, the influence of foundation size on primary settlements is shown. The settlements are calculated for layers of two meters over a depth of 20 meters. Even with small foundations, the settlements can quickly become in the order of tens of centimetres. This, however, is likely conservative, as it is calculated using a simplified method from NEN-EN-1997-1, and the porosity below 60cm is unknown.

After primary settlement, the foundation could be stuck with a rotation. With the height of the TLT and the large tip mass, this could result in large extra moments and loss of stability. There is insufficient knowledge about the underground at the Lunar South Pole and the Connecting Ridge to provide insights into how the soil will behave when settling, and whether irregularities from, for example, meteor remnants will result in differential settlements. This effect is also something to consider on the structural side; the materials should be able to take these bending moments and curvatures.

Lastly, when considering solar farms with multiple TLTs, the settlements could potentially affect other foundations, impacting the placement and, consequently, the necessary space for installing enough TLTs for energy harvesting.

In the end, it depends on what the possibilities in terms of adjustments to the structure and maximum allowable displacements will be.

Taking all failure mechanisms and the applied loads in the static situation into consideration, the possible design configurations are described by Figure 4.12. It can be seen that a small foundation is already sufficient to bear the loads in the static situation without seismic loading. The possible foundation configurations are actually smaller than the tower's width, previously determined as one metre. The foundation, therefore, will always be larger than the tower itself, resulting in a foundation that will always be sufficient for the static situation.

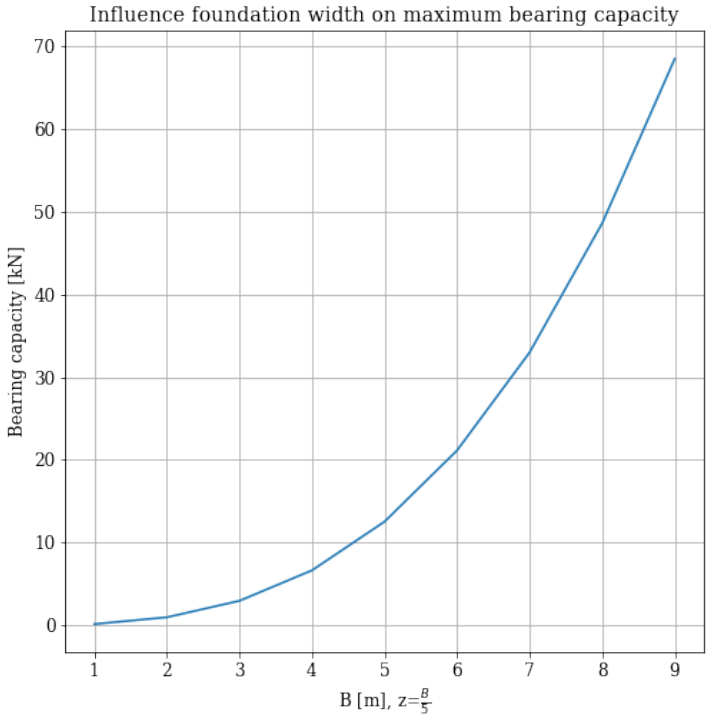

Figure 4.10: The influence of increasing the width of the foundation on the bearing capacity. The depth of the foundation is calculated by using a ratio of 1/5 to the width of the foundation.

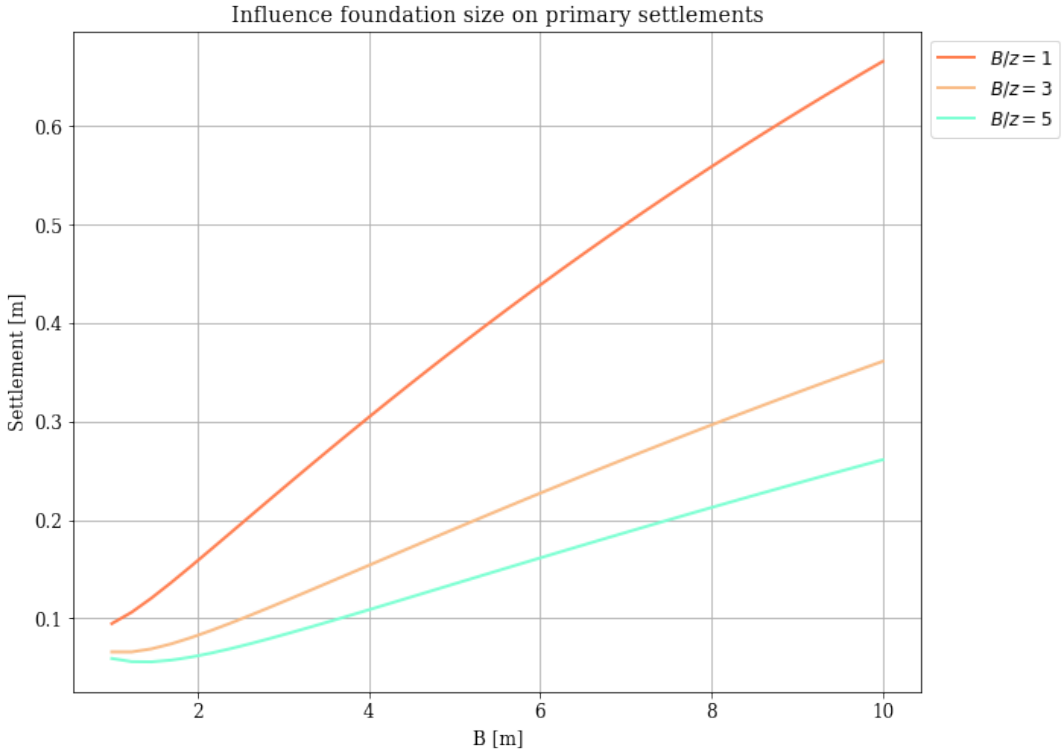

Figure 4.11: The settlements of the lunar regolith using three different foundation sizes and the primary compression index as defined in Table 3.3.

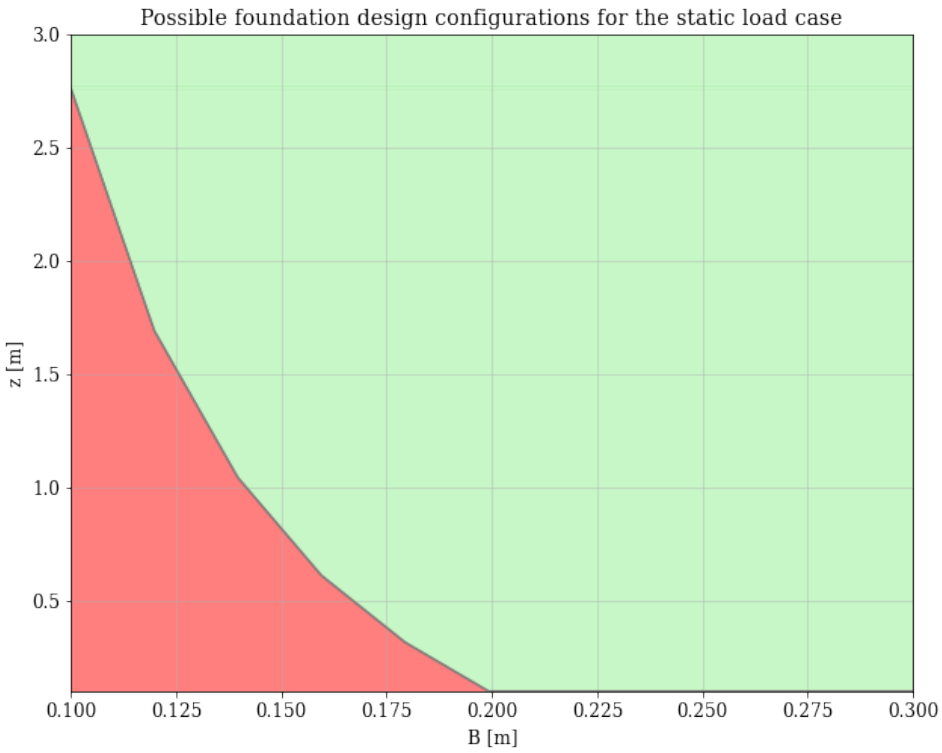

Figure 4.12: The design configurations possible in the static load case, as described in Table 4.1. The red area shows the square foundation configurations that lead to failure, where the green are safe configurations that can be used to choose a proper foundation format.

When examining the influence of microgravity on the calculations as visualised in Figure 4.13, the resulting graph differs little from the one without microgravity. The loads in the static situation are small, and even within Earth's gravity, most foundation configurations are easily able to withstand them. The area where failure occurs is slightly larger compared to the situation on the moon. This means that microgravity has a positive effect on foundation design, as it reduces the loads on the foundation, resulting in less bearing capacity needed to be generated by the soil itself.

The note here is that although the Ultimate Limit State suffices according to the Eurocode, the Serviceability Limit State could yield problems with (differential) settlements, likely resulting in the rotation of the foundation and large extra loads imposed on it. Depending on the allowed settlements, measures need to be taken to compact the soil or excavate until denser regolith is encountered at depth, characterised by a lower porosity and higher deformation modulus. It is also recommended to model the soil more accurately to better estimate the possible settlements and rotational effects.

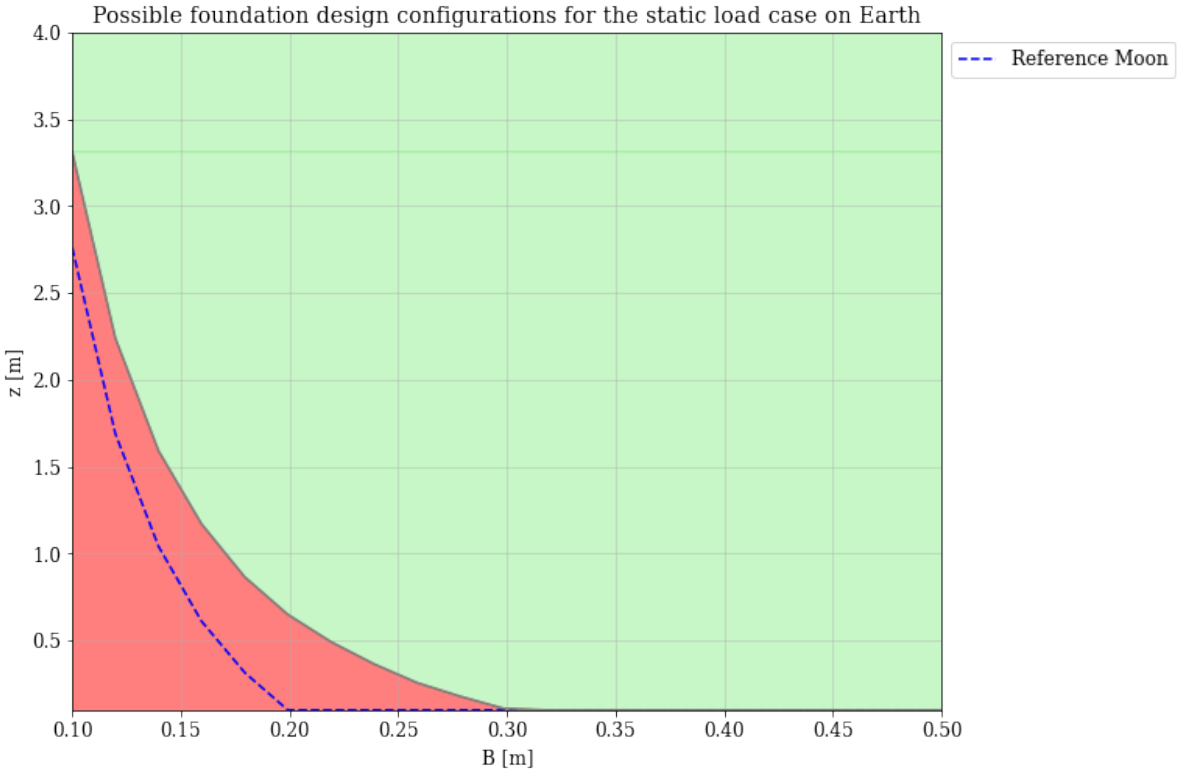

Figure 4.13: The design configurations for these static load case, as described in Table 4.1 on Earth. This illustrates the impact of microgravity on possible foundation configurations, as the reference line of the moon is lower than the grey line, which marks the beginning of viable foundation configurations.

5

Seismic analysis

5.1. Seismic analysis - no second order effects

5.1.1. Overview

Next to the vertical force due to the mass of the tower system, a small acceleration of the structure caused by a moonquake results in an additional horizontal force that is applied to the location of the tip mass of the tower, assuming the centre of mass is at the top of the tower. This horizontal force also causes a moment load on the foundation. According to NEN-EN 1998-5, the seismic action effects need to be taken into account using the following load combination.

$$E_{Fd} = E_{Fd,G}" + "\frac{\Omega_d \gamma_{Rd}}{\chi_H} E_{Fd,E} \tag{5.1}$$

The input for this analysis is summarised in Table 5.1, and in Figure 5.1, the load case is visualised.

5.1.2. Methodology

This section describes all the methods to verify the failure mechanisms in the Ultimate Limit State and the Serviceability limit state as described in the Eurocode NEN 1998-5.

Sliding failure

In a seismic situation, an additional horizontal force is applied to the system, requiring a calculation of the sliding resistance of the foundation. The resistance against this force comes from the shear resistance of the footing and the ground, the shear resistance of the two sides of the foundation and the horizontal component of the passive earth pressure. The EN 1998-5 states that only 30% of the

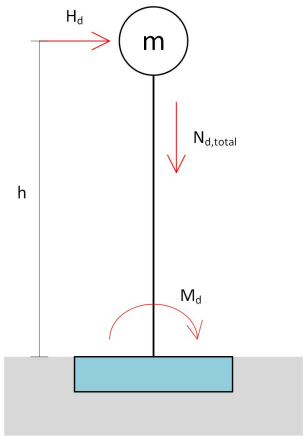

Figure 5.1: The seismic load case on the TLT modelled as a 1D oscillator. The seismic case consists of the vertical load and a horizontal force applied to the centre of mass of the system. This is assumed to be the location of the tip mass, resulting in a moment at the base of the tower.

Parameter	Description	Calculation	Value
$\Omega_d \gamma_{Rd}$	Given in 9.2 (13) EN 1998-5.	Bearing capacity shallow foundation. Sliding resistance shallow foundation.	1.2 1.0
χ_H	Based on Table 9.1 EN 1998-5, where values for χ_H can be found based on the range of permanent displacements. Since this range is unknown the most unfavourable value was chosen.	-	1.25
γ_G	The safety factor for the permanent loads. EN 1997-1, Table A.3.	Unfavourable Favourable	1.35 0.9
β_H	Given in Annex A of EN 1998-5. Using the most conservative value leads to the largest a_H.	-	1.0
a_H	The horizontal ground acceleration.	$a_H = \frac{\beta_H}{\chi_H} PGA_e = 1.0/1.25 * 2$	1.2 m/s^2
α_H	The horizontal seismic coefficient.	$\alpha_H = a_H/g = 1.21/(1/6 * 9.81)$	0.7
a_s	The acceleration of the structure. Determined in section 3.2.3.	-	0.1 m/s^2
$N_{d,total}$	The total vertical load. Same as the static vertical load except uses a favourable γ_G for sliding and rotational failure.	Bearing capacity Sliding, Rotational Failure	545 kN 363 kN
H_d	The horizontal load for the bearing capacity and for sliding, using different $\Omega_d \gamma_{Rd}$ values.	$\frac{\Omega_d \gamma_{Rd}}{\chi_H}(m_{TLT} + m_{solar}) * a_s/1000.$ Bearing capacity: $= (1.2/1.25)(200 + 1500) * 0.1/1000$ Sliding resistance: $= (1.0/1.25)(200 + 1500) * 0.1/1000$	0.16 kN 0.14 kN
M_d	The moment load.	$H_d * (h_{tower} + z) = 0.16 * (50 + 2)$	8.5 kNm

Table 5.1: The safety and combination factors for the seismic loads, combined with their sources and corresponding calculations. The final column shows the values used as input for the seismic analysis.

passive earth pressure should be considered when fully mobilised. This can be summarised by the formula:

$$V_{Ed} \leq F_{Rd} + V_{Rd,2} + 0.3V_{Rd,3} \tag{5.2}$$

V_{Ed} the horizontal sliding force on the foundation in kN;

F_{Rd} the shear resistance of the footing of the foundation in kN;

$V_{Rd,2}$ the shear resistance of the two sides of the foundation in kN;

$V_{Rd,3}$ the horizontal component of the passive earth pressure in kN.

To verify this condition, each contribution to the sliding resistance was determined. The sliding resistance from the footing of the foundation can be calculated by using:

$$F_{Rd} = (N_{Ed} - U)\frac{tan\delta_f}{\gamma_{tan\delta}} \tag{5.3}$$

F_{Rd} is the sliding resistance in kN;

δ_f is the friction angle between the foundation and ground in °;

$\gamma_{tan\delta}$ is the partial factor on δ_f;

N_{Ed} is the design vertical force on the foundation in kN;

U is the resulting force of the hydrostatic pore pressure in kN;

For the resistance of the 2 sides $V_{Rd,2}$, the same formula can be applied as for the resistance of the footing. Here, however, the force applied to the surface is not the vertical load, but rather the force related to the horizontal effective stress $\sigma_{h;d}$, which can be calculated from the vertical effective stress $\sigma_{v;d}$ by using the coefficient of lateral stress K_0.

$$\sigma_{v;d} = 1/2 * z * \gamma_d \tag{5.4}$$

$$\sigma_{h;d} = K_0 * \sigma_{v;d} \tag{5.5}$$

$$V_{Rd,2} = 2 * \sigma_{h;d} * z * B * \frac{tan\delta_f}{\gamma_{tan\delta}} \tag{5.6}$$

The last part is due to the passive earth pressure on one side of the foundation $V_{Rd,3}$. It requires calculating the passive earth pressure as per 10.3.2 of the NEN-EN 1998-5. This calculation requires passive earth pressure coefficients that account for the soil's weight and cohesion. No overburden is assumed, and thus there is no necessity for a coefficient related to a surcharge at the surface.

$$K_{PE\gamma} = [\frac{cos\delta_f}{cos(\beta_{sl} - \theta_{eq}) - \sqrt{sin^2\phi' - sin^2(\beta_{sl} - \theta_{eq})}}(cos\delta_f + \sqrt{sin^2\phi' - sin^2\delta_f})]\frac{cos\beta_{sl}}{cos\theta_{eq}}e^{-2\Psi_P tan\phi'} \tag{5.7}$$

$$K_{PEc} = \frac{K_{PE\gamma} - 1}{tan\phi'} \tag{5.8}$$

$$\Psi_P = 0.5(arcsin(\frac{sin\delta_f}{sin\phi'}) + arcsin(\frac{sin(\beta_{sl} - \theta_{eq})}{sin\phi'}) + \delta_f + \beta_{sl} + \theta_{eq}) \tag{5.9}$$

$$\sigma_P = K_{PE\gamma}(\sigma_v - u) + K_{PEc}c' + u \tag{5.10}$$

where:

β_{sl} is the inclination of the ground surface in °;

θ_{eq} is for the seismic situation, the inclination of the gravity field $\theta_{eq} = Atan(\alpha_H)$ in °;

$K_{PE\gamma}$ is the passive earth pressure coefficient accounting for the soil weight;

K_{PEc} is the passive earth pressure coefficient accounting for the cohesion;

σ_P is the passive earth pressure in kPa.

Then, the passive earth pressure becomes:

$$V_{Rd,3} = \sigma_P * z * B \tag{5.11}$$

Exceedance bearing capacity

In comparison to the static bearing capacity, a soil inertia force is applied to the foundation, necessitating a different approach. The seismic bearing capacity can be calculated according to Annex E of the NEN-EN 1998-5.

$$\frac{(1 - e\overline{F})^{c_T}(\beta\overline{V})^{c_T}}{(\overline{N})^a[(1 - m\overline{F}^k)^{k'} - \overline{N}]^b} + \frac{(1 - f\overline{F})^{c'_M}(\gamma\overline{M})^{c_M}}{(\overline{N})^c[(1 - m\overline{F}^k)^{k'} - \overline{N}]^d} - 1 \leq 0 \tag{5.12}$$

$$\begin{aligned} \overline{N} &= \frac{N_{Ed}}{N_{max}} \\ \overline{V} &= \frac{V_{Ed}}{N_{max}} \\ \overline{M} &= \frac{M_{Ed}}{BN_{max}} \end{aligned} \tag{5.13}$$

N_{max} is the design value of the bearing capacity under a vertical centred load as calculated in the static situation in kN;

N_{Ed}, V_{Ed}, M_{Ed} are the design values in the seismic situation for the vertical force, the horizontal force (here defined as a shear force) and an overturning moment;

B is the foundation width in m;

$\overline{F}$ is the dimensionless soil inertia force;

$a, b, c, d, e, f, m, k, k', c_T, c_M, c'_M, \beta, \gamma$ are numerical parameters related to the type of soil, either fine-grained or coarse-grained.

There are two options: one for fine-grained soils or saturated coarse-grained soils, and the other for dry soil, partially saturated coarse-grained soils or saturated coarse-grained soils. The Eurocode defines limits for the application of both versions of the dimensionless soil inertia force. These are shown below:

$$\begin{aligned} \overline{F}_{fine-grained} &= \kappa \frac{\rho a_H B}{\overline{c}} \qquad limit: \frac{\rho a_H B}{\overline{c}} \leq 2 \\ \overline{F}_{dry} &= \kappa \frac{\alpha_H}{tan\phi'} \qquad limit: 0 < \overline{N} \leq (1 - m\overline{F})^{k'} \end{aligned} \tag{5.14}$$

Rotational failure

For the rotational failure, the vertical force and moment load are most important. According to EN 1998-5 9.4.2.1.4, a maximum of one-third of the total foundation area cannot be in contact with the ground before the risk of rotational failure becomes too high. If more than 1/3th of the area is not in contact with the ground, a displacement-based approach should be taken to verify this failure mechanism. To provide an indication of the risk of rotational failure, the stresses on the underside of the foundation that the soil must withstand were calculated. The vertical force results in a compressive force, while the moment results in a compressive force on one side and a tensile force on the other side.

$$\sigma_N = \frac{N_d}{A} \tag{5.15}$$

$$\sigma_M = \frac{M_d * z}{I_{zz}} \tag{5.16}$$

σ_N is the normal stress at the bottom of the foundation in kPa;

N_d is the vertical force on the foundation in kN;

A is the area of the foundation in m^2;

σ_M is the bending stress at the bottom of the foundation at z in kPa

M_d is the moment load on the foundation in kNm;

z is the location from the center of the foundation in m;

I_{zz} is the moment of inertia of the analyzed cross section in m^4.

As soon as the stress changes from a compressive force to a tensile force, it is assumed that the soil and foundation are no longer in contact, since the soil is unable to provide tensile resistance.

$$\sigma_{LEFT} = \sigma_N + \sigma_M \qquad \sigma_{RIGHT} = \sigma_N - \sigma_M \tag{5.17}$$

$$\Delta_\sigma = \frac{\sigma_{LEFT} + \sigma_{RIGHT}}{B} \tag{5.18}$$

$$d_{nocontact} = \frac{\sigma_{LEFT}}{B\Delta_\sigma} * 100\% \tag{5.19}$$

This percentage $d_{nocontact}$ can be used to verify how much of the foundation is not in contact with the ground surface.

Settlements
The densification and settlements as a result of a seismic event need to be checked according to the Eurocode Annex C NEN-EN 1998-5. Most of this Annex, however, is focused on the effects of liquefaction, which is not a risk in the lunar underground thanks to the lack of hydrostatic pore pressure. When attempting to calculate the volumetric strain in clean, dry sand, the cyclic shear strain γ_{cyc} for lunar regolith is unknown. When a site response is not available, the Annex proposes to use γ_{ref}; however, this formula is dependent on the p_a, the atmospheric pressure, and therefore goes to infinity once calculated for the lunar situation. The lack of knowledge on the behaviour of lunar regolith under cyclic loads is an interesting future topic of investigation.

The EN 1998-5 suggests using ground improvement methods, especially to prevent densification from occurring. Since, in the static case, it was found that the upper layers of the lunar regolith have a lower density and at 30-60 cm a porosity of 0.44, ground improvement methods could reduce the risk of having (differential) settlements and of densification during a seismic event.

5.1.3. Results

This section contains the necessary calculations for the seismic case. As mentioned in the previous section, the sliding failure, exceedance of the bearing capacity and rotational failure are calculated.

Sliding failure
To calculate the sliding resistance, all three components of the sliding resistance were calculated.

The shear resistance of the footing of the foundation was calculated using formula 5.3. The $\gamma_{tan\delta}$ can be found in NEN-EN 1998-5 for the use in the Significant Damage (SD) and Near Collapse (NC) limit states and equals $\gamma_{tan\delta} = 1.0$. The δ_f is described in Table 9.b of the NEN-EN 1997-1. Assuming a rough surface, $\delta_f = 0.67 * \phi' k$. Since there is no hydrostatic pore pressure present, U is zero.

$$\delta_f = 0.67 * 35 = 26.7°$$

$$U = 0\ kN$$

$$F_{Rd} = (363 - 0)\frac{tan(26.7°)}{1.0} = 182.3\ kN$$

The shear resistance of the two sides of the foundation can be calculated by using 5.4, 5.5 and 5.6.

$$\sigma_{v;d} = 0.5 * 2 * 2.23 = 2.22\ kPa$$
$$\sigma_{h;d} = 0.45 * 2.22 = 1.00\ kPa$$
$$V_{Rd,2} = 2 * 1.00 * 2 * 7 * \frac{tan(26.7°)}{1.0} = 14.11\ kN$$

Lastly, the passive earth pressure was calculated. The inclination of the ground surface is assumed to be levelled before construction and therefore equals $\beta_{sl} = 0$. The inclination of the load is:

$$\theta_{eq} = Atan(1.2) = 35°$$

The passive earth pressure coefficients were calculated using 5.7, 5.8 and 5.9, where Ψ_P serves as input for the coefficients.

$$\Psi_P = 0.5(arcsin(\frac{sin26.7°}{sin35°}) + arcsin(\frac{sin(0 - 35°)}{sin35°}) + 26.7° + 0 + 35°) = 0.68$$

$$K_{PE\gamma} = [\frac{cos26.7°}{cos(0 - 35°) - \sqrt{sin^2 35° - sin^2(0 - 35°)}}(cos26.7° + \sqrt{sin^2 35° - sin^2 26.7°})]\frac{cos0}{cos35°}e^{-2*0.68*tan35°} = 6.68$$

$$K_{PEc} = \frac{6.68 - 1}{tan35°} = 8.17$$

With all the coefficients known, the horizontal component of the passive earth pressure was determined with 5.10 and 5.11.

$$\sigma_p = 6.68(2.22 - 0) + 8.17 * 1.6 + 0 = 23.06\ kPa$$

$$V_{Rd,3} = 23.06 * 2 * 7 = 322.86\ kN$$

Combining all terms results in the total force able to resist horizontal loads and check the sliding failure with 5.2:

$$0.14 \leq 182.3 + 14.11 + 0.3 * 322.86 = 293.28\ kN$$

With a horizontal force in this scenario of $H_d = 0.14\ kN$, the sliding resistance of 293.28 kN, is clearly sufficient.

Exceedance bearing capacity

For calculating the bearing capacity, first the loads need to be divided by the maximum static bearing capacity according to 5.13:

$$\overline{N} = \frac{545}{36330} = 0.015$$
$$\overline{V} = \frac{0.16}{36330} = 3.74 * 10^{-6}$$
$$\overline{M} = \frac{8.49}{7 * 36330} = 3.34 * 10^{-5}$$

The lunar regolith falls under both fine-grained soil and dry soil, making it difficult to choose between the two formulas for the dimensionless soil inertia force $\overline{F}$. Here, there are two options: one for fine-grained soils or saturated coarse-grained soils and the other for dry soil, partially saturated coarse-grained soils or saturated coarse-grained soils. Considering the absence of hydrosatic pore pressures in the lunar underground, the soil falls under the category of dry soil. However, the grain sizes as presented in Figure 3.5 make the lunar regolith a fine-grained soil.

The Eurocode defines limits for the application of both versions of the dimensionless soil inertia force. For the fine-grained variant, the following limit does not suffice:

$$\frac{1500 * 1.2 * 7}{1.0 * 1000} = 12.6 \nleq 2$$

Therefore, the formula for dry soil is used for the dimensionless inertia force. With this, only the numerical parameters need to be selected. Lunar regolith falls under fine-grained soil, so the numerical parameters from Table E.1 in the Eurocode become: $a = 0.70, b = 1.29, c = 2.14, d = 1.81, e = 0.21, f = 0.44, m = 0.21, k = 1.22, k' = 1.00, c_T = 2.00, c_M = 2.00, c'_M = 2.00, \beta = 2.57, \gamma = 1.85$.

To calculate the dimensionless soil inertia force with 5.14, most parameters are already known. One unknown is the κ value, which lies in the range of $0.3 \leq \kappa \leq 1.0$. This value is typically set to 1, but can be smaller if the fundamental period of the soil deposit and the structure differ significantly, as is the case for the TLT and the chosen moonquake event. The influence, however, of this parameter on the final check in the calculations is negligible; therefore, a conservative value of $\kappa = 1.0$ is assumed.

$$\overline{F} = 1.0 * \frac{0.73}{tan35^\circ} = 1.06\ kN \qquad limit: 0 < 0.015 \leq (1 - 0.21 * 1.06)^1 = 0.78$$

This then makes it possible to check the seismic bearing capacity using 5.12.

$$\frac{(1 - 0.21 * 1.06)^{2.00}(2.57 * 3.74 * 10^{-6})^{2.00}}{(0.015)^{0.7}[(1 - 0.21 * 1.06^{1.22})^{1.00} - 0.015]^{1.29}} + \frac{(1 - 0.44 * 1.06)^{1.00}(1.85 * 3.34 * 10^{-5})^{2.00}}{(0.015)^{2.14}[(1 - 0.21 * 1.06^{1.22})^{1.00} - 0.015]^{1.81}} - 1 \leq 0$$

$$= -1.0 \leq 0$$

Therefore, the bearing capacity in the seismic situation with the input loads described in Table 5.1, excluding second-order effects, is sufficient.

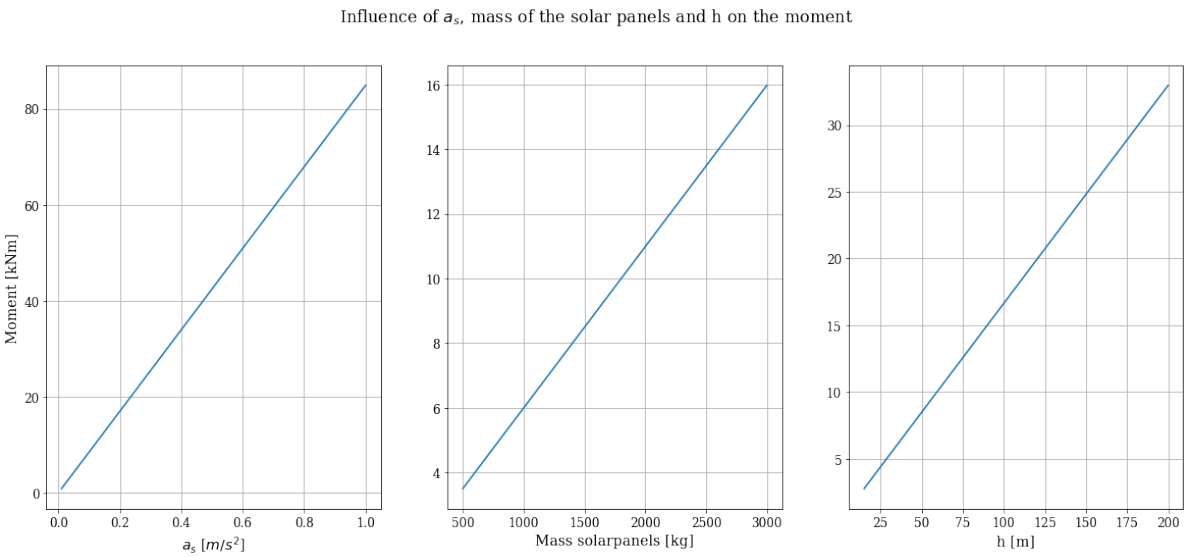

Figure 5.2: The influence of the structural acceleration a_s, the mass of the solar panels, and the height of the tower h on the moment load. The ranges of the parameters are chosen based on possible design configurations or estimated uncertainties in the parameters.

Rotational failure

Rotational failure can be checked by applying vertical and moment loads to determine if tensile stresses are occurring at the bottom of the foundation. Here, the foundation is assumed to be the end of a beam loaded in compression and bending.

$$\sigma_N = \frac{-363}{49} = -7.41\ kPa$$

$$\sigma_M = \frac{M_d * 1/2 * B}{\frac{1}{12} * B * B^3} = \frac{8.5 * 1/2 * 7}{1/12 * 7 * 7^3} = \pm 0.15\ kPa$$

With the vertical stress known and the maximum stress due to the bending moment at the edge of the foundation known, the stresses at both ends of the foundation were calculated using 5.17.

$$\sigma_{LEFT} = -7.41 + 0.15 = -7.26\ kPa \qquad \sigma_{RIGHT} = -7.41 - 0.15 = -7.56\ kPa$$

This indicates, however, that already the entire cross-section experiences compressive forces. Therefore, the foundation experiences no loss of contact, and the risk of rotational failure is low.

5.1.4. Discussion

The parameters for the structural acceleration a_s, the mass of the solar panels and the height of the tower have an influence on the seismic loads posed on the system. Especially the generated horizontal force is influenced by the acceleration of the structure, and this force is again responsible for generating a moment on the foundation.

The different parameters cannot be compared with each other, since they all use different units. However, when varying these design parameters within a considerable limit, the influence on the moment load and thus the foundation configuration is visualised.

The influence of these three parameters is shown in Figure 5.2. The variations of all parameters are based on estimated variations of the parameters. Varying these parameters all result in an increase in the moment load. The rate of increase, however, differs per parameter. This effect is shown on the boxplot in Figure 5.3.

The influence of a_s is mainly through the horizontal force, which increases linearly with an increase in structural acceleration. This horizontal force then generates a force by accelerating the tip mass of the structure, generating a moment on the foundation through multiplication by the height of the tower. With small variations in structural acceleration, the moment can increase considerably. A variation in the mass of the solar panels does not result in a significant increase in the moment load compared to

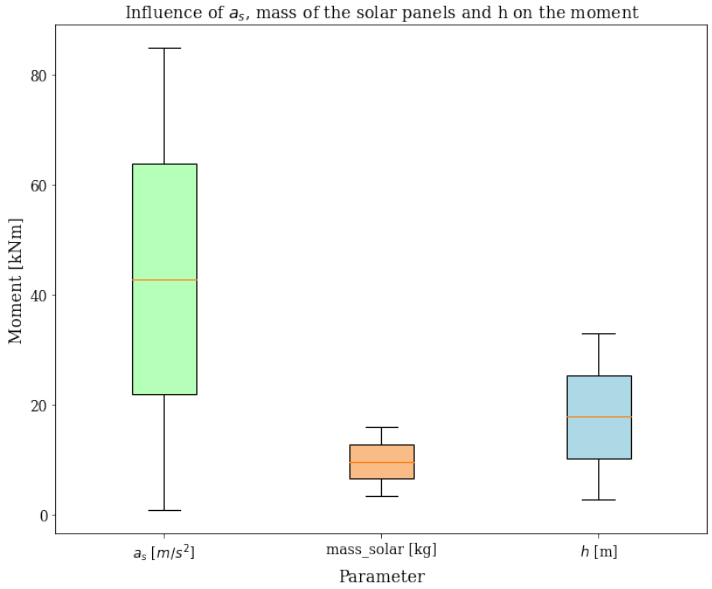

Figure 5.3: The influence of the structural acceleration a_s, the mass of the solar panels, and the height of the tower h on the moment load presented in a boxplot. The ranges of the parameters are chosen based on possible design configurations or estimated uncertainties in the parameters. For a_s the range is: $0.01 - 1.0\ m/s^2$, for the mass of the solar panels: $500 - 3000\ kg$ and for the height h: $15 - 200\ m$.

a slight increase in acceleration. Lastly, the height of the structure has a greater influence than the mass of the solar panels. This is logical, since it enlarges the arm of the moment. However, it is likely that the influence of height diminishes with larger foundations, since the centre of mass quickly moves lower. The foundation causes most of the weight on the lunar surface in those scenarios as described by Figure 4.6. This effect could be incorporated into future analyses to more accurately describe the influence of height. It is concluded that these parameters all influence the moment load, resulting in different foundation configurations.

When zooming in on the dimensionless inertia force, the effect of the horizontal seismic coefficient α_h and the internal friction angle ϕ_d was investigated. These effects are plotted in Figure 5.4. When α_h increases, $\overline{F}$ also increases. Since these have a linear correlation, this is logical. The more acceleration is present, the more inertia. When looking at the influence of ϕ_d, a different effect is observed. For increasing values of inertial friction angle, $\overline{F}$ reduces. This is expected, as with stronger soil, the forces can be more easily resisted. The lunar regolith has a large internal friction angle; therefore, the lunar underground has a positive effect on reducing the inertia forces generated by a moonquake.

In the seismic scenario, a horizontal force is present. This causes potential sliding behaviour. The risk of sliding for different foundation sizes compared to the present horizontal force can be seen in Figure 5.5. The resistance against sliding increases with larger foundations and larger depths. This is reasonable, since a wider foundation has more area to increase sliding resistance, and deeper foundations have more area to provide resistant forces on the sides, and provide a larger passive earth pressure. The sliding resistance with the given horizontal force is less than the sliding resistance provided by even small foundation elements.

However, as the input structural acceleration a_s changes, so does the horizontal force connected to it as shown in Figure 5.6. The horizontal force increases. This indicates that with larger a_s, the risk of sliding becomes bigger. Therefore, the determination of the structural acceleration should be done with care.

When comparing the sliding behaviour of the foundation with that of a foundation on Earth for a similar structure, using Earth's gravity instead of the microgravity present on the Moon, the larger vertical loads result in an increase in sliding resistance. This effect is visualized in Figure 5.7. A similar pattern as on the moon is visible on Earth, where the sliding resistance increases as the foundation

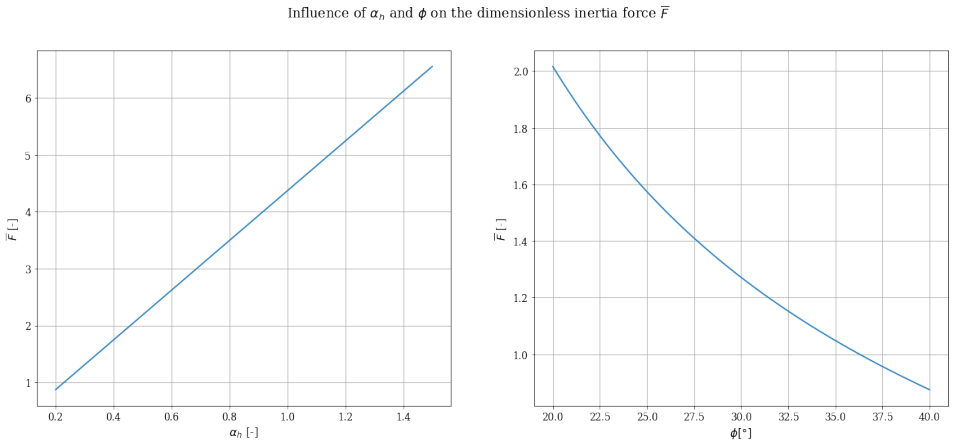

Figure 5.4: The effect of increasing the horizontal seismic coefficient α_H and the internal friction angle ϕ_d on the dimensionless inertia force $\overline{F}$. With a greater acceleration, the inertia effect is stronger. When the soil is able to resist inertia more easily, the force decreases.

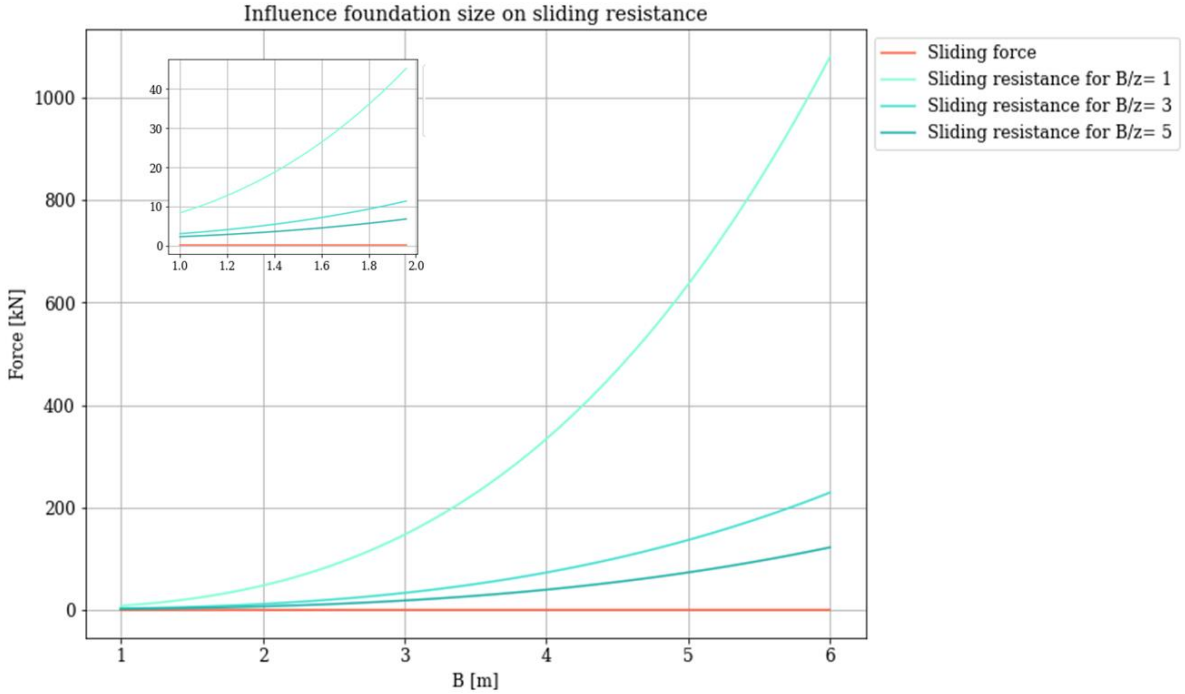

Figure 5.5: The sliding force plotted against different sliding resistances for foundation configurations. The width of the foundation varies, and the lines represent different ratios for the foundation that determine its depth. When the foundation size increases, the sliding resistance increases. This is the result of the larger area available to resist the sliding force and the greater passive earth pressure generated by the same effect.

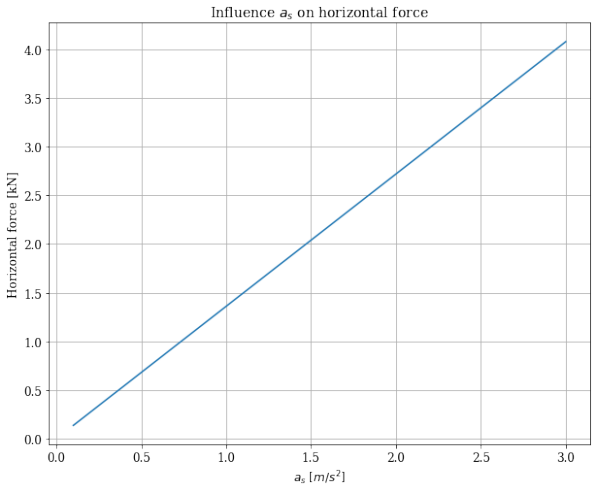

Figure 5.6: The increase in the horizontal force as the structural acceleration a_s increases. The horizontal force typically remains small; however, the sliding resistance may be compromised with larger horizontal forces.

size increases. This indicates that microgravity has a negative effect on the risk of sliding for shallow foundations.

Now that horizontal forces and moments are involved, the risk of rotational failure becomes a significant concern. When varying the size of the foundation, in the seismic loading case, only small foundations are at risk of losing more than 33 % of the contact. This effect can be seen in Figure 5.8. With a small foundation, these forces need to be divided over a small area. With a small foundation, there is less vertical weight present to counter the movement of the structure.

When looking at a smaller foundation to investigate the relationships of different parameters that influence the seismic load, it can be seen in Figure 5.9 that increasing a_s, the mass of the solar panels, and the height, all increase the risk of rotational failure, as all these parameters have a direct influence on the moment load. What is of interest is that the influence of a_s quickly leads to an exceedance of the rotational limit even with small deviations. The speed at which the loss of contact increases decreases as the mass of the solar panels and their height increase. The small deviations result in a rapid increase in the risk of contact. This is logical, since the loads on the foundation increase with these parameters, and small foundations are then prone to rotating for the reasons described above. When the moment then becomes even bigger, when using the preliminary method described in section 5.1.2, the loss of contact can only reach a maximum of 50 %, as the moment needs to be divided over two halves of the foundation.

When summarizing the different failure mechanisms in the seismic scenario, the resulting foundation configurations for the seismic scenario are represented in Figure 5.10. Larger foundation configurations are necessary compared to the static load situation alone.

To demonstrate the influence of microgravity on the seismic load situation, configurations for Earth's gravity with the same input parameters as described above were determined. The result can be seen in Figure 5.11.

Within a microgravity environment, there is less gravitational force to slow down the object's inertia; therefore, this effect is likely to be reflected in the dimensionless soil inertia force, as this value is dependent on Earth's gravitational constant through α_H. This horizontal seismic coefficient becomes smaller, resulting in a smaller dimensionless inertia force compared to the situation on the Moon. This is logical, since the acceleration on Earth is six times larger than the acceleration on the Moon, and the horizontal seismic coefficient is divided by this value. As shown before in Figure 4.13, there is a larger foundation necessary for the situation on Earth, due to the increase in forces. The forces and bearing capacity are impacted by the change in gravity, leading to smaller $\overline{N}$, $\overline{V}$ and $\overline{M}$. This combination leads to smaller values for the bearing capacity check in 5.12. This leads to more possible configurations

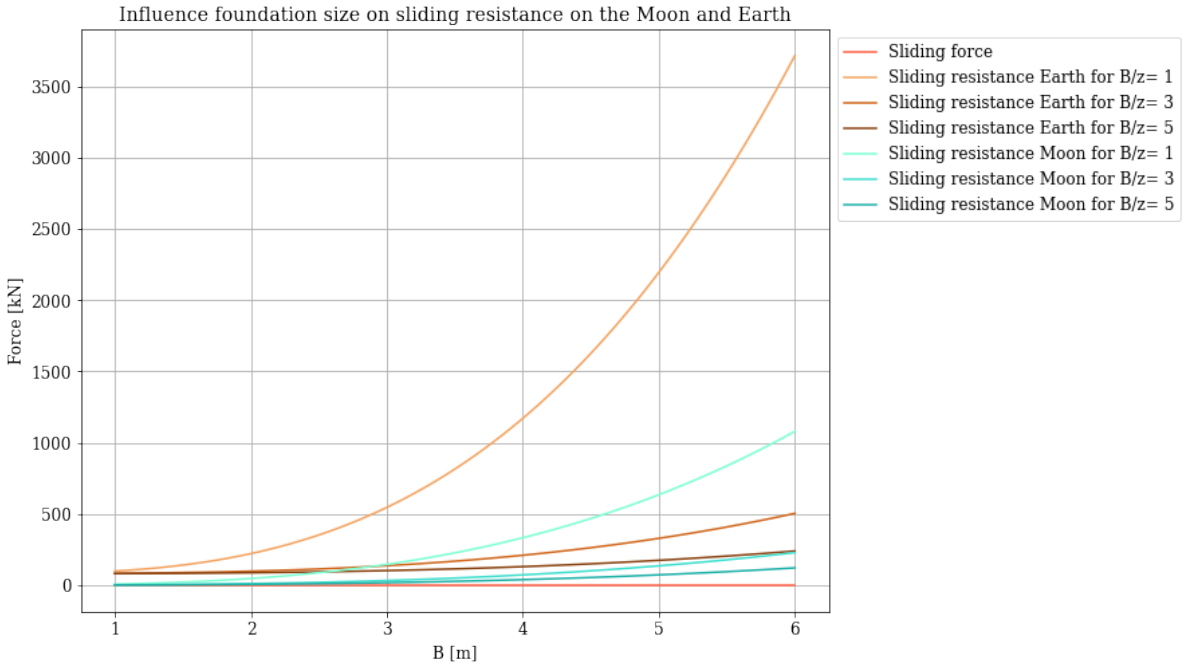

Figure 5.7: The comparison of the sliding resistance on Earth and on the Moon. On Earth, the sliding resistance is larger due to the greater vertical forces exerted by Earth's gravity, whereas the sliding resistance on the Moon is lower in the microgravity environment. The microgravity thus has a negative influence on the sliding resistance. Furthermore, the same increase in sliding resistance with size is observed on the analysis in Earth's gravity as the one in the Moon's microgravity.

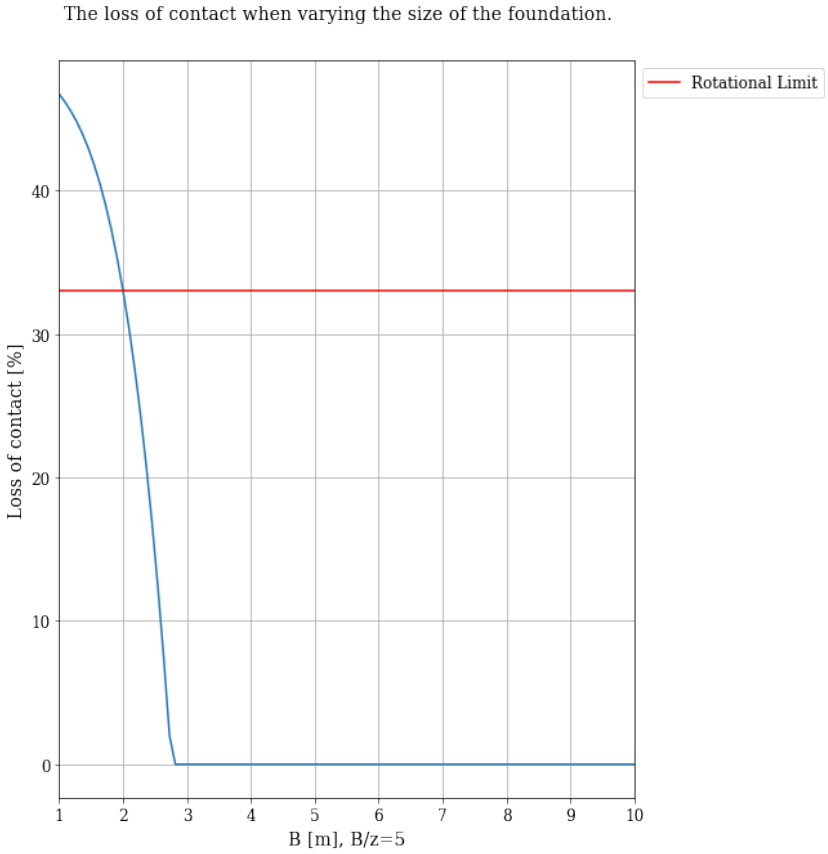

Figure 5.8: The rotational failure for different widths of the foundation. A limit of 33% contact loss is prescribed by the Eurocode to prevent rotational instability. For smaller foundations, therefore, the risk of rotational failure is higher, due to the lack of vertical mass and the moment that needs to be divided over a smaller area.

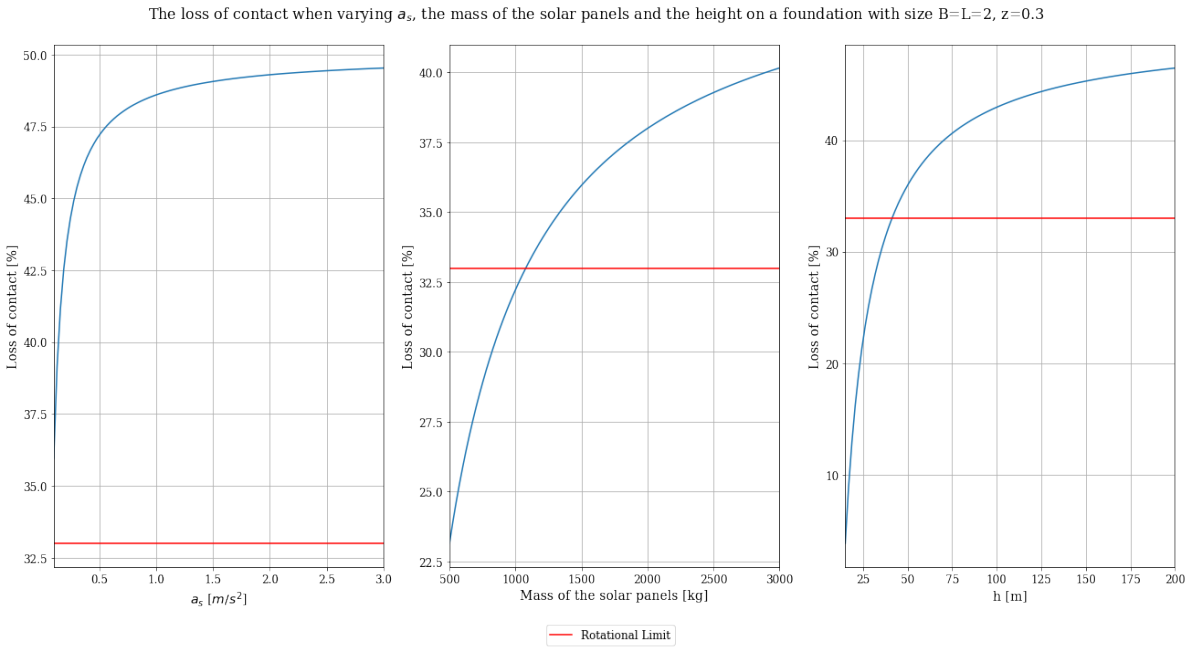

Figure 5.9: The influence of horizontal ground acceleration a_s, the mass of the solar panels, and the height h on the loss of contact. A limit of 33% contact loss is prescribed by the Eurocode to prevent rotational instability and is presented by the red line. An increase in these parameters results in extra moment loads on a small foundation, quickly increasing the risk of rotational failure. Due to the methodology used, only a maximum of 50 % of loss of contact can be reached, as the moment needs to be divided over two halves of the foundation.

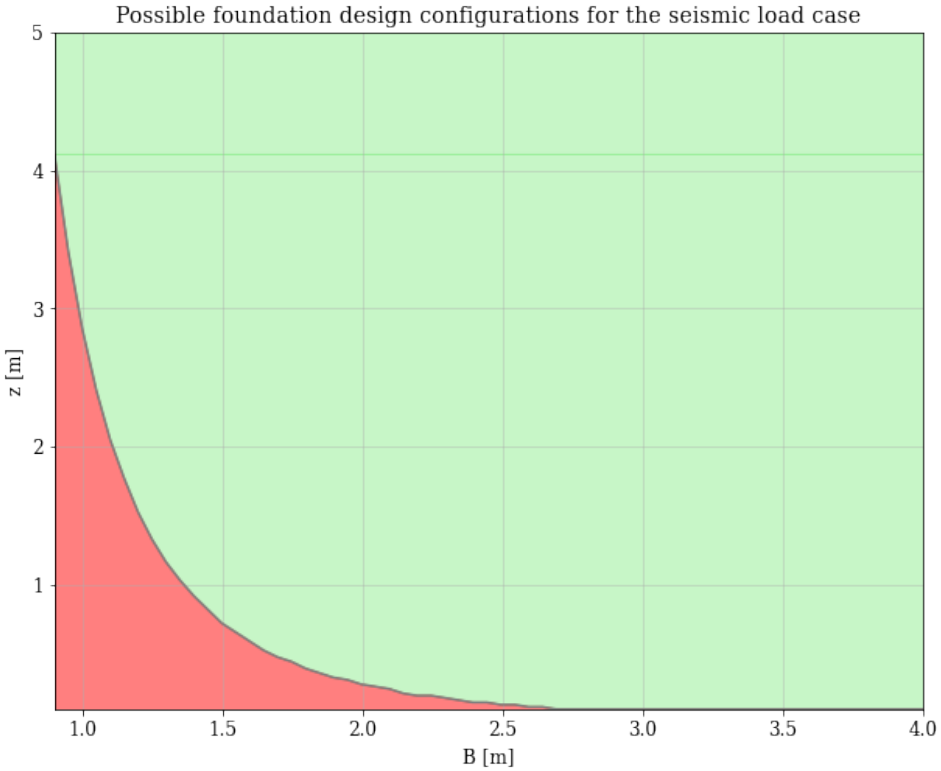

Figure 5.10: The foundation configurations possible for the seismic loading case as described in Table 5.1. The width of the foundation needs to be larger than that required for only static loads. The red area shows foundation configurations that lead to failure, while the green area shows safe configurations that can be used to choose a proper foundation format.

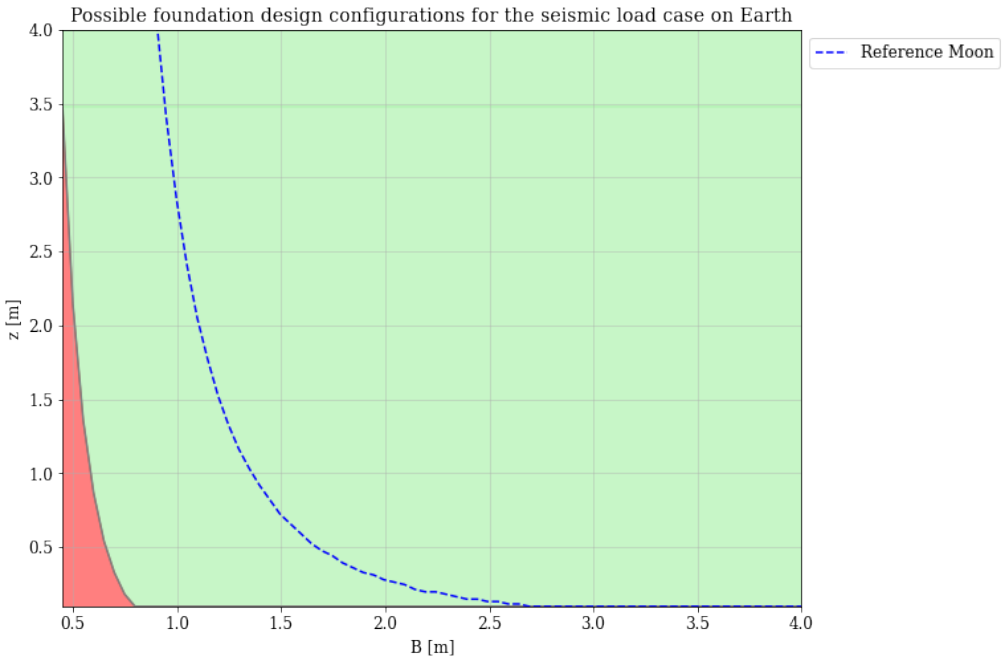

Figure 5.11: The design configurations for the seismic load case, as described in Table 5.1 on Earth. This illustrated the impact of microgravity on possible foundation configurations. Microgravity impacts inertia, as there is less gravitational force to slow down objects. Therefore, microgravity has a negative impact on foundation configurations.

and less risk of exceeding the seismic bearing capacity. Microgravity, therefore, has a negative impact on the seismic bearing capacity.

5.2. Seismic analysis - with second order effects

5.2.1. Overview

When the tip of the tower is displaced due to a seismic excitation, an extra moment is generated due to the second-order effect. To calculate this extra moment, the displacement of a simple clamped cantilever beam with a force applied on one end is assumed, as visualised in Figure 5.12. In Table 5.2, the extra displacement and increased moment are described.

Parameter	Description	Calculation	Value
w	The maximum displacement of the top of the tower.	$\frac{Fl^3}{3EI} = \frac{0.16*50^3}{3*70*10^6*2.21*10^{-4}}$	0.44 m
M_d	The moment load.	$Hd*(h+z)+(m_{TLT}+m_{solar})*g_{moon}*w = 0.16*(50+2)+(200+1500)*1/6*9.81*0.44$	1230 kNm

Table 5.2: The extra parameter and load needed for the calculation of the second-order effect in the seismic loading case. Includes the definition, calculation and final value.

The methodology for this analysis is the same as described in section 5.1.2.

5.2.2. Results

Only the bearing capacity and the risk of rotational failure change due to the addition of an extra moment load. The settlements would also change, but as concluded above, there is a lack of information on the cyclic behaviour of lunar regolith.

Exceedance bearing capacity

The bearing capacity changes due to the addition of an extra moment, resulting in a new term for the seismic bearing capacity.

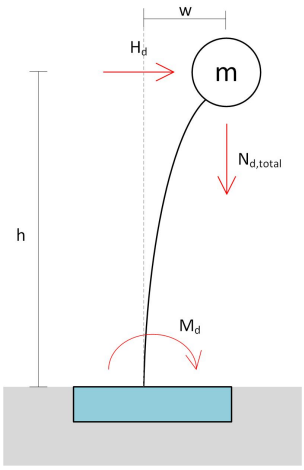

Figure 5.12: The seismic load case with the second-order effect on the TLT modelled as a 1D oscillator. This case involves a vertical load and a horizontal force applied at the location of the tip mass, assumed to be the centre of mass of the system. This results in a moment at the base of the tower. However, due to the displacement of the tip mass, the moment load changes as the vertical load now also generates a moment.

$$\overline{M} = \frac{1229.72}{7 * 36330} = 0.0048$$

$$\frac{(1 - 0.21 * 1.06)^{2.00}(2.57 * 3.74 * 10^{-6})^{2.00}}{(0.015)^{0.7}[(1 - 0.21 * 1.06^{1.22})^{1.00} - 0.015]^{1.29}} + \frac{(1 - 0.44 * 1.06)^{1.00}(1.85 * 0.0048)^{2.00}}{(0.015)^{2.14}[(1 - 0.21 * 1.06^{1.22})^{1.00} - 0.015]^{1.81}} - 1 \leq 0$$

$$-0.44 \leq 0$$

With the chosen foundation dimensions, the seismic bearing capacity in this analysis is sufficient. As can be seen, the seismic situation with the second-order effect is the governing design situation, characterised by the largest loads on the foundation.

Rotational failure

$$\sigma_N = \frac{-363}{49} = -7.41\ kPa \tag{5.20}$$

$$\sigma_M = \frac{M * 1/2 * B}{\frac{1}{12} * B * B^3} = \frac{1230 * 0.5 * 7}{\frac{1}{12} * 7 * 7^3} = \pm 21.52\ kPa$$

The stresses at both end of the foundation can now be calculated:

$$\sigma_{LEFT} = -7.14 + 21.52 = +14.38\ kPa \qquad \sigma_{RIGHT} = -7.14 - 21.52 = -28.66\ kPa$$

This means that on one side of the foundation, the compressive force becomes a tensile one, and therefore, there is a loss of contact. The percentage of loss was calculated with 5.18 and 5.19.

$$\Delta_\sigma = (7.14 + 28.66)/7 = 6.15\ kPa/m$$

$$d_{nocontact} = \frac{14.38}{7 * 6.15} * 100 = 32.78\%$$

This indicates that there is a considerable risk of rotational failure in a seismic situation with second-order effects, since the percentage of no contact is very close to the limit of 33%. It is advised to analyze this behaviour in a numerical simulation to verify the risk more accurately

5.2.3. Discussion

Just as in the seismic situation, the structural acceleration a_s has an influence on the seismic loads of the system. In Figure 5.13, the influence of a_s on the second-order displacement based on the force caused by the acceleration on the tip mass of a cantilever beam is shown. The displacement quickly becomes quite significant for a tower of only 50 meters in height. The moment caused by this displacement is visualised, and the direct effect of a structural acceleration on the moment is shown. Even with small structural accelerations, the moment load becomes considerably large. The second-order effect is therefore the most significant compared to the static load case and the seismic load case, where this effect is not considered. This moment needs to be countered by the lunar regolith.

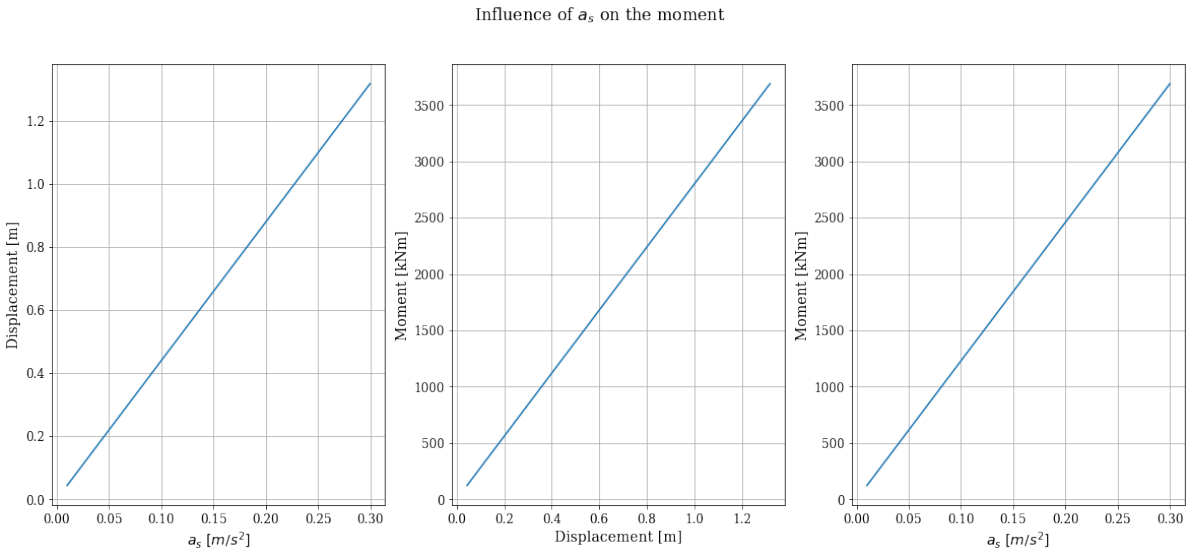

Figure 5.13: The influence of the structural acceleration a_s on the moment load generated by the second-order effect. Even with small accelerations, significant displacements occur, resulting in large moments on the foundations.

When using the larger second-order effect as input to calculate the foundation configurations, the result is shown in Figure 5.14. As expected, with a higher horizontal acceleration, a larger foundation width is required to stabilise the structure. When the ratio of foundation depth to foundation width is kept small, the foundation increases in size more quickly and therefore requires less width to provide the necessary mass to withstand the large moment load.

A part of this second-order effect is caused by the behaviour of the structure and its parameters as described in Table 3.2. When varying the material and choosing a material with higher stiffness, the effect on the moment load is visible in Figure 5.15. When choosing a larger stiffness, the displacement goes down. The greater the displacement, the greater the moment; therefore, reducing the displacement leads to a reduction in moment. Increasing the stiffness, therefore, reduces the moment load on the foundation by limiting the second-order displacement.

This effect can also be observed when calculating the required shallow foundation widths for different stiffness values, and can be seen in Figure 5.16. The stiffer the tower, the less wide the foundation has to be to provide enough mass for the system to stabilise. As stated before, the mass of the foundation increases more quickly with smaller width-to-depth ratios, explaining the shift to the right when this ratio grows.

Another parameter of the structure is the height. Increasing the height results in displacements at the top of the tower that quickly reach several meters, significantly affecting the moment load. This effect is shown in Figure 5.17. By increasing the height even slightly, the moment load increases exponentially. This effect is reduced at larger foundation sizes, as the centre of mass of the system moves downward, as explained before. To control the second-order behaviour, a trade-off must be made between required illumination conditions and the size of the foundation.

When plotting the influence of the height of the tower on the necessary foundation width, the width, just as with the increase in the second-order moment load, increases rapidly. This is shown in Figure

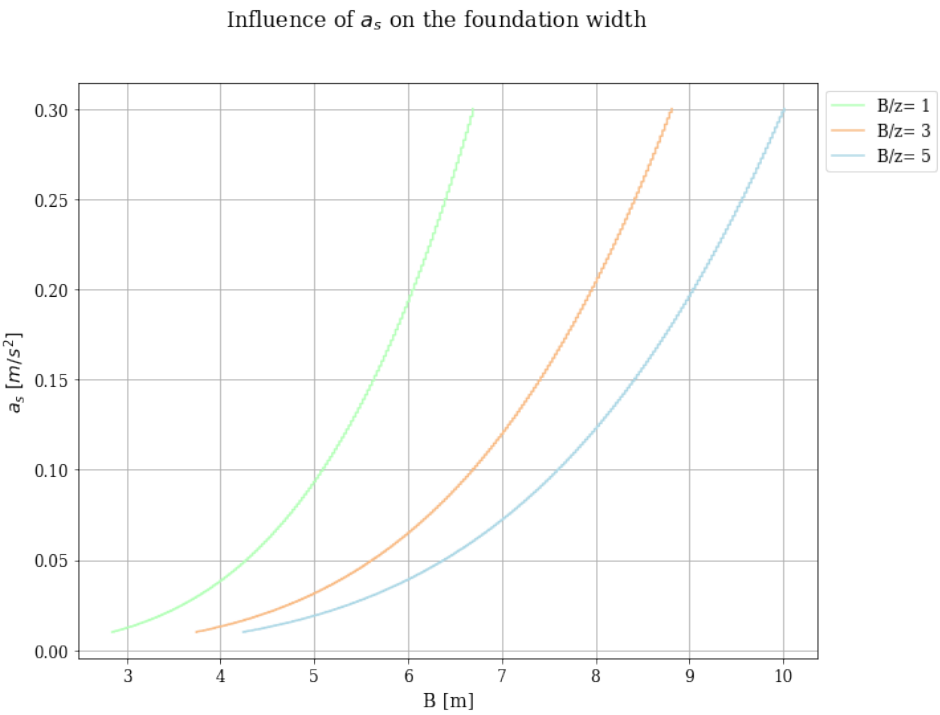

Figure 5.14: The influence of the structural acceleration a_s on the width of the foundation. With increased acceleration, a wider foundation is necessary.

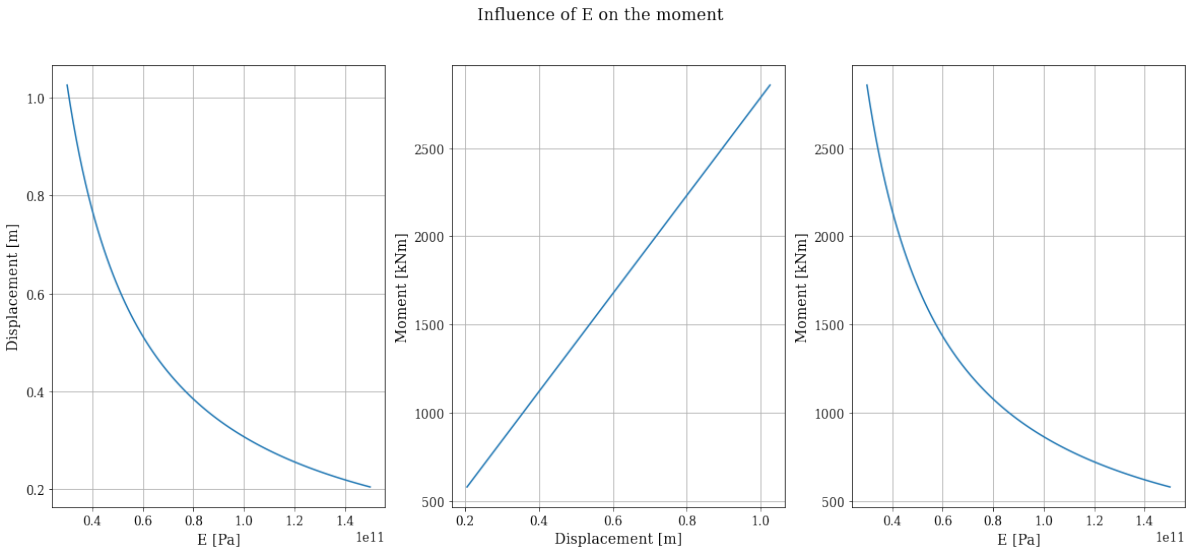

Figure 5.15: The influence of the stiffness E of the tower on the generated second-order moment. With a higher material stiffness, the displacement decreases, and the second-order moment consequently decreases.

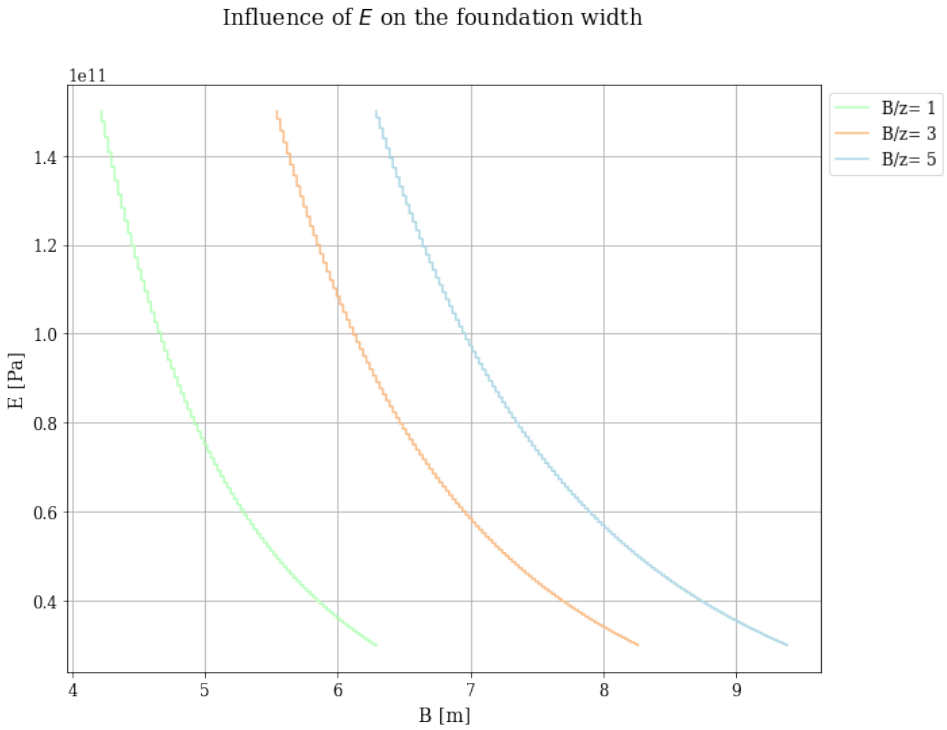

Figure 5.16: The influence of the stiffness E of the tower on the width of the foundation. With increased stiffness, a smaller foundation is required.

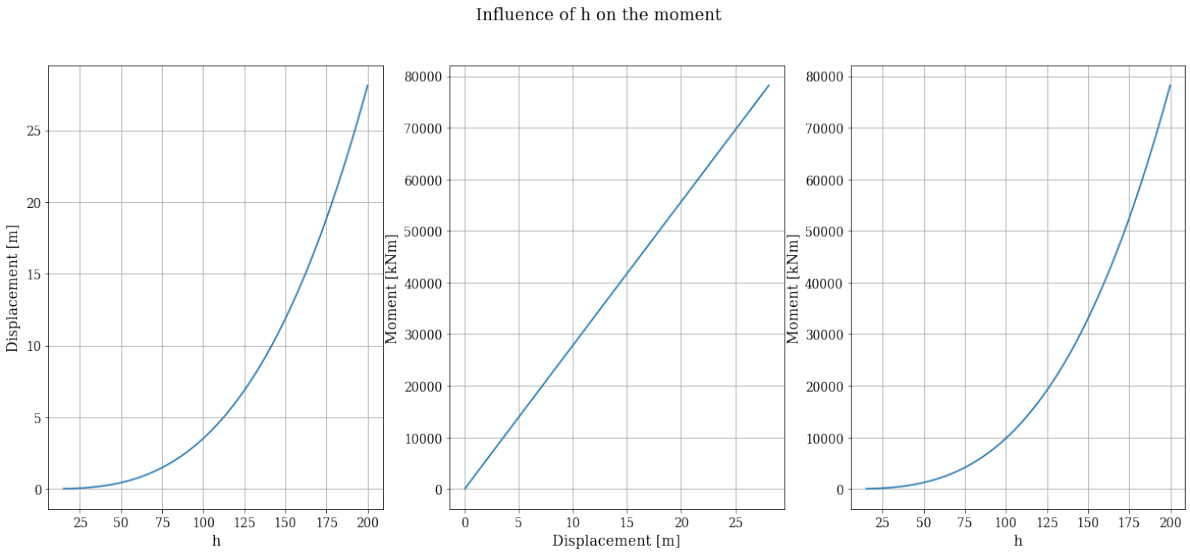

Figure 5.17: The influence of the height h of the tower on the generated second-order moment. With a higher tower, the displacement increases significantly, and therefore, the second-order moment increases.

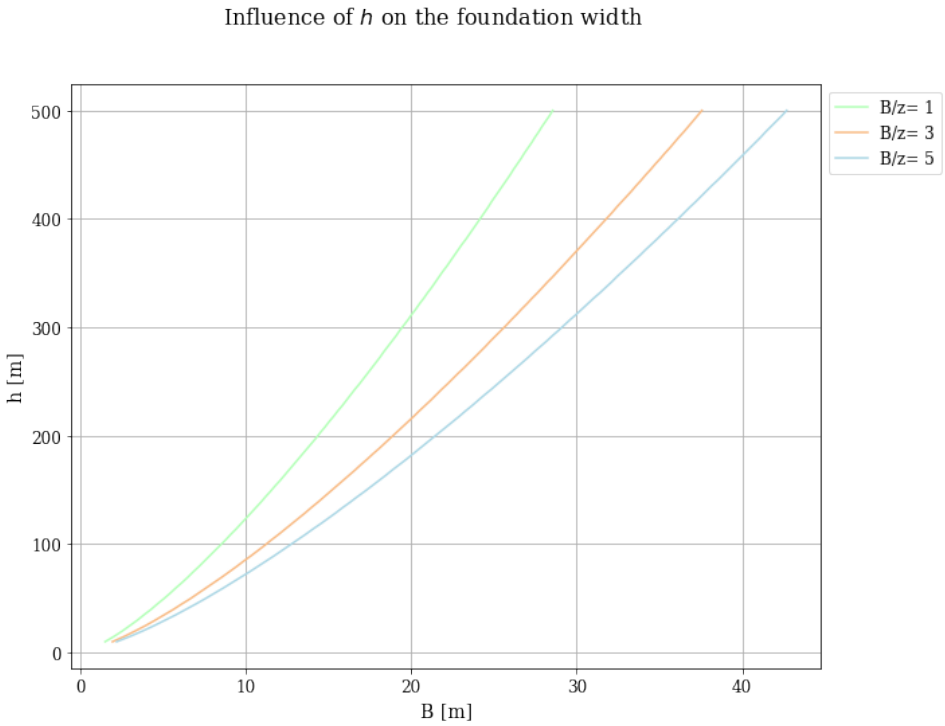

Figure 5.18: The influence of the height h of the tower on the foundation width. With a higher tower, the second-order displacement increases significantly, leading to a wider foundation.

5.18. The foundation width increases to tens of meters as the tower's height is slightly increased. For larger width-depth ratios, even wider foundations are required to provide the stabilising mass for the second-order moment.

As height is directly correlated to the available area for power generation for different illumination levels, as shown in Figure 2.9. For lower illumination levels, the available area is larger for different foundation configurations. With a larger foundation, a higher tower is possible, thereby increasing the area for solar power generation. As higher illumination percentages are required, less area is available to place towers, as confirmed by Ross et al. (2021). For one foundation configuration where depth increases linearly with width, this effect is plotted in Figure 5.20.

The moment of inertia I of the tower itself influences the displacement. As can be seen in Figure 5.21, the greater the moment of inertia, the smaller the displacement of the tip of the tower. The moment, therefore, decreases considerably once a higher moment of inertia is chosen for the profile of the tower. If the design is assumed as stated by Song, Mikulas, et al. (2023) to fall within the limits of a robotic assembly method, the options to vary the profiles and thus the moment of inertia are limited. Whether the second-order effect can be limited by increasing the moment of inertia of the tower depends on future material choices, profile choices, and construction method.

Similarly, for the tower's stiffness, increasing the moment of inertia reduces the required foundation width. This effect is visualised in Figure 5.22. As shown, the required foundation width decreases when a higher moment of inertia is used for the tower structure. This can be influenced in the design phase to balance foundation size and tower parameters.

Lastly, the mass of the solar panels can be varied to see the effect on the second-order effect (see Figure 5.23). Varying this parameter increases the horizontal force, and consequently, the moment on the foundation. Again, the second-order effect is considerably enlarged by an increase in the mass of the solar panels. This increase necessitates a larger foundation configuration. The mass of the solar panels is ultimately a choice based on the amount of solar energy required to be generated. However, this needs to be balanced with the amount of material that needs to be produced for a foundation.

As before, when plotting the mass of the solar panels versus the then required width of the foundation, an increase can be observed in Figure 5.24. The heavier the solar panels, the larger the second-order effect, and thus the larger mass of the foundation required to stabilise the structure. As before,

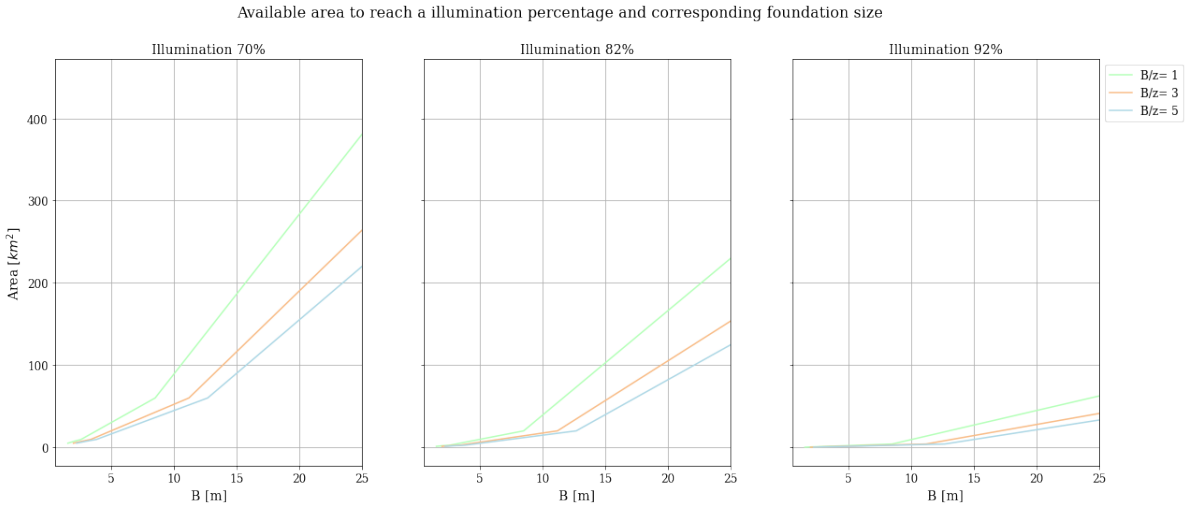

Figure 5.19: The available area for solar power generation on the Connecting Ridge for different foundation widths, ratios, and different illumination percentages.

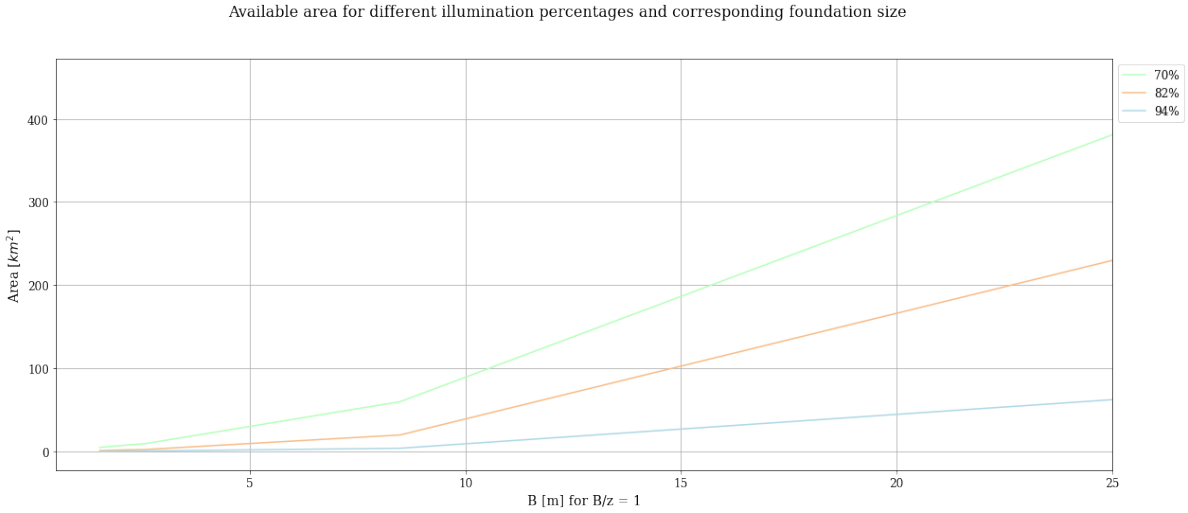

Figure 5.20: The available area for solar power generation, for different widths of a foundation with size B/z = 1 for the illumination percentages of 70%, 82% and 94%.

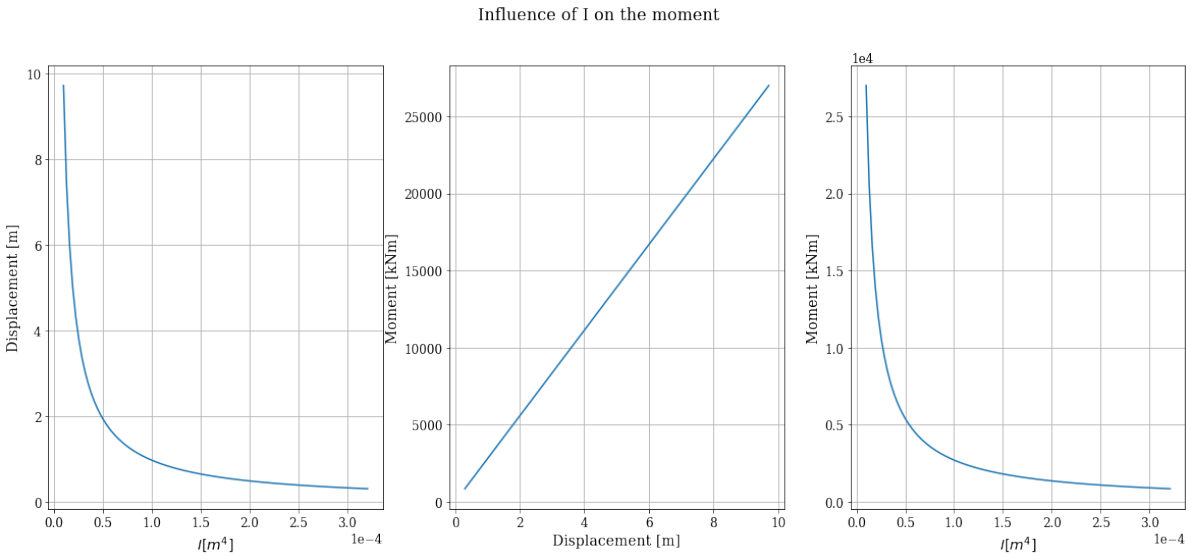

Figure 5.21: The influence of the moment of inertia I of the tower on the generation of a second-order moment. When the moment of inertia becomes larger, the displacements are, as a result, lower. This results in the second-order moment also becoming lower.

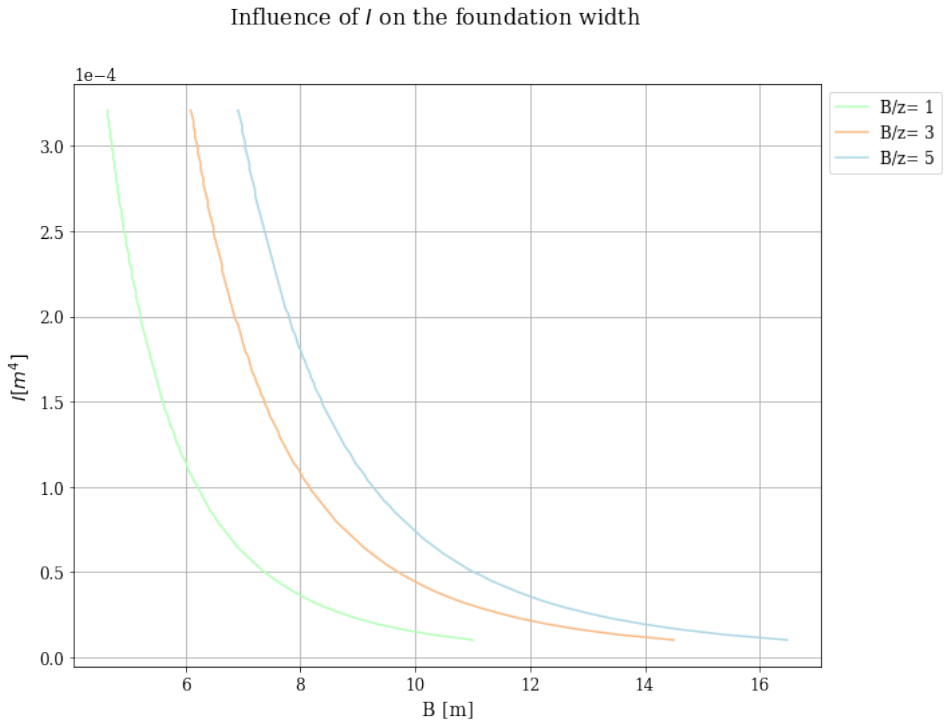

Figure 5.22: The influence of the moment of inertia I of the tower on the width of the foundation. With an increased moment of inertia, a smaller foundation is required.

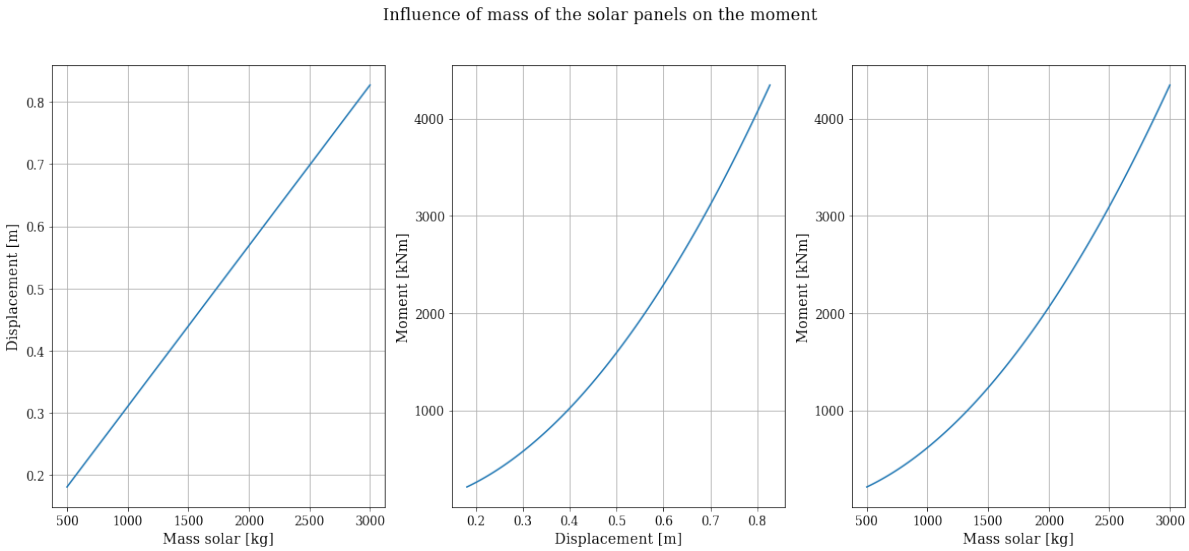

Figure 5.23: The influence of the mass of the solar panels on the generation of a second-order moment. As the mass of the solar panels increases, the displacement and, consequently, the second-order moment also increase.

when the ratio between width and depth of the foundation decreases, the mass increases more quickly; therefore, the smallest ratio requires the smallest foundation.

The influence of the structural acceleration a_s, the mass of the solar panels, and the height h of the tower on the seismic load case without second-order effects can be compared with the seismic load case that includes second-order effects. The influence of these parameter changes is visualised in Figure 5.25 on the generated moment load, as this is directly correlated to the foundation width. For a_s the range is: $0.01 - 1.0\ m/s^2$, for the mass of the solar panels: $500 - 3000\ kg$, and for the height h: $15 - 200\ m$, exactly the same as before. It can be seen that the influence of a_s has become smaller compared to the influence of the height. This is due to the displacement factor in the moment load. The displacement scales to the power of three with height, where the horizontal force only scales one-to-one with the displacement, where the horizontal force consists of the mass of the solar panels multiplied by the structural acceleration.

When comparing both the seismic load case without and with second-order effect in the same plot, Figure 5.26 is the result. For the same variations of these parameters, the plots with the second-order effects have an immense increase in moment load with the same variation through the second-order effect. The seismic situation without the second order reduces to a single line. Therefore, the second-order situation is the most governing situation, and the influence of the second-order effect is considerable. If, in the future, the towers need to increase in height, the design should be adapted to support these giant moment loads on the foundation.

The risk of rotational failure for the foundation configuration described in Figure 3.4 was investigated and the results can be seen in Figure 5.27. The loss of contact for smaller foundations exceeds the limit, calculated by dividing the width by five. Only larger foundations can withstand the large moment loads. With small increases in horizontal seismic acceleration a_s, the risk of rotational failure becomes significant. There is more leeway for the mass of the solar panels, but these also quickly pass the rotational limit for more solar panels. Increasing the height quickly results in the 50% limit being approached. This is all a result of these parameters quickly increasing the moment load through the second-order effect.

The risk of rotational failure, therefore, becomes problematic even with small deviations in the parameters. It is recommended to consider reducing moment loads by adjusting structural parameters or exploring alternative methods to minimise foundation size. It is also emphasised to model the structure and foundation to accurately assess the risk of rotational failure.

The final configuration for the seismic load case with second-order effects is presented in Figure 5.28. Compared to the static load case and the seismic load case without second-order effects, this

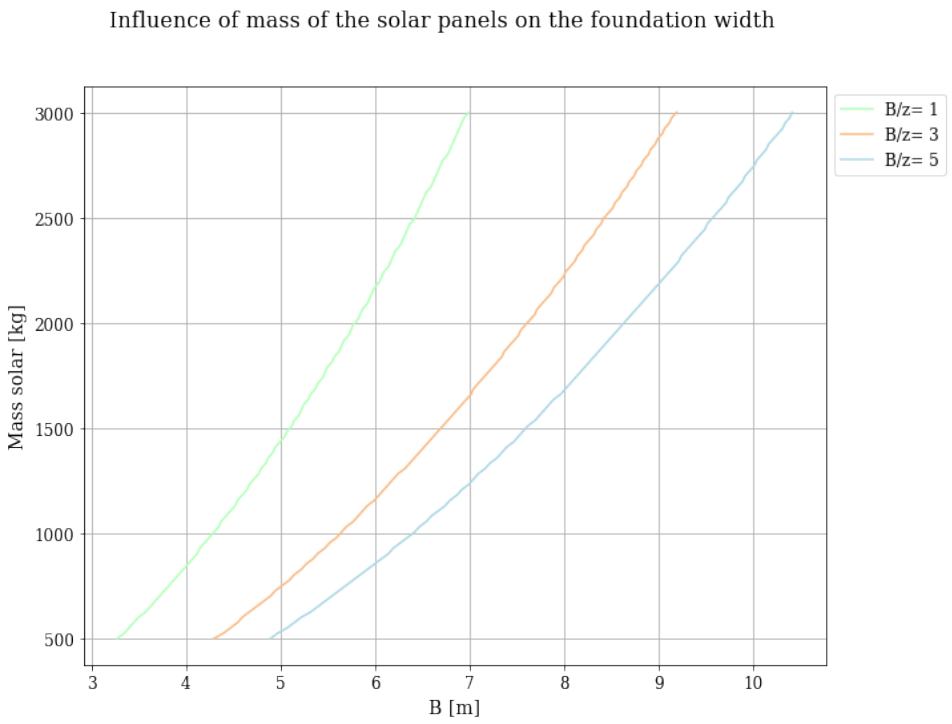

Figure 5.24: The influence of the mass of the solar panels on the width of the foundation. Increasing the mass of the solar panels requires a larger foundation.

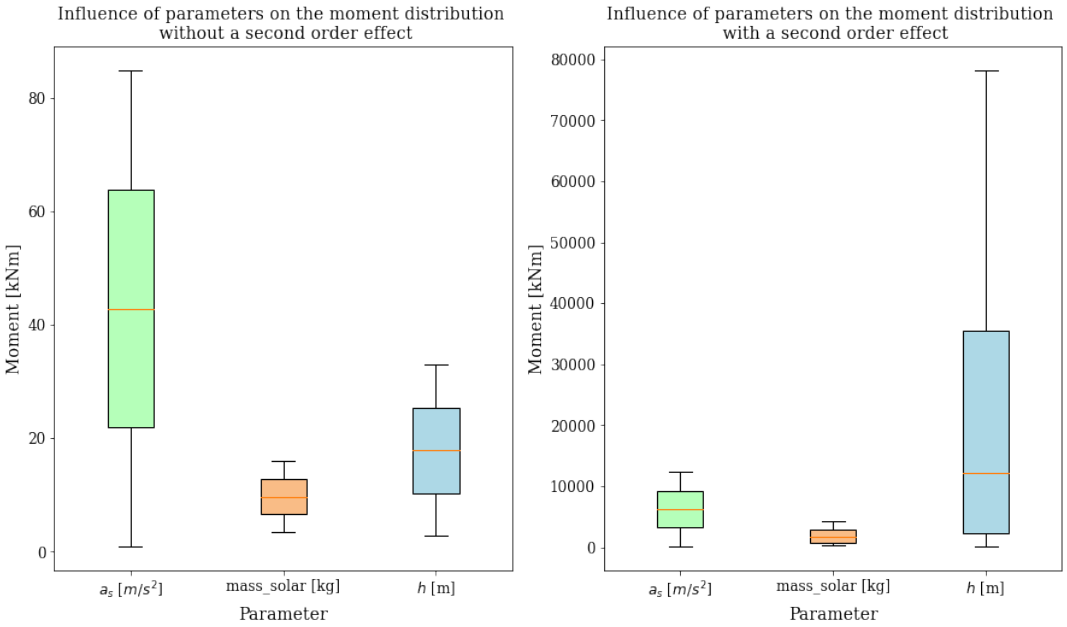

Figure 5.25: The influence of the structural acceleration a_s, the mass of the solar panels, and the height h of the tower on the moment load for the seismic load case with and without second-order effects. For a_s the range is: $0.01 - 1.0\ m/s^2$, for the mass of the solar panels: $500 - 3000\ kg$, and for the height h: $15 - 200\ m$. The influence of a_s is smaller in the seismic load case without the second-order effect, where the influence of the height has become considerable through the contribution to the displacement.

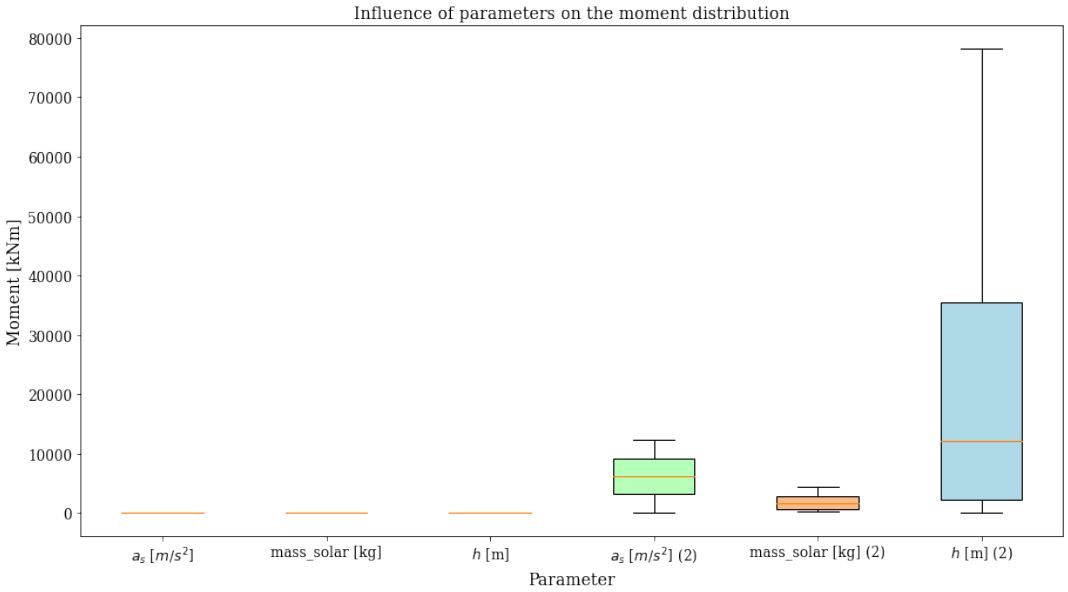

Figure 5.26: The comparison of the influence of the structural acceleration a_s, the mass of the solar panels, and the height h of the tower on the moment load for the seismic load case with and without second-order effects on one axis. For the same variations, the moment generated in the seismic load case with the second-order effect is immense. The influence of the parameters in the normal seismic load case gets even reduced to a single line.

load case needs the largest foundation configurations to support the loads. This is logical, since the loads of the second-order effects are significantly larger when this effect is not taken into consideration.

When examining the effect of microgravity, an interesting phenomenon was observed in Figure 5.29. Microgravity has no effect on the possible configurations for the seismic load case, considering second-order effects. This is likely due to the displacement and horizontal force not being generated by the gravitational acceleration, but rather by the acceleration of the moonquake event. Therefore, only the vertical force is impacted by the microgravity. This force has a minimal impact on the seismic bearing capacity of the structure, as the governing load is generated by the displacement-induced moment. Therefore, microgravity has a negligible effect on the design configurations when considering second-order effects.

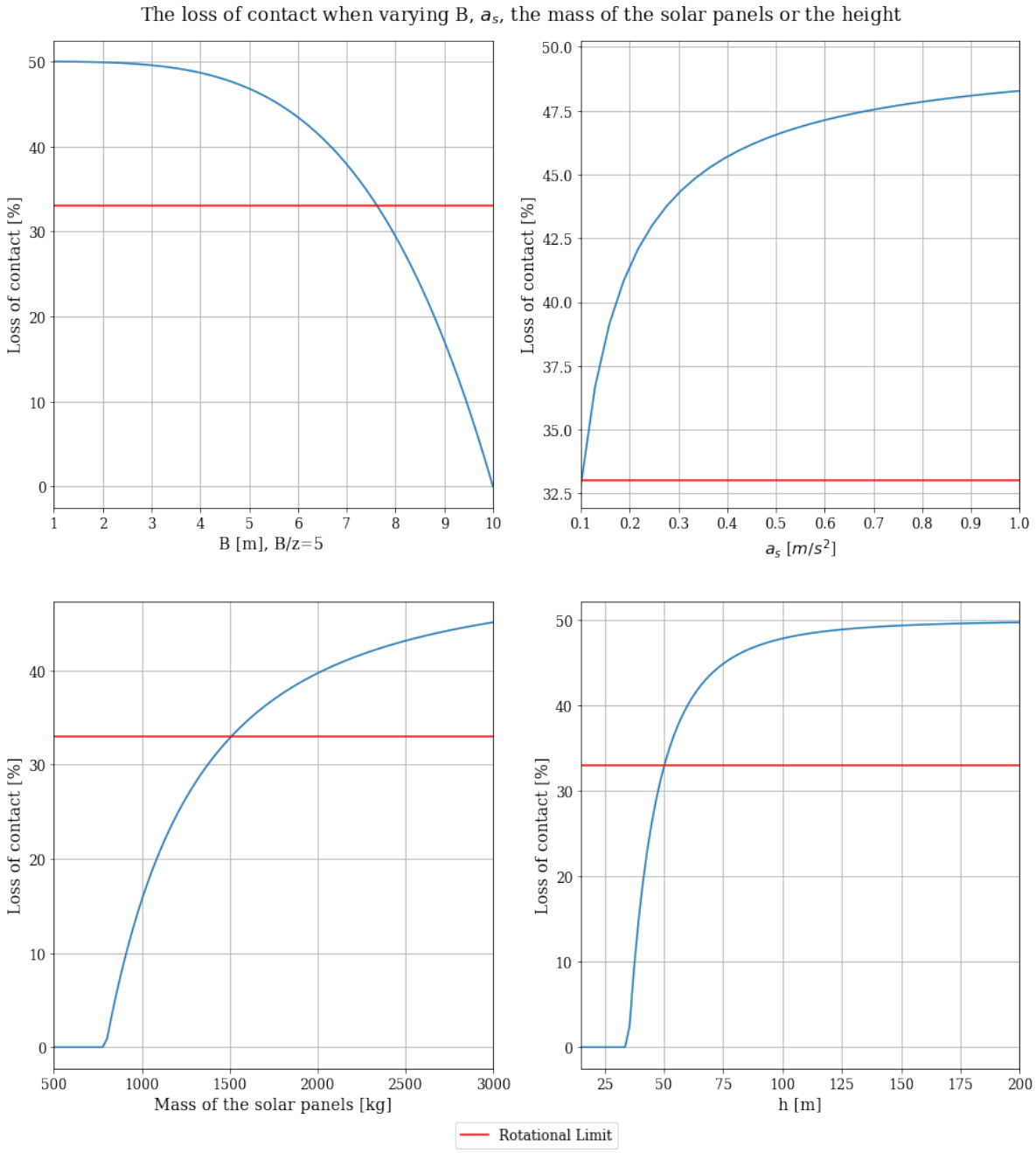

Figure 5.27: The influence of varying the size, horizontal seismic acceleration a_s, the mass of the solar panels, and the height h on the loss of contact, indicating a risk of rotational failure. Only large foundations can withstand the loads. The other influences were plotted based on the size in Table 3.4. Deviations in a_s have a significant influence on the risk of rotational failure, where the loss of contact by increasing the mass of the solar panels increases more slowly, and increasing height quickly leads to approaching the limit value of 50%. The influence of these parameters is primarily through the generation of the second-order moment.

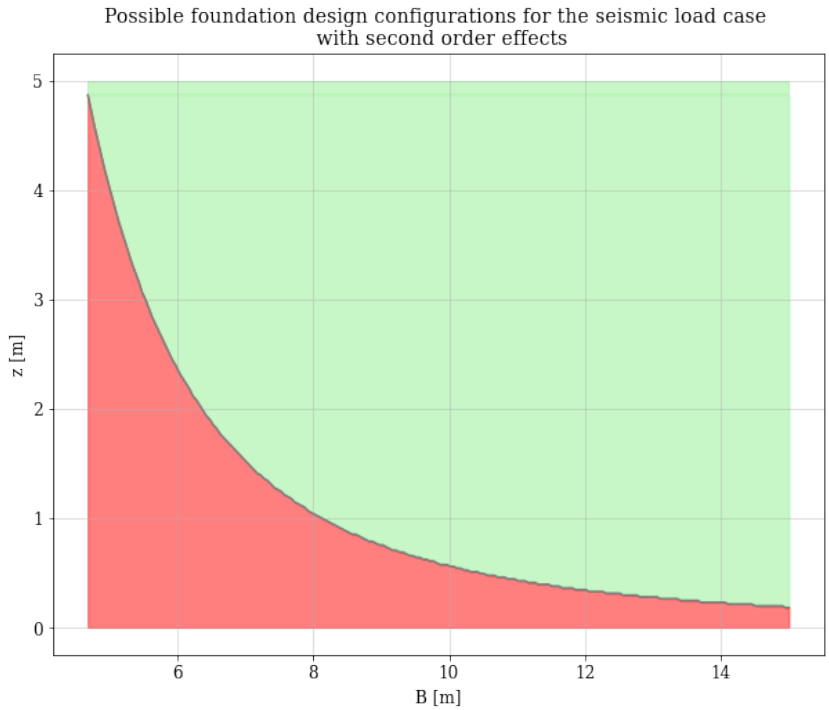

Figure 5.28: The foundation configurations possible for the seismic load case, including second-order effect as described in Table 5.2. The size of the foundation needs to be larger compared to the static and normal seismic load case. The red area indicates foundation configurations that lead to failure, while the green area indicates safe configurations that can be used to select a suitable foundation format.

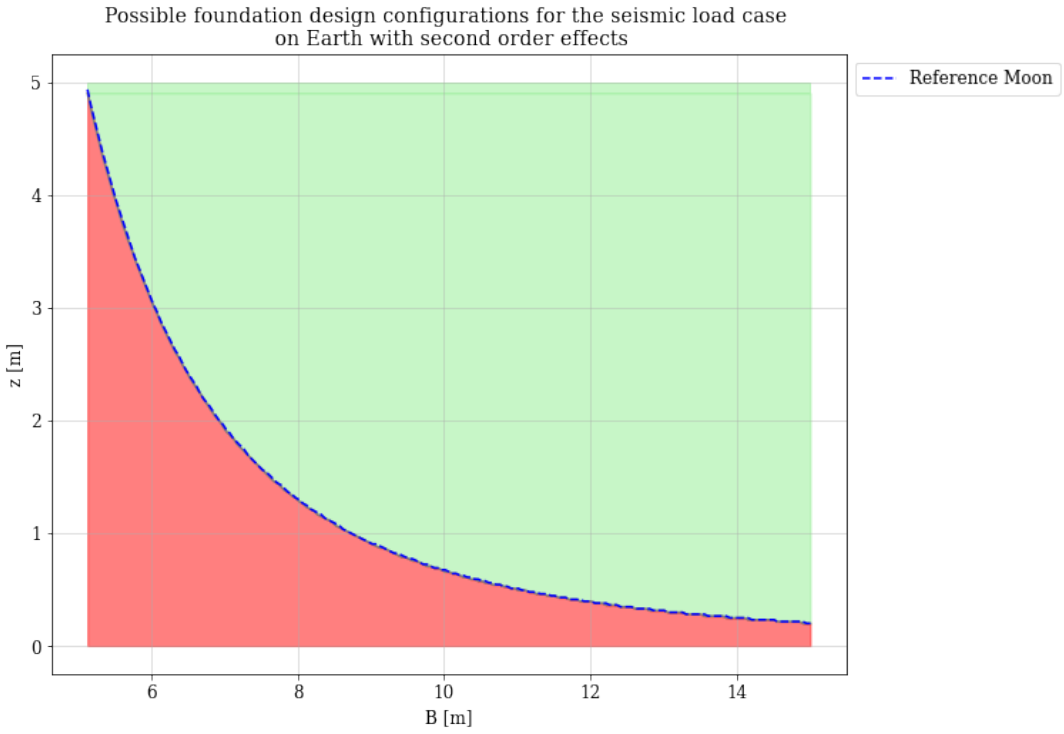

Figure 5.29: The design configurations for the seismic load case, including the second-order effect as described in Table 5.2. This illustrates the impact of microgravity on possible foundation configurations. The reference line of the situation on the Moon is the same as the grey line, which marks the beginning of viable foundation configurations on Earth. This is the result of the displacement and horizontal force being generated by the structural acceleration, rather than the gravitational acceleration.

6

Final Design

6.1. Final Design Configuration

When all parameters are taken into account as given by Table 3.3, 3.2, 4.1, 5.1, 5.2 and material properties and slope as defined in Table 3.4, the results for all failure mechanisms and foundation configurations are summarized by Figure 6.1. To ensure complete safety for all load cases, a foundation configuration should be chosen within the blue area.

For a foundation with the size as described in Table 3.4, the checks for all failure mechanisms are summarised in Table 6.1 for the governing failure mechanisms. This foundation is sufficient and, therefore, able to provide stability and resist microgravity and moonquake loading.

6.2. Material options

After determining the feasibility of a shallow foundation, some suggestions are made for the possible material configurations based on the obtained information in Section 2.7. To ensure the design behaves as assumed in the preliminary design calculations, the foundation must behave as a single unit to provide seismic resistance, properly stabilize the structure, and distribute the loads evenly over the underlying lunar regolith. Moreover, the tower must be properly connected to the foundation, and the material used should be able to withstand the forces in these connections.

The first option is shown in Figure 6.2a. Here, the foundation is cast in place with space concrete, such as geopolymer concrete. It needs to be possible to produce a relatively large amount of space concrete on the lunar surface. Additionally, a formwork that can be manufactured and set up in the lunar environment must be designed. The behaviour and setting of space concrete in a microgravity environment and under the lunar temperature fluctuations are also unknown factors. To provide reinforcement, metals could be extracted from the local lunar regolith and made into reinforcement bars. However, the extraction process is still in development. One alternative is to use fibre reinforcement, which must be thoroughly mixed into the concrete before it is cast.

To obtain another monolithic structure, cast basalt could be considered. This would require a large amount of energy to directly melt the lunar regolith and pour it into a suitable framework. It is preferred to focus on developing methods that require less energy, as this is one of the scarce resources, especially in early lunar colonisation.

Another option is visualised in Figure 6.2b, where sintered interlocking bricks or tiles are used to build a foundation. This would be more easily achievable, since the bricks can be made using a smaller microwave-like system and robotically assimilated. It needs to be investigated which configuration would work best to provide the proper behaviour to resist moonquake loading, without local failure of the masonry, for example. One advantage of using interlocking bricks is that they can be easily transported and reused elsewhere.

The third option is illustrated in Figure 6.2c, where the foundation is 3D printed as a whole. It is currently still being investigated how to 3D print in a microgravity environment and how to transport the necessary equipment to the moon. The setting of the 3D printed material and the bond strength of the different layers need to be investigated to ensure the foundation has sufficient resistance to moonquakes.

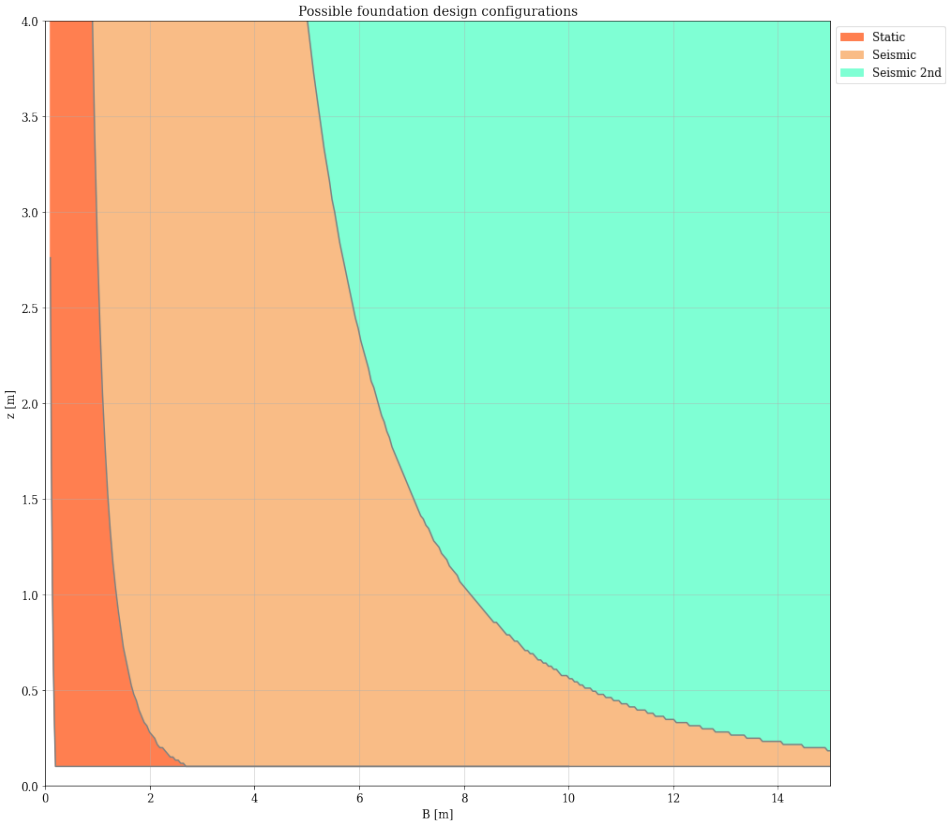

Figure 6.1: Possible foundation configurations for all 3 load cases. This figure summarises Figure 4.12, Figure 5.10 and Figure 5.28. The dimensions on the axes are described by Figure 3.7.

Static		
Bearing capacity	36330 kN	check = 545/36330
Settlements	0.20 m	-

Seismic		
Sliding	293 kN	check = 0.14 / 293
Bearing capacity	-1.0	check = -1.0 <= 0
Rotational failure	No loss of contact.	check = 0 < 33 %

Seismic 2nd		
Bearing capacity	-0.44	check = -0.44 ≤-1.0
Rotational failure	32.78 %	check = 32.78 < 33 %

Table 6.1: The values for the calculations for different failure mechanisms, performed on the foundation size configuration in Table 3.4. This foundation suffices under microgravity and moonquake loading.

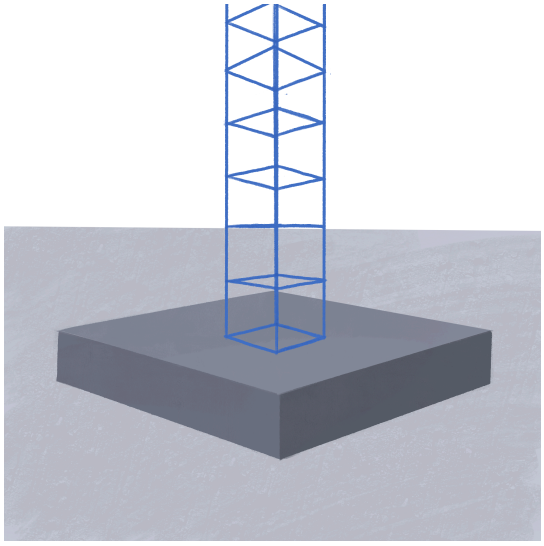

(a) A shallow foundation made out of a type space concrete. It needs to be cast in place. Another option is to create this slab from cast basalt.

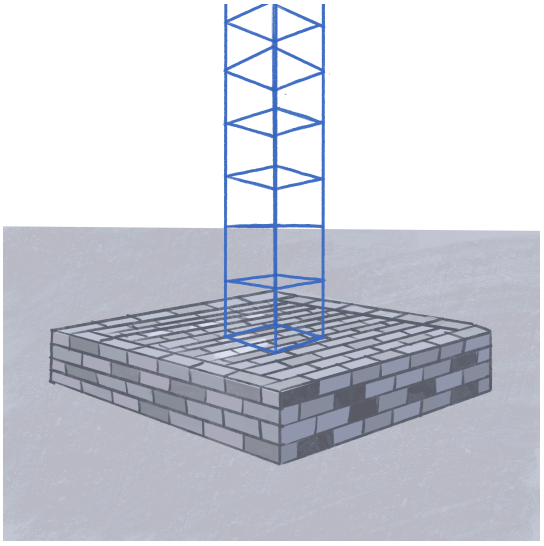

(b) A shallow foundation made of interlocking tiles. These could be produced locally and robotically assembled.

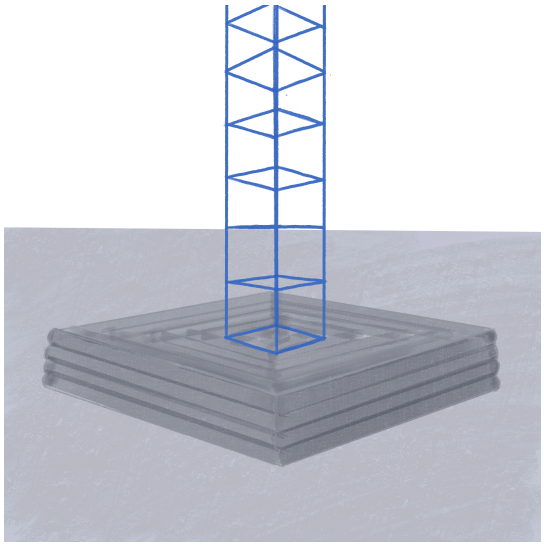

(c) A 3D printed shallow foundation. The equipment to 3D print this structure should be transported to the Moon. An investigation on 3D printing in the lunar environment is necessary.

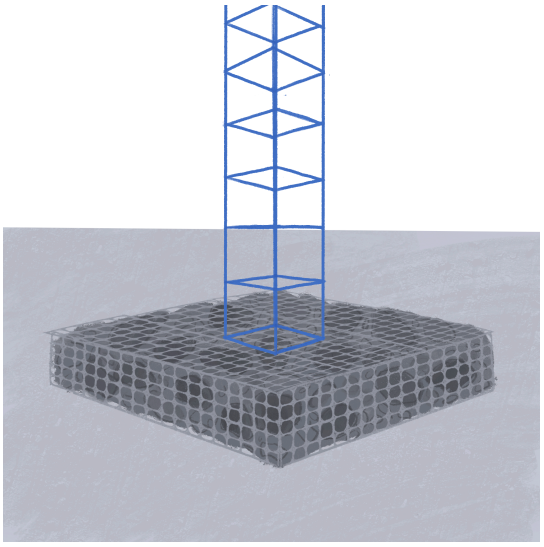

(d) A shallow foundation assembled from a gabion filled with local material or bags filled with regolith. The gabion can be locally 3D printed or otherwise manufactured, and the material to fill it can be easily obtained on the lunar surface.

Figure 6.2: Shallow foundation material configurations. It is required that the material behaves as a whole to provide stability, resist moonquakes, and distribute the load to the lunar regolith. It also needs to be able to withstand the lunar environment and the local connection forces of the tower.

Lastly, another option is a gabion, which can be 3d printed or otherwise manufactured, and filled with local material or bags holding local material. This would significantly reduce the amount of material that needs to be produced on the lunar surface. Again, it needs to be investigated if the moonquake resistance is sufficient, and if no local failure occurs when the material is distributed differently. Especially when post-tensioning tendons anchored in the foundation itself are taken into consideration. One of the advantages of this material option is that the gabion for the foundation can be easily transported over the lunar surface or reused by setting up the gabion and refilling it with the available material at the new location.

To protect the foundation against the aggressive lunar environment, it could be considered to cover the foundation with a layer of lunar regolith. This could protect the foundation against meteor impacts (Ruess et al., 2006), as well as radiation and temperature fluctuations (Jablonski & Ogden, 2008).

6.3. Shallow Foundation Size Reduction

This section explores alternative solutions or methods to enhance a shallow foundation, reducing the foundation's size and thereby minimising material production.

6.3.1. Post-tensioning

One option to reduce the size of the foundation is to utilise external or internal tendons, typically used in wind turbines. This could be in the form of guy wires through the truss structure of the TLT, or implementing tendons into the structure. By adding this wire, the tip of the tower gets pulled back once the second-order effect becomes too large. By reducing the displacement, the moment load on the foundation is also reduced.

Figure 6.3 illustrates how the TLT is affected by a guy wire connected to the foundation and the top of the tower. When the second-order effect is too small, the wire has a destabilising effect since the vertical tendon force is larger than the horizontal tendon force. This is a known effect of external tendons (Grünberg & Göhlmann, 2013). Once the displacement increases, the horizontal stabilising force also increases, pulling the tip of the tower back to the center.

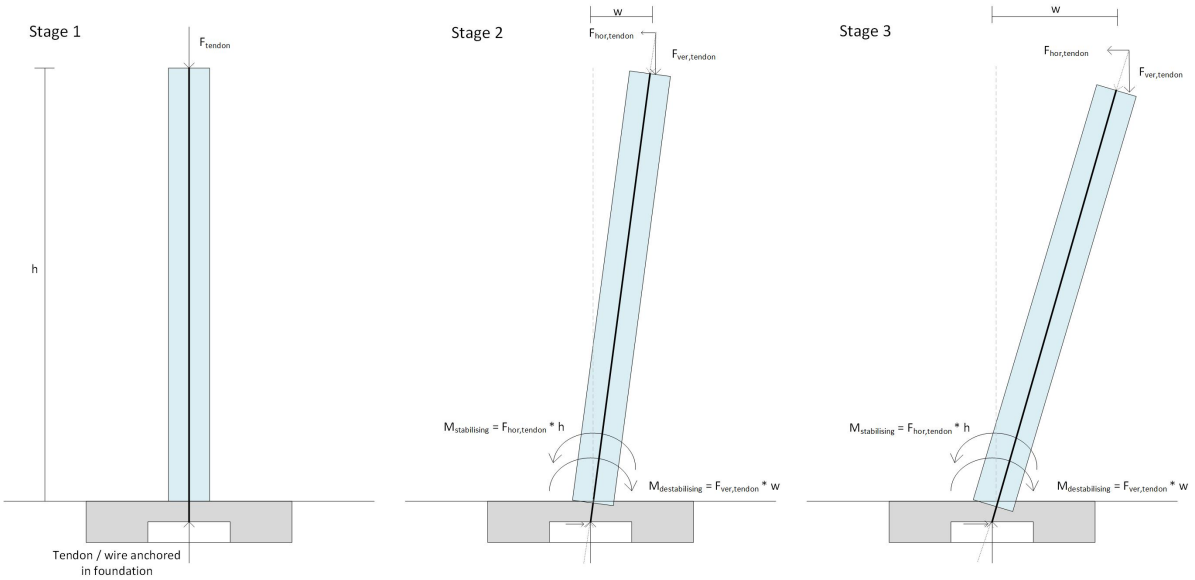

Figure 6.3: The effect of adding a post-tensioning tendon or wire to the TLT. The wire is connected to the top of the TLT and anchored in the foundation. When the TLT experiences a seismic event and starts moving due to the inertia, in the earlier stages, the vertical tendon force will destabilise the tower. Once, however, the displacement crosses a certain threshold, the horizontal tendon force generates a stabilising moment to recenter the TLT, as can be seen in stage 3, where $F_{hor,tendon}$ increases as the angle of the tower increases.

The use of a post-tensioning tendon or wire to reduce the second-order moment on the foundation design was investigated. From the literature review, it is known that basalt fibers can be produced from lunar regolith (Zhang et al., 2023). In the future, wires could be produced from multiple strands

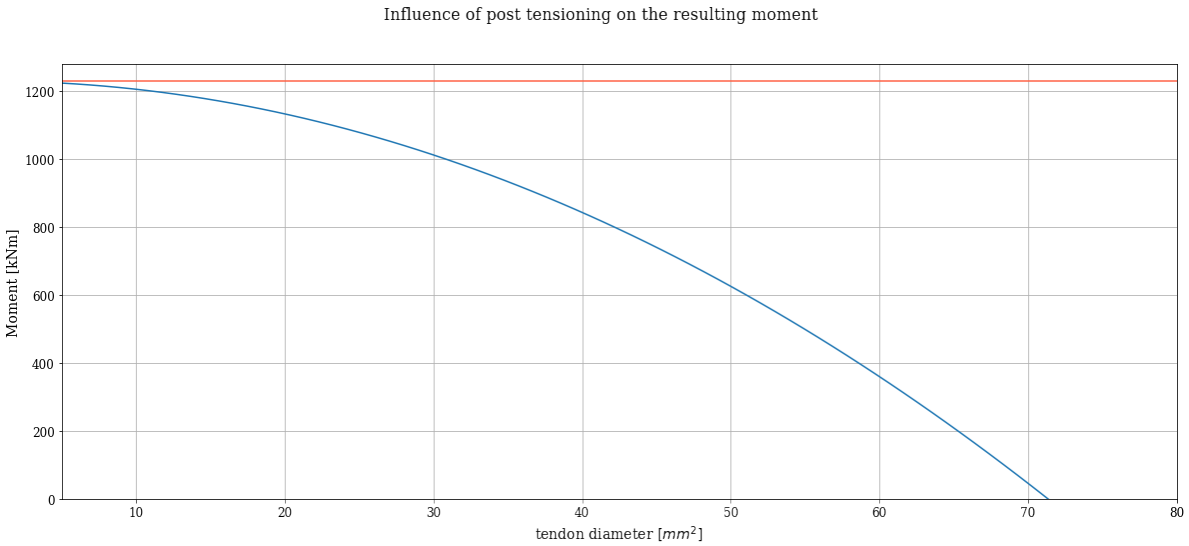

Figure 6.4: The reduction of the moment load depending on the diameters of the tendon or wire. The red line represents the original moment load in the seismic load case, taking into account second-order effects.

or filaments (Becker et al., 2019). It is known that one strand of basalt fiber has a tensile strength of $f_{tensile} = 1400\ MPa$ (Xing et al., 2020). It is assumed that the tendons are made of a similar material that can provide this tensile strength. Some standard dimensions for the diameters of tendon strands are 9, 12, 12.9, 15.2, 15.7, and 18 mm (STUBECO, 2015). When considering the use of multiple strands, larger areas become possible. With the force and area known, the tensile force in the tendon was calculated by:

$$F_{tendon} = f_{tensile} * \pi * r_{strand}^2 \tag{6.1}$$

To get the angle of the tendon force when the tower is not in its equilibrium position, the same assumption as for the displacement of the second-order effect is used. The tower is modeled as a cantilever beam with a tip mass, and the angle of the beam is taken as:

$$\alpha = \frac{1}{2}\frac{F * L^2}{EI} = \frac{1}{2}\frac{H_d * h_{tower}^2}{EI} \tag{6.2}$$

This enables the determination of both the horizontal and vertical tendon force and their corresponding moments:

$$F_{hor,tendon} = sin(\alpha) * F_{tendon} \tag{6.3}$$

$$F_{ver,tendon} = cos(\alpha) * F_{tendon} \tag{6.4}$$

$$M_{stabilising} = F_{hor,tendon} * h \tag{6.5}$$

$$M_{destabilising} = F_{ver,tendon} * w \tag{6.6}$$

The resulting effect on the moment load can then be summarised as:

$$\Delta M = M_{destabilising} - M_{stabilising} \tag{6.7}$$

With these equations, the difference in moment load, taking into account the second-order moment, can be visualised. As shown in Figure 6.4, a larger tendon or wire diameter results in a decreased maximum moment load. When the moment gets reduced, the foundation size can be reduced as well, as shown in Figure 6.5. To reach larger tendon diameters, it is suggested to use multiple strands of basalt filament.

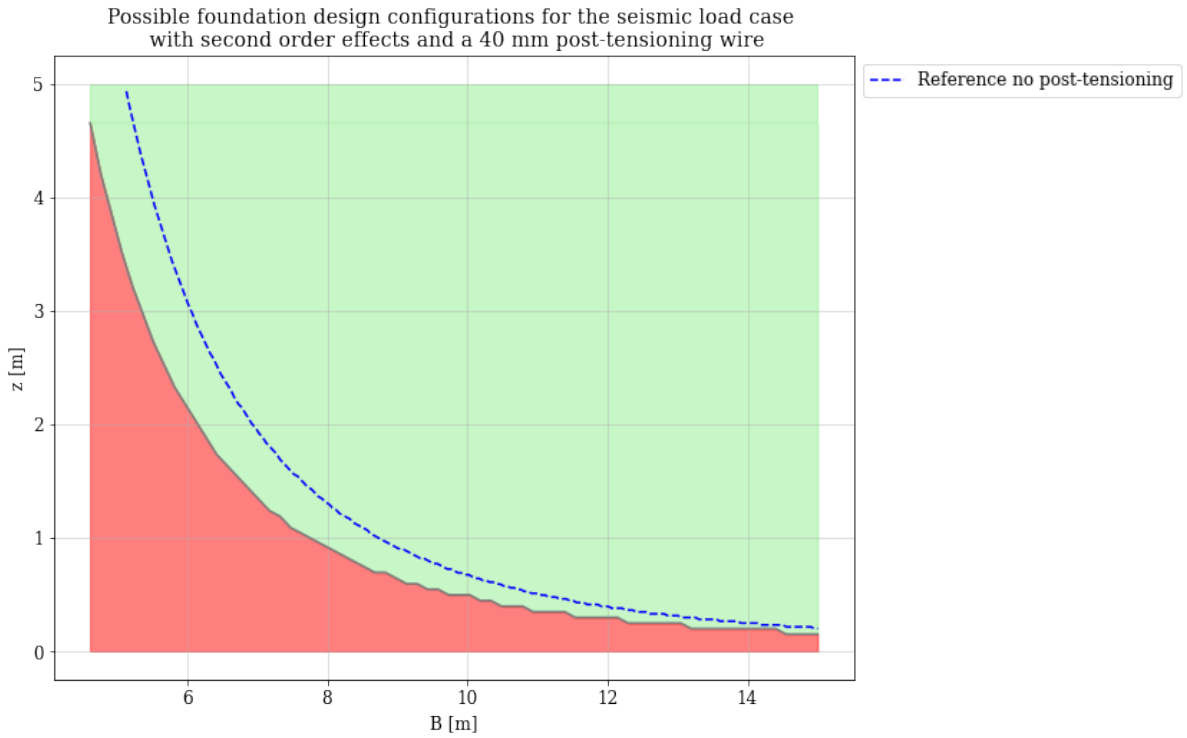

Figure 6.5: The possible foundation configurations while using the post-tensioning technique with a 40mm tendon or wire. The red area indicates foundation configurations that lead to failure, while the green area indicates safe configurations that can be used to select a suitable foundation format. The blue line visualises the border of foundation configurations before considering post-tensioning.

To visualise the effect on the border of the possible foundation configurations, the same line as in Figure 6.5 for a tendon of 40 mm was plotted for different tendon configurations, to observe the effect of increasing the tendon diameter. The result can be seen in Figure 6.6. For larger tendon or wire diameters, the possible foundation configurations increase as the boundary of possible solutions shifts to the left. This indicates that post-tensioning is a topic of interest for future investigations.

Several issues need to be explored when applying post-tensioning to the structure. The first is that the material for the wire is a yet-to-be-proven concept. The fibres and thread can be created (Becker et al., 2019; Xing et al., 2020), however, to make tendons or wires on the lunar surface from multiple filaments is a topic that demands investigation.

Another issue is the connection points of the tendon or wire. These connection points will create local forces that need to be countered by the material of the structure, foundation, or the soil if the anchor is created in the lunar regolith. For the structure, it also depends on where the tendons are connected inside the truss structure (Ghannam et al., 2017). The foundation needs to be modelled accurately with a chosen material type to see if the local forces can be distributed or lead to local failure. This will affect the possibilities for material choices.

6.3.2. Anchoring in lunar regolith

Another option to explore is the use of external wires anchored in the lunar regolith to enhance the structure's stability and mitigate the second-order effect. When examining the anchoring possibilities in Section 2.9, the current state of anchor designs for the lunar surface is in the very early stages of development. In addition, no ISRU options for anchors are available. When zooming in on the necessary tendon forces to reduce the moment load, it is crucial to determine how deep and how much force the anchor should resist.

In geotechnical engineering, anchors are typically pushed or drilled into the ground, utilising grout to create a bond with the surrounding soil. As stated earlier in Section 2.9, grout is currently unavailable. One possibility is to examine anchors on Earth that utilise no grout, such as the use of flip anchors. Yoshida and Xiong (2023) and Yoshida et al. (2023) experimented with this type of anchors. These anchors are pushed into the soil, and then open when a tension force is applied, as shown in Figure

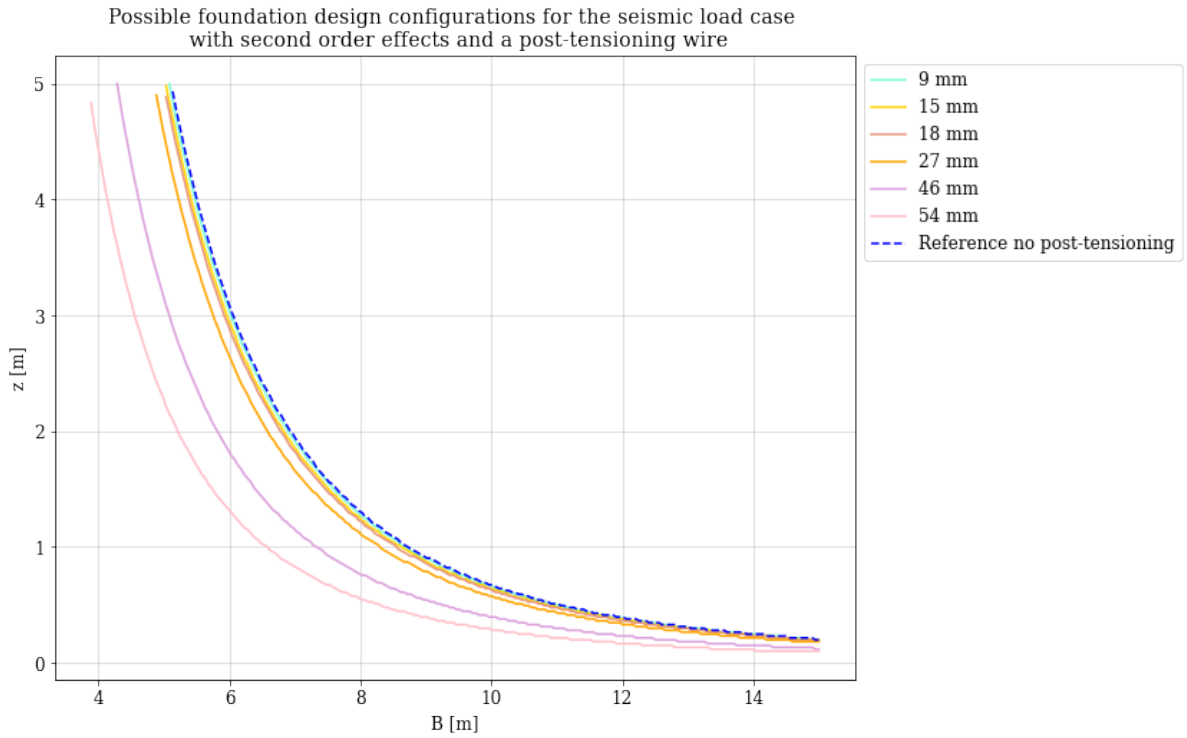

Figure 6.6: The possible foundation configuration borders for different tendon diameters. The border between safe and unsafe configurations, where safe is above the line and unsafe is below the line, shifts to the right as tendon diameter increases.

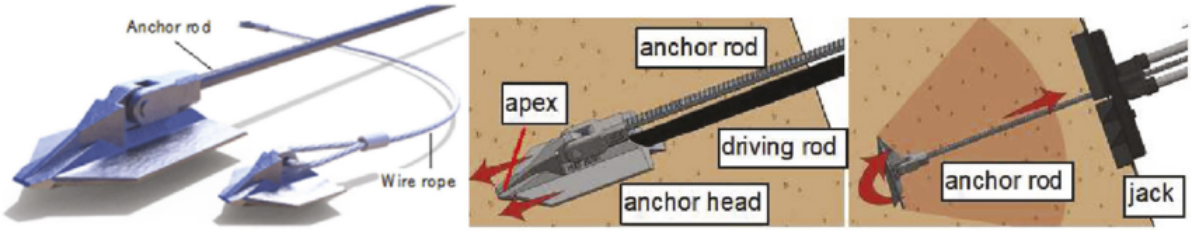

Figure 6.7: Flip anchor and their mechanism. The anchor is driven into the ground before being pulled back when the plate at the end rotates and provides a resisting force to the applied tensile force (Yoshida & Xiong, 2023).

6.7. The plate that appears at the end of the anchor provides resistance against pulling the anchor out of the soil again. These anchors depend on the weight of the soil above, which is affected by microgravity. The angle of the wedge and thus the amount of shear resistance is determined by the angle of internal friction; therefore, it is important to accurately determine the internal friction angle and density of the lunar regolith on the Connecting Ridge.

Ultimately, this leads back to the current drilling possibilities, as explained in Section 2.8. For the current state of lunar anchor designs, it should be verified how deep the anchors should be placed to resist a significant force and reduce the second-order effect, and if it is feasible to reach that depth with current or future drilling techniques. Placing an anchoring mechanism inside the lunar regolith would be a topic of future investigation.

6.3.3. Using fill material

The current failure mechanisms of the soil were investigated by treating the foundation as a single block of space concrete from the surface to the calculation level and calculating the mass. As this requires large amounts of space concrete to be produced, it is of interest to investigate if part of the height of the slab foundation can be replaced by other fill material with similar weight. The lowest compressive strength measured for geopolymer space concrete made from lunar simulant was 0.4 MPa using a 3D-printing technique (Wu et al., 2024). For tension, when taking about 1/10th of the compressive strength, the space concrete can support 40 kPa.

Using simple equilibrium and stress calculations as illustrated in 6.8. First, the resisting stress from the soil can be calculated. Here, the same method as for the rotational failure method is applied, except that an unfavourable safety factor is used.

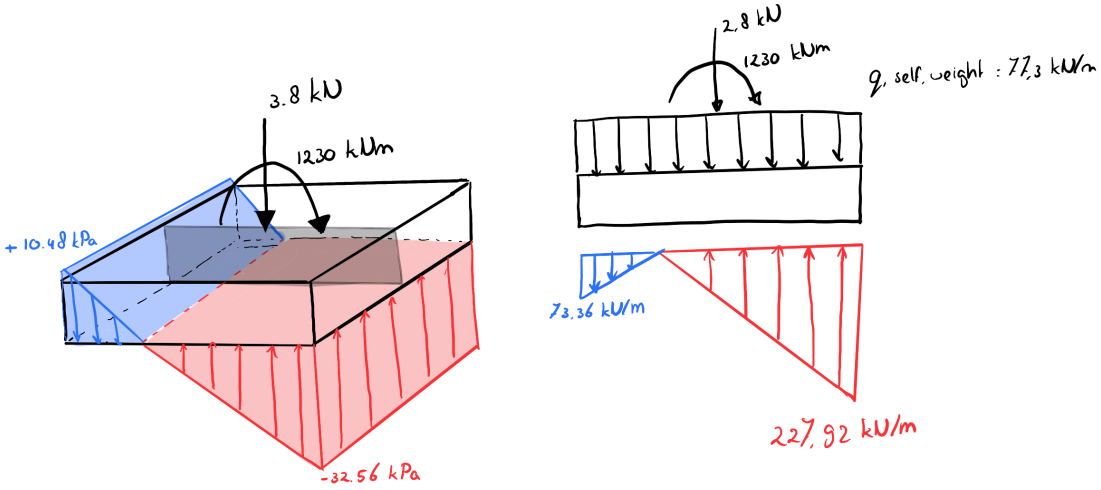

Figure 6.8: Illustration of the stresses and mechanical scheme used to calculate the stresses on the side of the slab foundation. The cross-section for the mechanical scheme is given by the grey rectangle in the left drawing.

$$\sigma_N = \frac{N}{A} = \frac{-540}{49} = -11.04\ kPa$$

$$\sigma_M = \frac{M * z}{I} = \frac{1230 * 0.5 * 7}{\frac{1}{12} * 7 * 7^3} = \pm 21.52\ kPa$$

The stresses at both ends of the foundation then become:

$$\sigma_{LEFT} = -11.04 + 21.52 = 10.48\ kPa \qquad \sigma_{RIGHT} = -11.04 - 21.52 = -32.56\ kPa$$

Both values are easily resisted by the space concrete, allowing the slab to be reduced in size and part of it replaced with fill material to achieve sufficient weight to resist moonquakes.

When looking in the other direction and calculating the stresses on the foundation's sides using the mechanical scheme as illustrated on the right in Figure 6.8, a similar calculation can be performed. As the weight of the tower is quite small, it is assumed that the tower will give a simple point load on the slab, and the moment is assumed to behave as a local moment. Because microgravity reduces the horizontal soil pressure on the sides of the foundation, a normal force is chosen to be omitted. As the maximum moment is present in the middle of the slab, the moment can be calculated over a section of the slab right before the point where the tower load and moment contribute.

These stresses can then be recalculated as a line load on a cross-section of the slab by multiplying them by the width of the foundation:

$$q_{LEFT} = 10.48 * 7 = 73.36\ kN/m \qquad q_{RIGHT} = -32.56 * 7 = -227.92\ kN/m$$

The resisting moment in the middle of the cross-section can then be calculated:

$$q_{MID} = 227.92 - \frac{(227.92 + 73.35)}{2} = 77.28\ kN/m$$

$$M_{MID,res} = 77.28 * \frac{7}{2} * \frac{1}{2} * \frac{7}{2} + (227.92 - 77.28) * \frac{1}{2} * \frac{7}{2} * \frac{2}{3} * \frac{7}{2} = 1088.5\ kNm$$

The acting forces from the self-weight of the slab generate another moment:

$$M_{MID,act} = \frac{540.8}{7} * \frac{7}{2} * \frac{1}{2} * \frac{7}{2} = 473.5\ kNm$$

The total moment in the cross-section then becomes:

$$M_{MID} = M_{MID,res} - M_{MID,act} = 1088.5 - 473.5 = 615\ kNm$$

Then the stress in the slab can be calculated, assuming the soil pressure of the lunar regolith on the sides of the slab is negligible:

$$\sigma_M = \frac{M * 1/2 * z}{\frac{1}{12} * B * z^3} = \frac{615 * 0.5 * 2}{\frac{1}{12} * 7 * 2^3} = \pm 132\ kPa$$

This is enough for the compressive strength of 0.4 MPa, however, for the tensile forces, this load is too high. Therefore, fibre or other types of reinforcement would be required. The design of potential reinforcement is deemed out of the scope of this thesis. It is noted that when other geopolymer concretes are used and a suitable construction technique is employed, higher strengths can be achieved. As higher strengths have already been measured in different types of geopolymer concrete (Wu et al., 2024), part of the slab could be replaced with fill materials to get the necessary weight to resist a moonquake load, reducing the size of the foundation that needs to be produced. As this is quite a simplified method to calculate the stresses in the slab, a more detailed calculation or simulation would be required. Similarly, for different foundation configurations, the stresses should be checked accordingly.

6.4. Difference from Earth

This section reflects on the differences in the design process for lunar conditions and how these were translated into the Eurocode calculations. The latter also offers suggestions for topics for a future lunar design standard.

6.4.1. Design process

After defining the possible foundation configurations on the lunar surface based on the design input and necessary assumptions, it is of interest to examine how designing for lunar conditions influences the design results.

Firstly, the design of the tower itself is significantly different from what it would be on Earth due to the influence of microgravity and atmospheric conditions. Such a tall, slender structure would be difficult to stabilise for horizontal wind loading. On the lunar surface, however, the lack of atmosphere removes this load. In addition, when building structures in seismic environments, special care is usually taken in foundation design to prevent large horizontal loads on the structure by either isolating the base or adopting other earthquake-resistant design measures. Due to the lunar environment, these earthquake-resistant building styles are not easily adaptable to the lunar surface, as equipment and materials are limited.

As it is impossible to bring everything required to build a foundation from Earth, not to mention the limitations of Earth's equipment that will not function under lunar circumstances, special equipment is required to produce and build on the lunar surface. The current state of development of this equipment imposes limitations on foundation design. Similarly, the local production of material from local resources and the necessary resistance against large thermal fluctuations and radiation impose limitations on the types of materials available on the lunar surface for constructing infrastructural elements. As the lunar environment is also hostile to humans, the construction process needs to rely on robotic construction. Because gravity is not the same as on Earth, penetrating deeper, denser layers of the lunar regolith remains a topic of investigation. In the microgravity environment and with the possibility of penetrating the lunar surface still limited, the use of anchors to stabilise the structure becomes uncertain as well. In conclusion, the current state of development of equipment and materials imposes unique constraints on foundation design.

Secondly, on Earth, when starting a construction project, information is available on the construction site and its history. The soil types are known, and field investigations can be easily conducted and samples collected. There is information available on the expected geology, and, from experience, the

risks and best practices are known for building economical, optimal solutions with a limited impact on the surroundings. When discussing seismicity, information is available to accurately define the seismic hazard on the construction site, as we know the sources of the quakes and can estimate the propagation through the underground. Using statistics, we can assess the reliability of the structure and design for earthquakes.

On the Moon, none of this information is available. The source of shallow moonquakes is unknown, and to assess seismic hazard, multiple assumptions had to be made (see section 2.6.2). It is known that moonquakes have a distinctly different pattern from earthquakes, possibly reducing damage to structures, but reaching a larger area. It is, however, unknown how big the moonquakes can be, and therefore, knowing the hazard that can be expected on our infrastructural elements becomes very uncertain.

The geological formation process has been described; however, it is unknown how much this affects the state of the lunar regolith. On Earth, constant ballistic sedimentation or the possibility of meteoroid strikes is not covered by any design practices. This process can also leave ejecta underground, which is unlikely to be encountered in Earth's environment.

Lastly, on Earth, the kinds of soils or rocks to be expected can be inferred from the geological formation process, as well as the expected geotechnical design parameters and their ranges when these soils or rocks are encountered. For the lunar regolith, however, there is very limited data available, and it is different from any material encountered on Earth's surface. This means that any correlations between soil parameters or standard calculations should be treated with care, as they may not be applicable to lunar regolith in the same way as formulas for sand are usually not applicable to soft layers like peat.

In addition, when performing field investigations on Earth, significant depths can be reached that can cover the influence depth of the future construction. On the Moon, the deepest measurements were taken only a few meters deep, meaning that there is only extrapolated information on the lunar regolith at depth available and limited knowledge of the risk of encountering weak pockets.

All these factors were involved in designing a foundation for a TLT and are significantly different from those involved in designing a foundation on Earth. The many unknowns and constraints require multiple assumptions to calculate preliminary foundation configurations, necessitating the translation of lunar conditions into a format interpretable by the Earth-based design standard.

6.4.2. Design standard

When examining the potential differences in the calculation steps in more detail, the points of interest for a future lunar design standard can be identified, and the differences between a normal Earth calculation for a shallow foundation and a calculation for a foundation on the Moon can be highlighted.

It already starts with the usual input factors used in design, as specified in the Eurocode. Every parameter has its own safety factor, based on research and engineering judgment from experience on Earth. These safety factors have to be translated to a lunar environment for corresponding adapted limit states and consequence classes. Additionally, for serviceability limit states, predefined settlement limits are usually used; these need to be defined for the lunar surface.

In seismic design, the seismic action index and class should be defined based on the seismic conditions on the lunar surface. In current standards, these depend on grain sizes, site categorisation, and topography, combined with information on the seismic hazard. The exact boundaries between classes are again related to consequence classes, where the boundaries in the seismic action index are defined by accelerations. To obtain the horizontal acceleration the system is subjected to, assumptions are made regarding the seismic hazard, factors related to spatial variation, the type of analysis, and the allowed permanent displacements of the system. These boundaries and factors are important in the seismic design process and should be considered in a lunar design standard accordingly.

To start the calculations, the loads due to the structure's weight need to be adjusted for microgravity. Similarly, the effective unit weight of the lunar regolith is 1/6th of the value measured on Earth. Applying the Eurocode standard under all assumptions, however, raises other concerns: Are the calculation methods still valid for lunar regolith? Does the extreme lunar environment cause any change in failure mechanisms? Because all calculation methods are based on Earth materials, which are usually limited to specific application ranges, the high friction angle of lunar regolith, for example, could introduce anomalies when extrapolated. Within the lunar environment, failure mechanisms could differ due to

extreme temperature gradients with depth, reduced gravity, and the lack of atmospheric pressure, and should be investigated before being included in a lunar design standard.

When performing the calculations, the major difference in the static case is the effect of microgravity and the absence of horizontal loads. As stated before, the failure mechanisms may differ on the lunar surface, and the formulas used to calculate bearing capacity might not hold for lunar regolith. The limit of stability for rotational failure might not apply, and the settlement calculation might not be applicable for lunar regolith.

In the seismic calculations, the factors related to horizontal acceleration, as described above, introduce uncertainty. For the sliding mechanism, the friction angle between the state-of-the-art materials and the lunar regolith is an unknown factor, as is the ”earth” pressure from the lunar regolith and its contribution to the sliding resistance. Both require research to be included in a lunar design standard. The seismic bearing capacity calculation, in particular, involves multiple decisions based on the differentiation between dry, fine-grained or coarse-grained soil, influencing the numerical factors used. The κ value describes how significantly different the fundamental periods of the soil deposit and the structure are, and must be defined within certain boundary values. For the lunar regolith, the range of possible κ values, the definition of the dimensionless soil inertia force and numerical factors should all be investigated or translated to the lunar environment. Lastly, a moonquake event could cause densification due to dynamic loading. The Eurocode prescribes formulas to predict these values, but they depend on atmospheric pressure. Therefore, new correlations should be developed for the lunar regolith and environment.

7

Conclusions & Recommendations

The design problem that this thesis had to solve with the corresponding objective is described in the following statements:

Problem Statement:
A foundation is critical for connecting a Tall Lunar Tower to the lunar surface, and relevant concepts are underdeveloped. Therefore, the stability of the Tall Lunar Tower under moonquake and microgravity loading cannot be guaranteed.

Design objective:
This thesis aims to provide a preliminary design of a foundation for a Tall Lunar Tower that guarantees stability and provides shallow moonquake resistance, within the constraints posed by the extraterrestrial lunar environment.

7.1. Conclusions

The design considered the cost of transporting material and equipment to the lunar surface, and the current state of equipment development. Excavating deeply into the lunar regolith was assumed to be unfeasible at the current time. In addition, the design focuses on the potential use of ISRU materials that can withstand the extreme temperatures and radiation, and on minimising size to prevent significant material production power requirements. The upper layer of the lunar regolith consists mainly of dust with a lower density than the deeper lunar regolith. This material is unsuitable for building on due to its low strength and risk of densification, and must be removed. A tilt of the underground will cause a large extra moment on the foundation. It is therefore assumed that the surface is levelled before beginning construction.

It was proposed to use a slab foundation as a prototype for a lunar foundation, due to its simplicity to construct and the optional use of local materials as building components, making it possible to construct it in its entirety on the lunar surface. Moreover, it requires less excavation compared to deep foundations, and given the current state of drills and excavators, it therefore poses less of a challenge. Material options include space concrete, possibly reinforced with fibre reinforcement, interlocking bricks made by sintering methods and constructed using automated robot technology, 3D printing the structure, or using a gabion that can be filled with regolith bags or local debris.

As expected, the seismic load case with a second-order effect is the governing situation for designing a foundation for a TLT. To obtain a foundation that can withstand seismic loads, a large, shallow foundation is necessary. The settlements of such a large foundation can become considerable. The risk of rotational failure is also present, and when potential differential settlements come into play, this should be thoroughly investigated and modelled. With a larger foundation, the risk of sliding and the bearing capacity being exceeded becomes lower. To reduce these sizes, post-tensioning tendons or wires can be used to recenter the tower, thereby reducing the second-order moment on the foundation. Another option is to use anchors to provide extra stability or to replace part of the foundation with fill material, provided the material's compressive and tensile strengths are sufficient.

The four research questions posed at the start of this thesis are answered below. The effects of different aspects of the system and their effect on foundation design were investigated.

How do the soil parameters influence foundation design under static and seismic loading conditions?

The strength parameters of the lunar regolith directly influence foundation size, as the bearing capacity in the static load case increases with higher strength parameters. The effect is dependent on the size of the foundation, as smaller foundations experience more pronounced effects of cohesion, where the influence of the friction angle causes significant variations in the maximum bearing capacity. The influence of volumetric weight becomes more apparent as the foundation size increases, since the foundation depth increases as well.

In seismic situations, the effect of strength parameters on foundation design is primarily evident through the internal friction angle. When the internal friction angle increases, the soil can more easily resist the movement due to the moonquake. As the internal friction angle of lunar regolith is high, this has a positive effect on the possible foundation sizes, as it reduces the inertial force applied by moonquakes.

The deformation values pose a significant risk to lunar infrastructure. Even with small foundations, the settlements can quickly become in the order of tens of centimetres. This, however, is calculated using a simplified and likely conservative calculation method from NEN-EN-1997-1 and with limited information on the porosity and soil deformation modulus. The risk of differential settlements resulting in extra moments on the structure is significant, as the rotation will pose extra forces on the system.

How does the foundation configuration affect the failure mechanisms given by the Eurocode design standards?

Even with small foundation configurations, the static loads are easily resisted. To resist the standard seismic load, small foundations remain sufficient, whereas the rotational failure mechanism could pose a risk. The foundation configuration options become problematic as second-order effects are taken into account. The risk of rotational failure and exceeding the seismic bearing capacity quickly becomes more pronounced, and larger foundation configurations are required to withstand these forces. Especially when the horizontal acceleration caused by the moonquake increases, the displacement and moment increase quickly as well, thereby increasing the risk of instability in the system. The risk of rotational failure, therefore, becomes problematic with even small deviations in the parameters.

How do the structural parameters of the TLT influence the foundation configuration?

The parameters for the natural frequency, the mass of the solar panels and the height of the tower have an impact on the seismic loads imposed on the system and consequently the foundation configuration. The natural frequency influences the structural acceleration a_s. An increase in a_s results in a larger horizontal force, leading to greater movement of the tip mass and a considerable increase in the second-order moment and necessary foundation width. As the horizontal force increases, the risk of sliding increases in the seismic situation. However, this effect is mitigated through the increase in the necessary foundation size to resist the second-order effect.

The second-order effect is considerably enlarged by an increase in the mass of the solar panels, as this mass is moved by the inertial force of the moonquake. As the second-order moment increases, a larger foundation configuration is required. However, this effect is not as pronounced as when increasing the height even slightly, as the moment load increases exponentially as the displacement of the tower skyrockets. When a larger area with a certain illumination percentage is required, taller towers are needed, which in turn require larger foundations.

The material and profile of the tower significantly influence the second-order effect. Increasing the stiffness reduces the moment load on the foundation by limiting the second-order displacement and thus reducing foundation size. In addition, the required foundation size decreases significantly when a higher moment of inertia is selected for the tower's profile.

How does microgravity influence the possible foundation configurations for the static and seismic load cases?

In the static load situation, the loads on the foundation are reduced by the microgravity. Therefore, the soil needs to counter less weight, leading to smaller possible foundation configurations than on Earth. However, in a seismic situation, lower weight means less friction at the foundation's base, increasing the risk of sliding. Additionally, there is less gravitational force to slow down moving objects. This increases the necessary foundation size on the lunar surface, as it negatively impacts the seismic bearing capacity. The second-order moment is not affected by the soil's inertia; therefore, there is no difference between the foundation configurations required on Earth compared to those on the Moon for this situation, as the displacement and thus second-order effect are not influenced by the soil's inertia.

7.2. Future recommendations

This section examines the limitations of the data and calculation methods and presents future recommendations and research opportunities to address these gaps.

This design only considers microgravity and moonquake loading. However, it is known that due to the lack of atmosphere, meteoroid impacts are a frequent occurrence on the lunar surface. As the effect of meteoroid impacts on the structure and the extent of the loads generated by these impacts is unknown, it is suggested to model this stochastic process to better identify the risk and loads posed on future lunar infrastructure.

The geotechnical parameters are based on the currently available data, which are typically limited to measurements from old experimental setups. In addition, the behaviour of the soil in microgravity and vacuum conditions, and whether the soil will fail in a similar manner as on Earth, is unknown. In particular, the bulk density over depth is an essential parameter to obtain, as it influences the internal friction angle and cohesion, as well as the grain sizes that can be observed in different layers. Furthermore, the known soil parameters are based on samples taken during the Apollo missions, which did not occur at the Lunar South Pole. The soil parameters on the Connecting Ridge, and whether and how they deviate from these values, are unknown. Data and samples should be gathered to determine whether the soil behaves fundamentally differently from the already obtained lunar regolith samples.

The bulk density is also influenced by porosity, in conjunction with specific density, which depends on the mineral and chemical composition of the lunar regolith. During loading, the lunar regolith becomes dense, resulting in considerable settlement. The geological formation process can also cause differential settlements, as there might be weak pockets that are covered by new layers through ballistic sedimentation. Moreover, larger ejecta and boulders can be encountered on the lunar surface, impacting the settlement behaviour of the surface. The behaviour of lunar regolith under cyclic deformations is also unknown. Ground improvement methods could reduce the risk of having (differential) settlements and of densification during a seismic event, and should be investigated as a possibility on the lunar surface, as well as to more accurately determine the deformation modulus and state of the lunar regolith as a function of depth on the Connecting Ridge.

The seismic hazard caused by shallow moonquakes is currently very uncertain. The structure of the moon's interior influences the depth of the lunar regolith, and still remains a subject of ongoing investigation. It is speculated that the northern side of the Moon is more seismically active than the southern side. The source of shallow moonquakes remains unknown due to the intense scattering in the subsurface and the extremely limited measurements available. As a consequence, there is no Ground Motion Prediction Equation for the lunar environment, rendering the limited data on seismic hazards unreliable and making it difficult to determine the seismic hazard to which future lunar infrastructure is subjected. As a result, the horizontal acceleration is very uncertain, spreading this uncertainty to the second-order effect and the foundation configuration options. It is recommended to gather more experimental data on seismic activity at the Lunar South Pole before constructing infrastructural elements, especially TLTs, as they are susceptible to small accelerations due to their height.

To reduce uncertainty in geotechnical parameters for foundation design, field investigations could be conducted on the Connecting Ridge. Tables 7.1 and 7.2 provide an overview of the Eurocode's recommendations for optional field investigations and laboratory tests to obtain the discussed parameters. However, these tests are usually conducted under Earth conditions and will need to be properly assessed and designed to function in lunar conditions. In addition, the indicated soil parameters are often derived from empirical correlations that may be invalid for the lunar terrain. For dynamic parame-

Subject	Field investigation
Soil types	CPT, SPT, DMT
Rock type	RDT
Extension of layers	CPT, SPT, DPL/DPM, WST, DMT
Grain sizes	SPT
Density	CPT, SPT, DMT, DPL/DPM
Shear strength soil	CPT, PMT, SPT (coarse soil), DPL/DPSM (coarse soil), WST (coarse soil), FVT (fine soil), DMT, PLT
Shear strength rock	PLT
Compressibility	CPT, PMT, RDT, FDT (fine soil), SPT, DPL/DPM, WST (coarse soil), DMT, PLT
Compressibility rock	RDT
Presence of ejecta/boulders in the underground	geophysical techniques e.g. Ground-Penetrating Radar
Shear wave velocities	geophysical techniques e.g. seismic profiling, seismometers

Table 7.1: Field investigation options for a future lunar mission. To take these measurements, it is advised to make boreholes and dig trenches to measure at different depths and to prevent taking measurements from the first layer of dust. A similar advice is recommended for taking samples. Methods to perform these field investigations on the lunar surface need to be developed.

CPT : cone penetration test
PMT : pressuremeter
DMT : flat dilatometer test
SPT : standard penetration test
DPL/DPM : dynamic probing light / dynamic probing medium
DPH/DPSH : dynamic probing heavy / superheavy
WST : weight sounding test
FVT : field vane test
DMT : flat dilatometer test
PLT : plate loading test
FDT : flexible dilatometer test
RDT : rock dilatometer test

ters, dynamic field testing methods like the dynamic cone penetrometer and laboratory tests simulating moonquake conditions would be preferable. If possible, the set-up of large-scale tests before building infrastructural elements is of interest in the earlier phases of the Artemis program. The detailed investigation and design of possible field investigation methods and how to obtain samples are research topics for the future.

When the uncertainty in the input values is reduced, the calculation methods have to be adapted to the lunar environment. For now, the NEN-EN 1997 and 1998 rules were used to provide a preliminary design of a foundation for a TLT. However, it is necessary to verify that the formulas and failure mechanisms in the design standards are applicable to the lunar environment, and special care is needed when using numerical values derived from Earth-based experimental results. This also applies to the seismic input variables related to the site categorisation, seismic indexes and classes. In addition, consequence classes, limit states, and safety factors for infrastructure on the lunar surface do not exist, and their influence on design calculations or on obtaining this information for the lunar environment is deemed a topic for future investigation.

When applying the design standards as they are, multiple factors related to the structure must be properly considered before a foundation configuration can be determined. The mass of the solar panels, the profile, and the material used for the tower, as well as the height, heavily influence the second-order effect experienced during a shallow moonquake event. To control the second-order behaviour, a trade-off must be made between required illumination conditions, or in other words, the height of the TLT and the size of the foundation. Whether the second-order effect can be limited by increasing the moment of inertia of the tower depends on future material choices, profile choices, and the possible construction methods. The structural parameters also influence the natural frequency of the tower, and should therefore be modelled accurately, combined with increased knowledge on the seismic hazard, to obtain a more accurate structural acceleration.

On the foundation side, there are multiple directions that can be further investigated. The material options need to be accurately modelled to see if the foundation can behave as a whole to provide the necessary seismic resistance, provide stability, and ensure that the loads are evenly distributed to the lunar regolith below. In addition, a more detailed stress distribution could indicate if fill material can be

Subject	Laboratory test
Bulk density	BDD
Internal friction angle	TX, SB
Cohesion	TX, SB
Residual shear strength	RS, SB
Deformation modulus	TX
Shear modulus	TX
Oedometer modulus	OED, TX
Primary compression index	OED, TX
Dynamic properties	Cyclic testing

Table 7.2: The following experiments can be performed on lunar regolith to obtain geotechnical design parameters. However, the Eurocode primarily recommends undisturbed samples for the silty upper layers of lunar regolith, which poses a challenge for future missions. For deeper layers, if particle sizes are more towards sand, a disturbed or remoulded version is likely to yield representative parameters. Routine tests for rock samples include: geological description, core recovery, Rock Quality Designation (RQD), degrees of induration, fracture log, weathering and fissuring. With an option for density of grains determination, wave velocity determination, Brazilian tests, shear strength of rock and joints determination, slake durability tests, swelling tests and abrasion tests.

BDD : bulk density determination
OED : oedometer test
TX : triaxial test
SB : translational shear box test
RS : ring shear box test

used to reduce the amount of material to be produced. The connections to the lunar tower and the local forces that the material must withstand should also be investigated. Furthermore, the size of the foundation could be reduced by using post-tensioning tendons or wires anchored in the foundation or in the lunar regolith, or by employing external anchors that are connected to the tower with wires. Both reduce the second-order moment by recentering the TLT. However, the wires made from local material have not been proven to be producible, and the connection to the foundation could lead to large local forces, which would need to be accurately modelled. Moreover, when considering anchoring in the lunar regolith, the microgravity, which reduces the weight of the soil above, could become problematic. It needs to be investigated whether the large internal friction angle can compensate for the effect of microgravity on anchoring.

The equipment to install these anchors and the anchors themselves do not exist. Making anchors from local material that can resist the forces exerted by recentering the TLT during a seismic event is a recommended subject for future investigation. One suggestion is to explore flip anchors, as these can be pushed into the lunar regolith and, when pulled back, open up on their own without requiring complex procedures. However, penetrating the denser lunar regolith at depth remains a challenge that needs to be addressed, and suitable drills and excavators require further investigation. Using vibrations to push the anchor or possibly in the future piles into the lunar regolith is not recommended, as the lunar regolith is very prone to densification. Auger piles are more suitable; experiments with larger drills are encouraged to determine whether the cohesion and high friction angle of lunar regolith can stabilise boreholes, possibly opening the way for pile foundations in the lunar regolith. Otherwise, the options of drilling fluid produced by ISRU techniques and its behaviour in microgravity are of interest.

The small, lightweight equipment required for constructing lunar infrastructure and producing ISRU materials is a topic for further consideration in the future. With more information on the lunar environment, more suitable equipment can be developed, and its power requirements and thus the necessary TLT assets can be determined. Then, the soil-structure interaction can be accurately modelled, and the actual foundation configuration can be determined. Once power and CPNT services become available on the lunar surface, constructing lunar infrastructure is the next step. A summary of further research directions related to the subsurface in order of importance for foundation design is provided in Table 7.3 and for general lunar infrastructure in Table 7.4.

This thesis has taken the state of the art into account to perform preliminary design calculations for a foundation for a TLT. By doing so, the research gaps for geotechnical engineering on the lunar surface were laid bare, and paths forward were identified. In the future, multiple opportunities lie ahead for researchers to experiment with lunar simulants and, hopefully, set up in situ measurements on the

lunar surface during the Artemis missions. With this data, new equipment and construction methods can be developed, as well as the infrastructure designed. As the risk of losing the power and CPNT services due to a shallow moonquake event can be reduced by designing a proper foundation, lunar colonisation can become a reality.

Topic of investigation	**Support**
Soil investigation methods	Supports the design of infrastructure by enabling information gathering of the lunar subsurface.
Sampling methods	Supports the design of infrastructure by enabling information gathering of the lunar subsurface. Through samples, geotechnical parameters can be obtained.
Geotechnical parameters: Internal friction angle, bulk density, cohesion at the Lunar South Pole (LSP)	Information about the behaviour and strength of lunar regolith at the LSP. This gives information to better design foundations for lunar infrastructure. In the case of a shallow foundation, the bearing capacity, sliding behaviour and risk of rotational failure can be more accurately calculated.
Grain sizes LSP	Insights in the geology, geomorphology, and behaviour of the lunar regolith. It also supports the design of lunar infrastructure in seismic conditions by influencing site categorisation and the formulas to be used.
In situ state LSP: porosity, specific density, deformation modulus	Supports calculations on (differential) settlements and future numerical simulations. Gives more information about the risk of densification and the geological formation process.
Soil behaviour microgravity and vacuum conditions	Gain insights into the in situ behaviour of lunar regolith to better inform design practices.
Seismic hazard at the LSP	More information about the accelerations that future infrastructure can be subjected to can inform seismic design. It also more accurately identifies the risk of shallow moonquake events.
Source shallow moonquakes	Directly supports identifying the seismic hazard on the lunar surface.
Presence of ejecta/boulders in the underground	Supports calculations on (differential) settlements. Identifies the risk of encountering large ejecta in the lunar underground at the construction location.
Geological formation process	This influences the expected states of lunar regolith and the risk of encountering weak pockets.
Behaviour of the lunar regolith under dynamic loads	Gives insights into the behaviour of the lunar regolith in seismic conditions and supports future numerical simulations.
Structure Moon's interior	With this information the depth of the bedrock formation can be determined and thus which layers are affected by seismic excitation. It gives information about the shear wave velocities that can be expected and serves as input for the seismic design of lunar infrastructure.
Ground improvement methods	Methods to reduce settlements by densification in microgravity and vacuum conditions.
Stability boreholes in lunar regolith	Informs the feasibility of pile foundations on the lunar surface.

Table 7.3: The potential research directions related to the lunar subsurface and what they would support in order of importance for foundation design.

Topic of investigation	Support
Natural frequency of the TLT	Gives the opportunity for a more accurate seismic design for a TLT and its foundation.
Model foundation behaviour for different material types	Investigate if the foundation can move as a whole and can provide the required resistance against microgravity and moonquake loading.
Stochastic process meteoroid impacts	Gain insights into how to design for meteoroid loads and what the risk of meteoroid impacts is.
ISRU produced wires	Can support an investigation to use wires to provide stability or use post-tensioning in lunar structures.
Connection forces post-tensioning wires	If wires are anchored in the foundation, accurately modelling these forces supports foundation design and gives insights into ISRU material design.
Anchoring lunar regolith	Gives possibilities for stabilising wires for lunar construction or post-tensioning. In addition, it informs design for microgravity and vacuum conditions, as well as insights into the behaviour of the lunar regolith.
ISRU produced anchors	Supporting ISRU production by locally producing anchors.
Suitable drills and excavators	Determines boundary conditions for foundation and infrastructure design. With suitable drills, pile foundation options might become available.
ISRU drilling fluid and its behaviour in microgravity	Supports ISRU principles and can potentially stabilise excavations and boreholes, expanding construction options.
Small and lightweight construction equipment	Supports construction possibilities.
Small and lightweight production equipment ISRU materials	Supports ISRU material production possibilities.
Design standard lunar environment	Informs the design of lunar infrastructure.

Table 7.4: Potential research directions that can inform the development of lunar infrastructure.

References

Agavriloaie, L., Oprea, S., Barbuta, M., & Luca, F. (2012). Characterisation of polymer concrete with epoxy polyurethane acryl matrix. *Construction and Building Materials*, *37*, 190–196. https://doi.org/10.1016/j.conbuildmat.2012.07.037

Anastasopoulos, I., Gazetas, G., Loli, M., Apostolou, M., & Gerolymos, N. (2010). Soil failure can be used for seismic protection of structures. *Bulletin of Earthquake Engineering*, *8*(2), 309–326. https://doi.org/10.1007/s10518-009-9145-2

Baker, A. H. M., Setiawan, M. I., & Prawito, A. (2022). The Foundations in Construction, a General and Comprehensive Study from an Engineering and Historical Perspective [Number: 1]. *IJTI International Journal of Transportation and Infrastructure eISSN 2597-4769 pISSN 2597-4734*, *6*(1), 19–25. https://doi.org/10.29138/ijti.v6i1.2025

Bao, C., Feng, P., Zhang, D., Wang, Q., & Yang, S. (2024). Conceptual design and experimental investigation of regolith bag structures for lunar *in situ* construction. *Journal of Building Engineering*, *95*, 110245. https://doi.org/10.1016/j.jobe.2024.110245

Barker, M. K., Mazarico, E., Neumann, G. A., Smith, D. E., Zuber, M. T., & Head, J. W. (2021). Improved LOLA elevation maps for south pole landing sites: Error estimates and their impact on illumination conditions. *Planetary and Space Science*, *203*, 105119. https://doi.org/10.1016/j.pss.2020.105119

Becker, T., Lüking, A., Meinert, T., & Panajotovic, S. (2019, May). Moonfibre - fibres from lunar regolith. https://doi.org/10.13140/RG.2.2.12287.36007

Bernhardt, H., Robinson, M. S., & Boyd, A. K. (2022). Geomorphic map and science target identification on the Shackleton-de Gerlache ridge. *Icarus*, *379*, 114963. https://doi.org/10.1016/j.icarus.2022.114963

Bleacher, J. E., George, T., & Esty, C. C. (2024, February). *Lunar Site Selection* (tech. rep.) (NTRS Author Affiliations: Goddard Space Flight Center, Johnson Space Center NTRS Document ID: 20230016267 NTRS Research Center: Headquarters (HQ)). Retrieved March 13, 2025, from https://ntrs.nasa.gov/citations/20230016267

Boazman, S. J., Shah, J., Harish, Gawronska, A. J., Halim, S. H., Satyakumar, A. V., Gilmour, C. M., Bickel, V. T., Barrett, N., & Kring, D. A. (2022). The Distribution and Accessibility of Geologic Targets near the Lunar South Pole and Candidate Artemis Landing Sites [Publisher: IOP Publishing]. *The Planetary Science Journal*, *3*(12), 275. https://doi.org/10.3847/PSJ/aca590

Bussey, D. B. J., McGovern, J. A., Spudis, P. D., Neish, C. D., Noda, H., Ishihara, Y., & Sørensen, S. .-. (2010). Illumination conditions of the south pole of the Moon derived using Kaguya topography. *Icarus*, *208*(2), 558–564. https://doi.org/10.1016/j.icarus.2010.03.028

Carrio, L. F., Palmer, R., Lillard, A., Hilliard, S., Morzel, J., Harvey, A., Ball, N., Gebhardt, A., Dietz, H., & Cichan, T. (2023, October). System-of-Systems Analysis Approach to Establishing Lunar Infrastructure. In *ASCEND 2023*. American Institute of Aeronautics; Astronautics. https://doi.org/10.2514/6.2023-4612

Chang, B. C., Bernold, L. E., & Lee, T. S. (2010). Experimental Study of Lunar Regolith Anchoring Forces | Request PDF. *ResearchGate*. https://doi.org/10.1061/41096(366)127

Cheng, S., Gao, Y., Shi, Y., Xiao, L., Ding, L., Zhou, C., & Zhou, Y. (2024). Advances in in-situ resources utilization for extraterrestrial construction. *Advances in Space Research*, *74*(7), 3297–3325. https://doi.org/10.1016/j.asr.2024.06.029

Creech, S., Guidi, J., & Elburn, D. (2022). Artemis: An Overview of NASA's Activities to Return Humans to the Moon [ISSN: 1095-323X]. *2022 IEEE Aerospace Conference (AERO)*, 1–7. https://doi.org/10.1109/AERO53065.2022.9843277

Csank, J. (2023, April). NASA Lunar Surface Operations & Power Grid.

De M. Wahrhaftig, A., Brasil, R. M. L. R. F., & Balthazar, J. M. (2013). The first frequency of cantilevered bars with geometric effect: A mathematical and experimental evaluation. *Journal of the Brazilian Society of Mechanical Sciences and Engineering*, *35*(4), 457–467. https://doi.org/10.1007/s40430-013-0043-9

Doggett, W. R., Heppler, J., Mahlin, M. K., Pappa, R. S., Teter, J., Song, K., White, B., Wong, I., & Mikulas, M. (2022, February). Towers: Critical Initial Infrastructure for the Moon. In *AIAA SCITECH 2023 Forum*. American Institute of Aeronautics; Astronautics. https://doi.org/10.2514/6.2023-0383

Ebert, T., & Larochelle, P. (2016). Simulation of soft regolith dynamic anchors for celestial exploration. *2016 IEEE Aerospace Conference*, 1–7. https://doi.org/10.1109/AERO.2016.7500767

Edwards, B. (2023, September). Communications and Navigation [NTRS Author Affiliations: Goddard Space Flight Center NTRS Meeting Information: NASA STMD Game Changing Division 2023 Annual Review; 2023-09-19 to 2023-09-21; undefined NTRS Document ID: 20230013057 NTRS Research Center: Goddard Space Flight Center (GSFC)]. Retrieved December 12, 2024, from https://ntrs.nasa.gov/citations/20230013057

Edwards, B., Wagner, R., Zemba, M., Millard, W., Braham, S., Gifford, K., & Somerlock, O. (2023). 3GPP Mobile Telecommunications Technology on the Moon [ISSN: 1095-323X]. *2023 IEEE Aerospace Conference*, 1–12. https://doi.org/10.1109/AERO55745.2023.10115746

El Samid, N. A., Thangavelautham, J., Richard, J., Boucher, D., & D'Eleuterio, G. M. (2008). Infrastructure robotics: 59th International Astronautical Congress 2008, IAC 2008. *International Astronautical Federation - 59th International Astronautical Congress 2008, IAC 2008*, 2045–2058. Retrieved April 18, 2025, from http://www.scopus.com/inward/record.url?scp=77950476978&partnerID=8YFLogxK

Faßwald, J., Kömle, N. I., Bentley, M. S., & Weiss, P. (2012). Considerations on a suction drill for lunar surface drilling and sampling: II. experimental tests in vacuum conditions. *Acta Geotechnica*, *7*(2), 115–127. https://doi.org/10.1007/s11440-011-0155-2

Feng, Y., Li, H., Tong, X., Li, P., Wang, R., Chen, S., Xi, M., Sun, J., Wang, Y., He, H., Wang, C., Xu, X., Xie, H., Jin, Y., & Liu, S. (2024). Optimized Landing Site Selection at the Lunar South Pole: A Convolutional Neural Network Approach [Conference Name: IEEE Journal of Selected Topics in Applied Earth Observations and Remote Sensing]. *IEEE Journal of Selected Topics in Applied Earth Observations and Remote Sensing*, *17*, 10998–11015. https://doi.org/10.1109/JSTARS.2024.3407070

Ferdous, W., Manalo, A., Wong, H. S., Abousnina, R., AlAjarmeh, O. S., Zhuge, Y., & Schubel, P. (2020). Optimal design for epoxy polymer concrete based on mechanical properties and durability aspects. *Construction and Building Materials*, *232*, 117229. https://doi.org/10.1016/j.conbuildmat.2019.117229

Fincannon, J. (2007). Lunar South Pole Illumination: Review, Reassessment, and Power System Implications. In *5th International Energy Conversion Engineering Conference and Exhibit (IECEC)*. American Institute of Aeronautics; Astronautics. https://doi.org/10.2514/6.2007-4700

Fincannon, J. (2008). Characterization of Lunar Polar Illumination from a Power System Perspective. In *46th AIAA Aerospace Sciences Meeting and Exhibit*. American Institute of Aeronautics; Astronautics. https://doi.org/10.2514/6.2008-447

Frohlich, C., & Nakamura, Y. (2006). Possible extra-Solar-System cause for certain lunar seismic events. *Icarus*, *185*(1), 21–28. https://doi.org/10.1016/j.icarus.2006.07.002

Gawronska, A. J., Barrett, N., Boazman, S. J., Gilmour, C. M., Halim, S. H., Harish, McCanaan, K., Satyakumar, A. V., Shah, J., Meyer, H. M., & Kring, D. A. (2020). Geologic context and potential EVA targets at the lunar south pole. *Advances in Space Research*, *66*(6), 1247–1264. https://doi.org/10.1016/j.asr.2020.05.035

Ghannam, M., Mahmoud, N. S., Badr, A., & Salem, F. A. (2017). Numerical Analysis for Strengthening Steel Trusses using Post Tensioned Cables.

Gillet, K., Margerin, L., Calvet, M., & Monnereau, M. (2017). Scattering attenuation profile of the Moon: Implications for shallow moonquakes and the structure of the megaregolith. *Physics of the Earth and Planetary Interiors*, *262*, 28–40. https://doi.org/10.1016/j.pepi.2016.11.001

Gläser, P., Scholten, F., De Rosa, D., Marco Figuera, R., Oberst, J., Mazarico, E., Neumann, G. A., & Robinson, M. S. (2014). Illumination conditions at the lunar south pole using high resolution Digital Terrain Models from LOLA. *Icarus*, *243*, 78–90. https://doi.org/10.1016/j.icarus.2014.08.013

Goins, N. R., Dainty, A. M., & Toksöz, M. N. (1981). Seismic energy release of the Moon. *Journal of Geophysical Research: Solid Earth*, *86*(B1), 378–388. https://doi.org/10.1029/JB086iB01p00378

Gracia, V., & Casanova, I. (2012). Sulfur Concrete: A Viable Alternative for Lunar Construction [Publisher: American Society of Civil Engineers], 585–591. https://doi.org/10.1061/40339(206)67

Grugel, R. N., & Toutanji, H. (2008). Sulfur “concrete” for lunar applications – Sublimation concerns. *Advances in Space Research*, *41*(1), 103–112. https://doi.org/10.1016/j.asr.2007.08.018

Grünberg, J., & Göhlmann, J. (2013). References. In *Concrete structures for wind turbines* (pp. 209–215). John Wiley & Sons, Ltd. https://doi.org/https://doi.org/10.1002/9783433603291.refs

Heffels, A., Knapmeyer, M., Oberst, J., & Haase, I. (2017). Re-evaluation of Apollo 17 Lunar Seismic Profiling Experiment data. *Planetary and Space Science*, *135*, 43–54. https://doi.org/10.1016/j.pss.2016.11.007

Heiken, G., Vaniman, D., & French, B. (1991). Lunar sourcebook.

Hiesinger, H. (2006). New Views of Lunar Geoscience: An Introduction and Overview [Place: Washington, D.C. : Publisher: The Mineralogical Society of America,]. *Reviews in mineralogy and geochemistry.*, *60*(1).

Hilburger, M. (2024, April). An envisioned future for lunar infrastructure - technology development status & needs.

Hu, T., Yang, Z., Li, M., van der Bogert, C. H., Kang, Z., Xu, X., & Hiesinger, H. (2023). Possible sites for a Chinese International Lunar Research Station in the Lunar South Polar Region. *Planetary and Space Science*, *227*, 105623. https://doi.org/10.1016/j.pss.2022.105623

ICON. (2021). 3D-printed Rocket Pad. Retrieved April 18, 2025, from https://www.iconbuild.com/projects/3d-printed-rocket-pad

Jablonski, A. M., & Ogden, K. A. (2008). Technical Requirements for Lunar Structures [Publisher: American Society of Civil Engineers]. *Journal of Aerospace Engineering*, *21*(2), 72–90. https://doi.org/10.1061/(ASCE)0893-1321(2008)21:2(72)

Jakus, A. E., Koube, K. D., Geisendorfer, N. R., & Shah, R. N. (2017). Robust and Elastic Lunar and Martian Structures from 3D-Printed Regolith Inks [Publisher: Nature Publishing Group]. *Scientific Reports*, *7*(1), 44931. https://doi.org/10.1038/srep44931

Jaumann, R., Hiesinger, H., Anand, M., Crawford, I. A., Wagner, R., Sohl, F., Jolliff, B. L., Scholten, F., Knapmeyer, M., Hoffmann, H., Hussmann, H., Grott, M., Hempel, S., Köhler, U., Krohn, K., Schmitz, N., Carpenter, J., Wieczorek, M., Spohn, T., … Oberst, J. (2012). Geology, geochemistry, and geophysics of the Moon: Status of current understanding. *Planetary and Space Science*, *74*(1), 15–41. https://doi.org/10.1016/j.pss.2012.08.019

Jayathilake, B. A. C. S., Ilankoon, I. M. S. K., & Dushyantha, M. N. P. (2022). Assessment of significant geotechnical parameters for lunar regolith excavations. *Acta Astronautica*, *196*, 107–122. https://doi.org/10.1016/j.actaastro.2022.04.008

Jung, K.-C., Roh, I.-T., & Chang, S.-H. (2014). Evaluation of mechanical properties of polymer concretes for the rapid repair of runways. *Composites Part B: Engineering*, *58*, 352–360. https://doi.org/10.1016/j.compositesb.2013.10.076

Kalapodis, N., Kampas, G., & Ktenidou, O.-J. (2020). A review towards the design of extraterrestrial structures: From regolith to human outposts. *Acta Astronautica*, *175*, 540–569. https://doi.org/10.1016/j.actaastro.2020.05.038

Klosky, J. L., Sture, S., Ko, H. Y., & Barnes, F. (1998). Helical anchors for combined anchoring and soil testing in lunar operations. *In Space 98*, 489–494.

Knapmeyer-Endrun, B., & Hammer, C. (2015). Identification of new events in Apollo 16 lunar seismic data by Hidden Markov Model-based event detection and classification. *Journal of Geophysical Research: Planets*, *120*(10), 1620–1645. https://doi.org/10.1002/2015JE004862

Knez, D., & Zamani, M. A. M. (2021). A Review of the Geomechanics Aspects in Space Exploration [Number: 22 Publisher: Multidisciplinary Digital Publishing Institute]. *Energies*, *14*(22), 7522. https://doi.org/10.3390/en14227522

Konstantatou, M., Sena, A., Cann, G., Gallou, I., Perez, S. N., Punch, O., Guberman, M., Goodloe, D., & Boyd, P. (2025). Conceptual Design, Manufacturing, and Assembly of a Tall Lunar Tower. In L. Bensch, T. Nilsson, M. Nisser, P. Pataranutaporn, A. Schmidt, & V. Sumini (Eds.), *Advancing human-computer interaction for space exploration (spacechi 2025)* (12:1–12:13, Vol. 130). Schloss Dagstuhl – Leibniz-Zentrum für Informatik. https://doi.org/10.4230/OASIcs.SpaceCHI.2025.12

Keywords: Space Architecture, Lunar Infrastructure, Lunar Tower, Additive Manufacturing, In Situ Resource Utilisation (ISRU), Solar Energy.

Kramer, G. (2020). Origin, Geography, and Geology of the Moon. In P. Eckart & A. Aldrin (Eds.), *Handbook of Lunar Base Design and Development* (pp. 1–22). Springer International Publishing. https://doi.org/10.1007/978-3-030-05323-9_52-1

Krasilnikov, A. S., Ivanov, M. A., Krasilnikov, S. S., & Head, J. W. (2024). Stratigraphic cross-sections, geologic history, and provenance of material at the candidate landing sites of the Artemis missions. *Icarus*, *420*, 116190. https://doi.org/10.1016/j.icarus.2024.116190

Lammlein, D. R., Latham, G. V., Dorman, J., Nakamura, Y., & Ewing, M. (1974). Lunar seismicity, structure, and tectonics. *Reviews of Geophysics*, *12*(1), 1–21. https://doi.org/10.1029/RG012i001p00001

Latham, G., Ewing, M., Dorman, J., Lammlein, D., Press, F., Toksoz, N., Sutton, G., Duennebier, F., & Nakamura, Y. (1971). Moonquakes [Publisher: American Association for the Advancement of Science]. *Science*, *174*(4010), 687–692. https://doi.org/10.1126/science.174.4010.687

Latham, G., Ewing, M., Dorman, J., Press, F., Toksoz, N., Sutton, G., Meissner, R., Duennebier, F., Nakamura, Y., Kovach, R., & Yates, M. (1970). Seismic Data from Man-Made Impacts on the Moon [Publisher: American Association for the Advancement of Science]. *Science*, *170*(3958), 620–626. https://doi.org/10.1126/science.170.3958.620

Lawrence, S. (2022, April). Lunar Exploration in the 21st Century [NTRS Author Affiliations: Johnson Space Center NTRS Meeting Information: 2022 Korean Aerospace Research Institute Space Lecture Series; 2022-04-26 to 2022-04-26; undefined NTRS Document ID: 20220006004 NTRS Research Center: Johnson Space Center (JSC)]. Retrieved October 17, 2024, from https://ntrs.nasa.gov/citations/20220006004

Lucas, M. P., Neal, C. R., Long-Fox, J. M., & Britt, D. (2024). Simulating lunar highlands regolith profiles on Earth to inform infrastructure development and ISRU activities on the Moon. *Acta Astronautica*, *224*, 161–171. https://doi.org/10.1016/j.actaastro.2024.08.019

Mazarico, E., Neumann, G. A., Smith, D. E., Zuber, M. T., & Torrence, M. H. (2011). Illumination conditions of the lunar polar regions using LOLA topography. *Icarus*, *211*(2), 1066–1081. https://doi.org/10.1016/j.icarus.2010.10.030

Meyers, C., & Toutanji, H. (2007). Analysis of Lunar-Habitat Structure Using Waterless Concrete and Tension Glass Fibers [Publisher: American Society of Civil Engineers]. *Journal of Aerospace Engineering*, *20*(4), 220–226. https://doi.org/10.1061/(ASCE)0893-1321(2007)20:4(220)

More, C. V., Alsayed, Z., Badawi, M. S., Thabet, A. A., & Pawar, P. P. (2021). Polymeric composite materials for radiation shielding: A review. *Environmental Chemistry Letters*, *19*(3), 2057–2090. https://doi.org/10.1007/s10311-021-01189-9

Moriarty, D., Neal, C., & Lawrence, S. (2021). The Moon is a Special Place. *Bulletin of the AAS*, *53*(4). https://doi.org/10.3847/25c2cfeb.13220a63

Mueller, R. P., Howe, S., Kochmann, D., Ali, H., Andersen, C., Burgoyne, H., Chambers, W., Clinton, R., De Kestellier, X., Ebelt, K., Gerner, S., Hofmann, D., Hogstrom, K., Ilves, E., Jerves, A., Keenan, R., Keravala, J., Khoshnevis, B., Lim, S., … Zelhofer, A. (2016). Automated Additive Construction (AAC) for Earth and Space Using In Situ Resources. *Earth and Space 2016*, 354–377. https://doi.org/10.1061/9780784479971.036

Nakamura, Y., Latham, G. V., Dorman, H. J., Ibrahim, A.-B. K., Koyama, J., & Horvath, P. (1979, January). *Shallow moonquakes - Depth, distribution and implications as to the present state of the lunar interior* [NTRS Author Affiliations: Marine Science Inst., Texas, University NTRS Meeting Information: Lunar and Planetary Science Conference; 1979-03-19 to 1979-03-23; undefined NTRS Document ID: 19800039522 NTRS Research Center: Legacy CDMS (CDMS)]. Retrieved January 16, 2025, from https://ntrs.nasa.gov/citations/19800039522

Nakamura, Y. (1977). HFT events: Shallow moonquakes? *Physics of the Earth and Planetary Interiors*, *14*(3), 217–223. https://doi.org/10.1016/0031-9201(77)90174-1

Nakamura, Y. (1982). Lunar Seismic Data Analysis, Final Technical Report, NASA Grant NSG-7418 30 June 1982. UTIG Galveston [Publisher: Institute for Geophysics]. Retrieved January 16, 2025, from http://hdl.handle.net/2152/65409

Nakamura, Y., Latham, G. V., & Dorman, H. J. (1982). Apollo Lunar Seismic Experiment—Final summary. *Journal of Geophysical Research: Solid Earth*, *87*(S01), A117–A123. https://doi.org/10.1029/JB087iS01p0A117

NASA. (2022a). NASA Identifies Candidate Regions for Landing Next Americans on Moon - NASA [Running Time: 120 Section: Goddard Space Flight Center]. https://www.nasa.gov/news-release/nasa-identifies-candidate-regions-for-landing-next-americans-on-moon/

NASA. (2022b). Why artemis will focus on the lunar south polar region.

NASA. (2023). Nasa's moon to mars strategy and objectives development. https://www.nasa.gov/wp-content/uploads/2023/04/m2m_strategy_and_objectives_development.pdf?emrc=c21aff

National Space Council. (2020). *Nasa's plan for sustained lunar exploration and development* (tech. rep.). NASA.

Nunn, C., Garcia, R. F., Nakamura, Y., Marusiak, A. G., Kawamura, T., Sun, D., Margerin, L., Weber, R., Drilleau, M., Wieczorek, M. A., Khan, A., Rivoldini, A., Lognonné, P., & Zhu, P. (2020). Lunar Seismology: A Data and Instrumentation Review. *Space Science Reviews*, *216*(5), 89. https://doi.org/10.1007/s11214-020-00709-3

Oberst, J., & Nakamura, Y. (1992). A seismic risk for the lunar base [NTRS Author Affiliations: Texas Univ. NTRS Report/Patent Number: CONTRIB-769 NTRS Document ID: 19930008250 NTRS Research Center: Legacy CDMS (CDMS)]. Retrieved October 3, 2024, from https://ntrs.nasa.gov/citations/19930008250

Oberst, J. (1987). Unusually high stress drops associated with shallow moonquakes. *Journal of Geophysical Research: Solid Earth*, *92*(B2), 1397–1405. https://doi.org/10.1029/JB092iB02p01397

Ockleston, A. (1950). The structural use of sorel cement concrete.

Onodera, K. (2024). New Views of Lunar Seismicity Brought by Analysis of Newly Discovered Moonquakes in Apollo Short-Period Seismic Data. *Journal of Geophysical Research: Planets*, *129*(7), e2023JE008153. https://doi.org/10.1029/2023JE008153 e2023JE008153 2023JE008153.

Osio-Norgaard, J., Hayes, A. C., & Whiting, G. L. (2021). Sintering of 3D printable simulated lunar regolith magnesium oxychloride cements. *Acta Astronautica*, *183*, 227–232. https://doi.org/10.1016/j.actaastro.2021.03.016

Paul, J., & Wamelink, H. (2017). Introduction to seismic essentials in groningen. https://ocw.tudelft.nl/courses/introduction-seismic-essentials-groningen/

Pilehvar, S., Arnhof, M., Pamies, R., Valentini, L., & Kjøniksen, A.-L. (2020). Utilization of urea as an accessible superplasticizer on the moon for lunar geopolymer mixtures. *Journal of Cleaner Production*, *247*, 119177. https://doi.org/10.1016/j.jclepro.2019.119177

Przwerlócki, D., & Świniański. (2005). (PDF) Review of historical buildings' foundations. *ResearchGate*. https://doi.org/10.1680/geot.55.5.363.66017

Ross, A., Ruppert, S., Glaser, P., & Elvis, M. (2021). Towers on the Peaks of Eternal Light: Quantifying the Available Solar Power. Retrieved January 8, 2025, from https://www.semanticscholar.org/paper/Towers-on-the-Peaks-of-Eternal-Light%3A-Quantifying-Ross-Ruppert/25d0eaed43f8ec3d25a9172189778a8fc1122870

Ruess, F., Schaenzlin, J., & Benaroya, H. (2006). Structural Design of a Lunar Habitat [Publisher: American Society of Civil Engineers]. *Journal of Aerospace Engineering*, *19*(3), 133–157. https://doi.org/10.1061/(ASCE)0893-1321(2006)19:3(133)

Ruiz, S., Cruz, A., Gomez, D., Dyke, S. J., & Ramirez, J. (2022). Preliminary approach to assess the seismic hazard on a lunar site. *Icarus*, *383*, 115056. https://doi.org/10.1016/j.icarus.2022.115056

Ruppert, S., Ross, A., Vlassak, J., & Elvis, M. (2022, February). Tall Towers on the Moon [arXiv:2103.00612 [astro-ph]]. https://doi.org/10.48550/arXiv.2103.00612
Comment: 12 pages, 10 figures, submitted for publication in New Space.

Scott, A. N., & Oze, C. (2018). Constructing Mars: Concrete and Energy Production From Serpentinization Products. *Earth and Space Science*, *5*(8), 364–370. https://doi.org/10.1029/2017EA000353

Slyuta, E. N. (2014). Physical and mechanical properties of the lunar soil (a review). *Solar System Research*, *48*(5), 330–353. https://doi.org/10.1134/S0038094614050050

Sollberger, D., Schmelzbach, C., Robertsson, J. O. A., Greenhalgh, S. A., Nakamura, Y., & Khan, A. (2016). The shallow elastic structure of the lunar crust: New insights from seismic wavefield gradient analysis. *Geophysical Research Letters*, *43*(19), 10, 078–10, 087. https://doi.org/10.1002/2016GL070883

Song, K., Mikulas, M., Mahlin, M. K., & Cassady, J. T. (2023, January). Sizing and design tool for tall lunar tower. In *Aiaa scitech 2023 forum*. https://doi.org/10.2514/6.2023-0382

Song, K., Stark, A. E., Amundsen, R. M., Mikulas, M., Mahlin, M. K., & Cassady, J. T. (2023, October). Sizing, Buckling, and Thermal-Structural Analysis of Tall Lunar Tower. In *ASCEND 2023*. American Institute of Aeronautics; Astronautics. https://doi.org/10.2514/6.2023-4753

Stopar, J., & Meyer, H. (2019). Topographic Map of the Moon's South Pole (80°S to Pole) [Publisher: Lunar and Planetary Institute, Regional Planetary Image Facility]. Retrieved March 12, 2025, from https://hdl.handle.net/20.500.11753/1254

STUBECO, S. (2015). Voorspanning. https://www.stubeco.nl/7-voorspanning.html

Taveau, J. (2024, October). NASA Provides Update on Artemis III Moon Landing Regions - NASA. Retrieved January 27, 2025, from https://www.nasa.gov/news-release/nasa-provides-update-on-artemis-iii-moon-landing-regions/

Thesis Prep course. (n.d.). General lecture notes for hydraulic structures.

Tiffin, D., & Mahlin, M. (2023, October). Tall lunar towers: Systems analysis of lunar-surface-assembled power, communication, and navigation infrastructure. In *Ascend 2023*. https://doi.org/10.2514/6.2023-4754

Toklu, Y. C., & Akpinar, P. (2022). Lunar soils, simulants and lunar construction materials: An overview. *Advances in Space Research*, *70*(3), 762–779. https://doi.org/10.1016/j.asr.2022.05.017

Valinia, A., Grunsfeld, J. M., Hess, M. G., Green, J., Schier, J., Haas, J. P., Weber, R. C., Dischinger, C., White, N. E., McClenskey, C. M., John, K. K., Edwards, R. D., & Stalcup, E. J. (2022). Unique Science from the Moon in the Artemis Era.

Wang, Y., Wang, J., Zhang, G., Gao, M., Zhang, X., & Xie, H. (2024). Advances in Drill-Based Sampling Technology for Extraterrestrial Bodies. *Space Science Reviews*, *220*(6), 66. https://doi.org/10.1007/s11214-024-01100-2

Wu, C., Yu, Z., Shao, R., & Li, J. (2024). A comprehensive review of extraterrestrial construction, from space concrete materials to habitat structures. *Engineering Structures*, *318*, 118723. https://doi.org/10.1016/j.engstruct.2024.118723

Xing, D., Xi, X., Guo, Z., Yue, X., Hao, B., Liang, C., Gu, Y., Chen, T., Wang, R., & Ma, P. (2020). Study on the feasibility of preparing a continuous fibre using lunar soil simulant [Publisher: Science China Press]. *SCIENTIA SINICA Technologica*, *50*(12), 1625–1633. https://doi.org/10.1360/SST-2020-0141

Xiong, G., Guo, X., Yuan, S., Xia, M., & Wang, Z. (2022). The mechanical and structural properties of lunar regolith simulant based geopolymer under extreme temperature environment on the moon through experimental and simulation methods. *Construction and Building Materials*, *325*, 126679. https://doi.org/10.1016/j.conbuildmat.2022.126679

Yazici, S. (2018). Building in Extraterrestrial Environments: T-Brick Shell [Publisher: American Society of Civil Engineers]. *Journal of Architectural Engineering*, *24*(1), 04017037. https://doi.org/10.1061/(ASCE)AE.1943-5568.0000293

Yoshida, S., & Xiong, X. (2023, August). A limit equilibrium method for estimating pull-out resistance of flip-type ground anchors in sand grounds. https://doi.org/10.1201/9781003299127-150

Yoshida, S., Xiong, X., & Matsumoto, T. (2023). Experimental and numerical study on reinforcement effect of plate anchors or flip anchors on model slopes. *Soils and Foundations*, *63*(2), 101285. https://doi.org/10.1016/j.sandf.2023.101285

Young, K., Jr., J. M. H., Graff, T. G., Moriarty, D. P., Valencia, S., Watkins, R., Petro, N., Runyon, K., Morse, Z. R., Fagan, A., Neal, C. R., & Watkins, J. (2021). The Importance of Human Exploration in Accomplishing High Priority Lunar Science Objectives. *Bulletin of the AAS*, *53*(4). https://doi.org/10.3847/25c2cfeb.812f2213

Zacny, K. (2012). Lunar Drilling, Excavation and Mining in Support of Science, Exploration, Construction, and In Situ Resource Utilization (ISRU). In V. Badescu (Ed.), *Moon: Prospective Energy and Material Resources* (pp. 235–265). Springer. https://doi.org/10.1007/978-3-642-27969-0_10

Zarzycki, P. K., & Katzer, J. (2019). Multivariate comparison of lunar soil simulants. *Journal of Aerospace Engineering*, *32*. https://doi.org/10.1061/(ASCE)AS.1943-5525.0001075

Zhang, P., Dai, W., Niu, R., Zhang, G., Liu, G., Liu, X., Bo, Z., Wang, Z., Zheng, H., Liu, C., Yang, H., Bai, Y., Zhang, Y., Yan, D., Zhou, K., & Gao, M. (2023). Overview of the Lunar In Situ Resource Utilization Techniques for Future Lunar Missions [Publisher: American Association

for the Advancement of Science]. *Space: Science & Technology*, *3*, 0037. https://doi.org/10.34133/space.0037

Zhong, C., & Christopoulos, C. (2022). Self-centering seismic-resistant structures: Historical overview and state-of-the-art [Publisher: SAGE Publications Ltd STM]. *Earthquake Spectra*, *38*(2), 1321–1356. https://doi.org/10.1177/87552930211057581

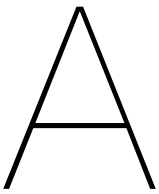

Appendix A: Consideration MCA scores

Transportation cost

- Slab: Can be made from local material, but it is necessary to bring equipment to produce these materials.
- Slab + anchors: Anchors need to be brought from earth. Slab can be built locally.
- Pile: Slab and piles could be produced locally, but equipment to ”auger” piles and make the slab needs to be brought from Earth
- Piled raft: Equipment to made piles should be brought from Earth as well as equipment to make the slab
- Rocking podium: Equipment to make slab and column structure needs to be brought, but all material can be produced locally.
- Isolation bearing: Equipment to make slab needed and equipment to produce elastic material,
- Friction pendulum bearing: The precision of the friction pendulum likely requires it to be brought from Earth.
- Gothic: Local debris and a binding agent made from local material needs to be used, binder needs to be produced by equipment.
- Brick column: Sintering devices need to be brought, but bricks can be produced locally.
- Strap: Can be made from local material, but it is necessary to bring equipment to produce these materials.

Material Production Energy

This one is hard to use, since there is no information available on the power consumption of different techniques in comparison to others. Only preliminary guesses were made based on engineering judgement.

- Slab: Needs to be 3D-printed / assembled. Depending on the material, production energy would be high.
- Slab + anchors: Needs to be 3D-printed / assembled. Depending on the material, production energy would be high. Anchors are imported from Earth, however.
- Pile: Material required to pour into holes that are assumed to be quite deep
- Piled raft: Large amount of material required
- Rocking podium: Needs more material than only a slab, has large columns

- Isolation bearing: Needs both a rubber-like material to be produced and a slab
- Friction pendulum bearing: Most of the foundation needs to be brought from Earth, so barely any material is likely to be produced.
- Gothic: Only mortar needs to be produced, and regolith gathered
- Brick column: Bricks can be produced with the sintering technique
- Strap: Needs to be 3D-printed / assembled. Depending on the material, production energy would be high.

Ease of Construction

- Slab: Slabs are close to the surface and easy to cast/assemble
- Slab + anchors: Only a few anchors required to be placed, and an easy shallow foundation
- Pile: Assumed auger technique available
- Piled raft: Assumed auger technique available, need to get deep into the regolith and make a relatively complex structure
- Rocking podium: Easy shapes that can be made with various techniques
- Isolation bearing: Requires several steps to produce the material and precision to put them together
- Friction pendulum bearing: Steel components can be brought from Earth; they just need to be precisely assembled with difficult geometric components.
- Gothic: Can be made from randomly found material and can be assembled easily.
- Brick column: Bricks are easily produced and stacked together.
- Strap: Slabs are close to the surface and easy to cast/assemble. The pattern takes more care to be produced.

Use of local materials

- Slab: Can be completely produced from local materials
- Slab + anchors: Slab can be made from local material; anchors need to be brought from Earth.
- Pile: Can be completely produced from local materials
- Piled raft: Can be completely produced from local materials
- Rocking podium: Can be completely produced from local materials
- Isolation bearing: material Jakus et al. (2017) has elastic properties, can be made from local material, but the compressive strength is heavily dependent on the geometry, porosity and loading conditions. Assumed to work; if not, the material needs to be brought from Earth.
- Friction pendulum bearing: Slab can be made from local material; however, in literature, these friction pendulum bearings are usually made from steel and are high-precision elements that likely need to be produced on Earth.
- Gothic: Can be completely produced from local materials
- Brick column: Can be completely produced from local materials
- Strap: Can be completely produced from local materials

Excavatbility

- Slab: Depending on a possible embedment, but will remain shallow.
- Slab + anchors: Depending on a possible embedment of the slab, but will remain shallow.
- Pile: Assumed to need to go deep into lunar regolith.
- Piled raft: Assumed to need to go deep into lunar regolith.
- Rocking podium: To get an effective rocking mechanism going under the ground so accessibility for maintenance remains, needs to go deeper than isolation bearings likely.
- Isolation bearing: Will likely need to be embedded depending on the vertical dimensions of the isolation bearing. Probably needs more than a slab foundation.
- Friction pendulum bearing: Will likely need to be embedded depending on the vertical dimensions of the friction pendulum bearing. Probably needs more than a slab foundation.
- Gothic: Assumed it needs to go less shallow than a slab foundation, but not as deep as to provide base isolation.
- Brick column: Assumed it needs to go less shallow than a slab foundation, but not as deep as to provide base isolation.
- Strap: Depending on a possible embedment, but will remain shallow.

Experience with the construction method on Earth

- Slab: Common. If interlocking tiles are used, this score lowers.
- Slab + anchors: Experience with anchors, but not with the specific anchors available for lunar construction. Not used for foundations.
- Pile: Pile foundations are common.
- Piled raft: Common.
- Rocking podium: Something that was historically done, but is not used explicitly anymore.
- Isolation bearing: These base isolation methods are being used in earthquake-prone environments.
- Friction pendulum bearing: These base isolation methods are being used in earthquake-prone environments.
- Gothic: Something that was historically done, but is not used explicitly anymore. Random array of rocks introduces uncertainty.
- Brick column: Something that was historically done, but is not used explicitly anymore.
- Strap: Common.

Sensitivity to settlements

- Slab: Will rest on soil with a lower deformation modulus and a less dense state. Therefore, it will cause settlements.
- Slab + anchors: Will rest on soil with a lower deformation modulus and a less dense state. Therefore, it will cause settlements. The size of the slab is reduced compared to the slab alone, as the forces on the slab are reduced by the anchors.
- Pile: Will be resting on the denser rocks, but the deformation modulus of lunar regolith at 3 meters is still low
- Piled raft: Will be resting on the denser rocks, but the deformation modulus of lunar regolith at 3 meters is still low

- Rocking podium: Depending on the length of the columns, the excavation will allow the foundation to rest on layers with a higher deformation modulus
- Isolation bearing: Will be put several meters into the soil, where the density of the lunar regolith is better and therefore, fewer settlements will occur. The deformation modulus of lunar regolith at a depth of 3 meters, however, is still low.
- Friction pendulum bearing: Will be put several meters into the soil, where the density of the lunar regolith is better and therefore, fewer settlements will occur. The deformation modulus of lunar regolith at a depth of 3 meters, however, is still low.
- Gothic: Rests on shallow soil, introduces uncertainties in weight distribution and likely causes differential settlements and thus rotations of the top structure.
- Brick column: Will be put several meters into the soil, where the density of the lunar regolith is better and therefore, fewer settlements will occur. The deformation modulus of lunar regolith at a depth of 3 meters, however, is still low.
- Strap: Will rest on soil with a lower deformation modulus and a less dense state. Therefore, it will cause settlements. Can easily be subject to differential settlements.

B

Appendix B: Alternative Pile Foundation

An alternative for a shallow foundation, once more data is available and equipment is developed, is a pile foundation. To use the NEN-EN 1997-1 design standards for axially loaded piles, Cone Penetration Test (CPT) data is normally used. During Apollo 16, several penetrometer tests were performed, but these only reached a depth of almost 80 cm, where the maximum stress reached was about 1500 kPa. The CPT data from Apollo 16 can be found in Figure B.1.

B.1. Methodology

When looking at the NEN-EN 1997-1 calculation method, the maximum bearing capacity $R_{c;cal;i}$ for a pile can be determined by adding the maximum tip bearing capacity $R_{b;cal;max;i}$ and the shaft resistance $R_{s;cal;max;i}$:

$$R_{c;cal;i} = R_{b;cal;max;i} + R_{s;cal;max;i} \tag{B.1}$$

Where the tip bearing capacity is calculated by:

$$\begin{aligned} R_{b;cal;max;i} &= A_b * q_{b;max;i} \\ A_b &= 1/4 * \pi * D_{eq}^2 \end{aligned} \tag{B.2}$$

$$q_{b;max} = \frac{1}{2} * \alpha_p * \beta * s * (\frac{q_{c;I;gem} + q_{c;II;gem}}{2} + q_{c;III;gem}) \tag{B.3}$$

$$s = \frac{1 + \frac{sin\phi}{r}}{1 + sin\phi} \tag{B.4}$$

Where:

$R_{b;cal;max;i}$ the maximum bearing capacity of the pile near CPT i in kN;

A_b the area of the pile tip in m^2;

$q_{b;max;i}$ the maximum tip bearing capacity of the pile near CPT i in kN/m^2;

D_{eq} the equivalent outer diameter of the pile, dependent on the type of pile in m;

α_p the pile class factor for the tip bearing capacity, dependent on the type of pile;

β the factor that considers the influence of the shape of the base of the pile;

s the factor that considers the cross-section of the base of the pile;

$q_{c;I;gem}$, $q_{c;II;gem}$, $q_{c;III;gem}$ are all average values over certain sections of the CPT, however, due to the lack of data, an average value is assumed in kPa;

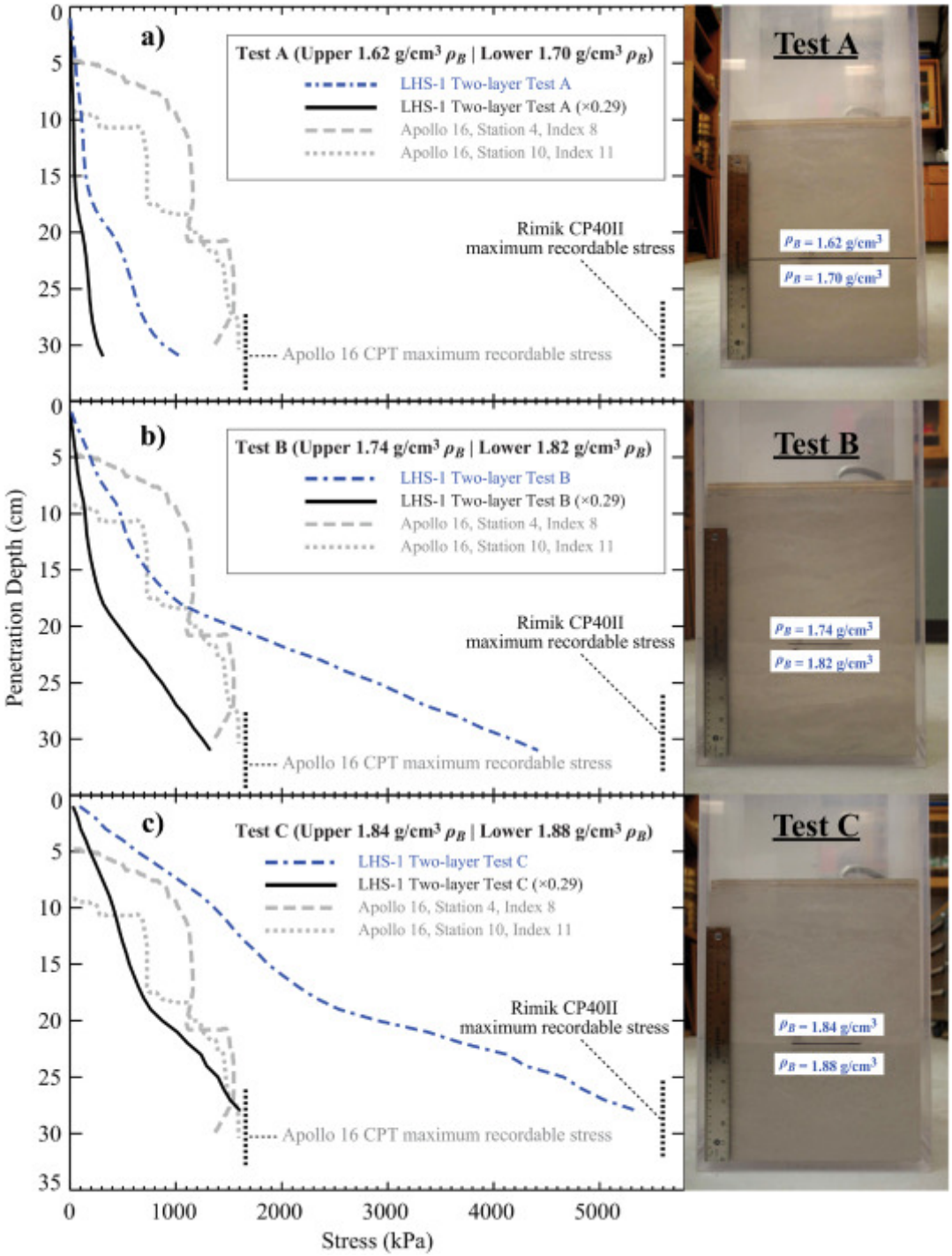

Figure B.1: A CPT test over 35 cm on a lunar simulant created by Lucas et al. (2024) to imitate the lunar regolith measurements during Apollo 16, the blue line is adjusted to the lunar conditions.

ϕ is the internal friction angle in °;

r is the radius of a circle, or the ratio of b/a for rectangular piles, where b is the largest distance of the pile base and a the smallest in m;

And the shaft resistance by:

$$R_{s;cal;max;i} = O_{s;\Delta L;gem} * \int_{\Delta L} q_{s;max;z;i}\, dz \tag{B.5}$$

$$q_{s;max;z} = \alpha_s * q_{c;z;a} \tag{B.6}$$

$$\begin{aligned} Circular:\ O_{s;\Delta L;gem} &= \pi * d_{eq} \\ Rectangular:\ O_{s;\Delta L;gem} &= 2a + 2b \end{aligned} \tag{B.7}$$

Where:

$R_{s;cal;max;i}$ the maximum share resistance at CPT i in kN;

$O_{s;\Delta L;gem}$ the average circumference of the pile tip in m;

ΔL the length of the part of the pile where shaft resistance can be included in m;

$q_{s;max;z;i}$ the maximum shaft friction at depth z, near CPT i in kN/m^2;

α_s the pile class factor for the shaft resistance dependent on the type of pile;

$q_{c;z;a}$ the cone resistance after applying reduction factors for excavating, OCR, grain sizes, and determining the average CPT values in kN/m^2;

d_{eq} the equivalent outer diameter for circular piles in m.

For piles under tension, the following formula can be used:

$$R_{t;d} = \int_0^L O_{s;gem} * q_{s;z;d}\, dz \tag{B.8}$$

$$q_{s;z;d} = \alpha_t * q_{c;z;d} \tag{B.9}$$

Where:

$R_{t;d}$ the value for the tension resistance of the pile in kN;

$O_{s;gem}$ the average circumference of the pile in m;

L the length of the part of the pile where shaft resistance can be included in m;

$q_{s;z;d}$ the shaft friction at depth z in kPa;

α_t the pile class factor for the tension resistance dependent on the type of pile;

$q_{c;z;d}$ the value of the cone resistance at depth z in kPa.

B.2. Results

The pile bearing capacity depends on the type of pile that will be used. In the lunar environment, there are limited options available. Therefore, this thesis assumes four types of piles to compare:

- Concrete prefabricated square pile. This pile needs to be hammered into the lunar soil, and this is highly unlikely due to the risk of densification and the lack of piling driving rigs available on the lunar surface. The pile needs to be fabricated using ISRU principles as well.
- Concrete prefabricated circular pile, which has similar limitations as described directly above.
- Auger pile. This type is likely more possible in the lunar environment. However, the equipment currently does not exist.
- Pile formed from supporting fluid. When drilling fluid is developed, combined with the equipment to form these piles, the piles could be made in situ.

These pile types have the following pile class factors:

Pile type	α_p	α_s	α_t
Concrete prefabricated	0.70	0.01	0.007
Auger Pile	0.30	0.006	0.0045
Pile formed from supporting fluid	0.35	0.006	0.0045

Table B.1: Pile class factors.

For the β factors, it is unknown what shape the pile foot is going to be in the future, as the value ranges from 0.6 - 1.0, a value of 1.0 is assumed.

The shape factor s is calculated for a circular foundation with radius of $0.1\ m$ and a square foundation that has the two sides $a = 0.2\ m$ and $b = 0.2\ m$.

$q_{c;I;gem}$, $q_{c;II;gem}$, $q_{c;III;gem}$, $q_{c;z;a}$, $q_{s;z;d}$, $q_{c;z;d}$ are all related to the CPT data. As there is limited data available, and only for approximately the first meter, a value of $1500kPa$ is assumed for these calculations. Pile group effects are not considered for the resistance against tension.

Pile type	$q_{b;max}$ [kPa]	$q_{s;max;z}$ [kPa]	$q_{s;z;d}$ [kPa]
Concrete prefabricated square	525.0	15.0	10.5
Concrete prefabricated circle	525.0	15.0	10.5
Auger Pile	225.0	9.0	6.8
Pile formed from supporting fluid	262.5	9.0	6.8

Table B.2: The values for the tip bearing capacity, shaft friction and shaft friction under tensile forces.

Each pile type requires its own D_{eq}, which is dependent on the type of equipment used to install the pile. For the square pile this is described as $D_{eq} = 1.13 * a * \sqrt{b/a}$, the D_{eq} for circular piles however, is based on the radius of the auger or other drilling equipment, and is therefore assumed to be the same as the pile radius of $0.1\ m$. The shaft resistance is also dependent on the length of the pile, which is assumed to be $3\ m$, based on the current maximum drilling depth.

Pile type	$R_{b;cal;max;i}$ [kN]	$R_{s;cal;max;i}$ [kN]	$R_{c;cal;i}$ [kN]	$R_{t;d}$ [kN]
Concrete prefabricated square	42	29	71	20
Concrete prefabricated circle	33	18	51	13
Auger Pile	14	11	25	8
Pile formed from supporting fluid	16	11	28	8

Table B.3: The tip bearing capacity, the shaft friction, the combined resistance under compression and the tension resistance of a pile.

For the static load of $V_{d,static} = 545\ kN$, the amount of piles can be calculated by dividing this value over the bearing capacity of a single pile:

$$nr\ of\ piles = V_{d,static}/R_{c;cal;i}$$

For the dynamic situation, the large second-order moment loads need to be divided over the piles. As a slab of $5\ m$ is assumed to be connected to the TLT to transfer the loads to the piles, the moment load can be divided in two forces by dividing it by $2/3 * B$. The number of tensile piles at one half of the foundation will then be:

$$F_{tension} = \frac{M_{dynamic;2nd}}{2/3 * B}$$

$$nr\ of\ piles = \frac{F_{tension}}{R_{t;d}}$$

Number of piles	r = 0.1, a=b= 0.1		r=0.3, a=b=0.3	
Pile type	$V_{d,static}$	$M_{dynamic;2nd}$	$V_{d,static}$	$M_{dynamic;2nd}$
Concrete prefabricated square	8	19 * 2	2	3 * 2
Concrete prefabricated circle	11	29 * 2	2	5 * 2
Auger Pile	22	45 * 2	4	7 * 2
Pile formed from supporting fluid	20	45 * 2	4	7 * 2

Table B.4: The number of piles for two different pile sizes under static and dynamic loading.

B.3. Discussion

Depending on the diameter or dimensions of the pile, the number of piles beneath a small slab would become unfeasible. With a large pile diameter, these numbers become more feasible. However, the technology to construct these piles does not exist. The auger piles and piles formed from supporting fluids are the most likely candidates to be deployed on the lunar surface, as they may be derived from current drilling techniques. The drilling fluid to stabilise the bored holes and its behaviour is, as stated before, also unknown. If it can be experimentally verified that the internal friction angle and cohesion on the Connecting Ridge are indeed high enough to stabilise bored holes up to multiple meters, this problem can be mitigated.

Furthermore, this calculation is based on cone penetration data from a different area of the Moon. As is known, the geological conditions can vary immensely depending on the formation process of the surrounding soil, and therefore, the cone tip resistance is an unknown factor. If the resistance is higher than the used calculation value of 1500 kPa, as is possible considering that lunar regolith at depth could be denser than the first meter, the resistance of a single pile can be improved dramatically.

If the piles can resist moonquake loading without losing their structural integrity, if they are affected by settlements, and the group resistance of piles is currently not considered in this analysis. This should be modelled accurately to see if this is a suitable alternative to a shallow foundation. A pile foundation reduces the material that needs to be produced compared to a shallow foundation, especially when only small piles or possibly even micropiles are used. However, this also depends on the chosen material type of the shallow foundation, and whether the technology to produce, e.g., interlocking bricks, is more energy-efficient than an augering system and producing the piles themselves.

In conclusion, it ultimately depends on what the technology can provide in terms of material production and drilling capability to determine whether a pile foundation is a suitable alternative.